STRUCTURAL CONFIGURATION STUDY

FOR AN ACOUSTIC WAVE SENSOR

by

BIAOBIAO ZHANG

W.STEVE.SHEPARD JR, COMMITTEE CHAIR
MARK E. BARKEY
KEITH A. WILLIAMS
JIALAI WANG
XIANGRONG SHEN

A DISSERTATION

Submitted in partial fulfillment of the requirements
for the degree of Doctor of Philosophy
in the Department of Mechanical Engineering
in the Graduate School of
The University of Alabama

TUSCALOOSA, ALABAMA

2012

ABSTRACT

A continuous structure has several response characteristics that make it a candidate for a sensor used to locate an acoustic source. Primary goals in developing such a sensor structure are to ensure that the response is rich enough to provide information about the impinging acoustic wave and to detect the direction of travel without being too sensitive to background noise. As such, there are several factors that must be examined with regard to sensor configuration and measurement requirements. This dissertation describes a set of studies that examine various configuration requirements for such a sensor. Some of the parameters of interest include the size, or aperture of the structure, boundary conditions, material properties and thickness. The response of the structure to transient sinusoidal wave excitations will be examined analytically. The time-domain response of an Euler–Bernoulli beam excited by a traveling sinusoidal excitation is obtained based on modal superposition and verified by using a finite element method. Then, an approach using simple basis functions will be applied to achieve the goal of more efficient response and force identification. The moving force will be identified in the time domain by extending previous inverse approaches. The Tikhonov regularization technique provides bounds to the ill-conditioned results in the identification problem. Both simulated displacement and velocity are considered for use in the inverse. To evaluate the method and examine various

configurations, simulations with different numbers of sinusoidal half-cycles exciting the sensor structure will be studied. Various levels of random noise are added to the simulated displacements and velocities responses in order to study the effect of noise in moving wave load identification. Such a new approach in acoustic sensing will have wide applications in the areas of security and disaster recovery.

DEDICATION

This dissertation is dedicated to everyone who helped me and guided me through the trials and tribulations of creating this manuscript. In particular, my family and close friends who stood by me throughout the time taken to complete this masterpiece.

LIST OF ABBREVIATION AND SYMBOLS

GMRES	Generalized minimum residual
RRGMRES	Range Restricted GMRES
LSQR	Sparse Equations and Least Squares
FRF	Frequency response function
SVD	Singular value decomposition
TSVD	Truncated singular value decomposition
CGM	Conjugate gradient method
MFIS	Moving Force Identification System
FEM	Finite element method
DOF	Degree-of-freedom
LS	Least square
TLS	Total least square
F	Spatial force load
V	Response
$[D]$	Structural operator
$\tilde{V}$	Response from inverse

δ	Background noise level
W	Displacement response
X	Beam location
t	Time
E	Young's modulus of the beam
I	Constant moment of inertia of Beam cross section
μ	Constant mass per unit length
ω_b	Circular frequency of damping for the beam
$\omega(j)$	Circular frequency of the jth mode
C_{1j}, C_{2j}	Unknown constants
B_i	Force series amplitude
β_i	Circular frequency
φ_i	Phase
$[q]$	System displacement vector
$[F]$	Corresponding force vector
$[M]$,$[K]$	Mass and stiffness matrices of the system
$[K]_t$,$[M]_t$	Mass and stiffness matrices at time step t
$\{\tilde{F}\}_{\Delta t+t}$	The external loads on the system at time $t + \Delta t$
k	Acoustic wave number
V_n	Beam structure vibration velocity amplitude

$V_j(t)$	Displacement amplitude
$V_j'(t)$	Velocity amplitude
$V_j''(t)$	Acceleration amplitude
$\emptyset_{\mathrm{n}}$	Clamped-free beam shape function
$u(x)$	New shape function for intermediate beam
A_n, B_1, B_0	Initial unknown constants
L_E	Beam Lagrangian function
T_E	The kinetic energy
V_E	The potential energy
W_E	The external force work
α, β	Integration parameters
$f(x,t)$	Moving wave load
H	Heaviside step function
$\psi_{e1}, \psi_{e2}, W_{e1}, W_{e2}$	Beam element two nodes' rotation and translation
$N_{ei}(x)$*(i=1,2,3,4)*	Shape functions of element
K_f	Foundation stiffness matrix
τ	Traveling time across the beam
W_0	Static displacement at beam middle location
D_d	Transient response divided by the static one
A	Force amplitude

L	Beam length
B	Beam width
h	Beam thickness
c	Wave speed
T	Half-cycle period
N	Number of half-cycles
ρ	Beam material density
E	Beam young's modulus
ν	Poisson's ratio
a	Left constraint
b	Right constraint
E_F	Foundation Young's modulus
TH	Foundation thickness
$C_i (i = 1,2,3,4)$	Unknown constants
ϕ_n	Elastically foundation beam shape functions
$q_n(t)$	nth amplitude
ζ_n	Damping ratio for n
ω_n	Natural frequency
Δt	Sampling time interval
λ	The regularization parameter

F_λ	Filter function
(x,y,z)	Spatial point at coordinates *x,y,z*

ACKNOWLEDGEMENTS

I would like to express my sincere gratitude and appreciation to my advisor, Dr. W. Steve Shepard Jr. His invaluable knowledge and support were indispensable for this work in the past years. Having the opportunity of working in his Structural Acoustics Laboratory also made me realize the power of a creative and professional research atmosphere.

Thanks are given to Dr. Mark E. Barkey, Dr. Keith A. Williams, Dr. Jialai Wang, Dr. K.Clark Midkiff and Dr. David A. Francko for their contributions as committee members. Special thanks are given to Dr. Mark E. Barkey, Dr. Keith A. Williams, Dr. Jialai Wang, to whom I owe much of my knowledge in their courses.

I would also like to acknowledge the financial support from the Natural Science Foundation and the Graduate School of the University of Alabama during the past years.

I would like to express my deep gratitude to my cousin Mr Hui Wang for his financial support during my stay in China within recent two years. I am forever grateful to my family for their love, kindness, and belief in me.

CONTENTS

LISTS OF TABLES

LISTS OF FIGURES

Chapter 1 Introduction

Many acoustic sensors have been developed to date. Research regarding about acoustic sensor applications can be seen in previous journal papers. These articles mainly cover areas such as military and industry fields, for example, acoustic sensors are often employed to monitor manufacturing lines and detect a breakdown of running machines.

Application of acoustic sensor technology can be traced back to the early 1900s for military battlefield purposes [1], first to detect vehicles as target locations. This technology was further developed for determining speed and detecting direction of moving objects so that people could monitor the battlefield more easily. However, exposure to background noise and a strong atmospheric environment, acoustic sensor system long-range detection capabilities were discounted because they were strongly influenced.

Beside the above applications, acoustic sensor applications can be found for object tracking due to their abilities for being deployed easily and quickly, they can be applied in diverse fields such as submarine fields, through objects tracking, soldiers monitor targets in surveillance systems. But disadvantages are obvious especially when acoustic sensors are applied to track multiple objects, for example, noise background disturbance causing random effects on measurement data has significant negative influence on acoustic sensor estimation performance.

Furthermore, a large footprint is often required for microphone arrays.

With recent advances in force reconstruction, it has recently become feasible to consider development of a wave sensor device capable of detecting the direction of a traveling acoustic wave. With such a device, one could detect the direction of moving vehicles on the road. Such a device could also be used to detect people locations and movements in dangerous threat situations. Also the need to detect persons trapped in a collapsed building, such as after a natural disaster like an earthquake, provides a motivation for the development of such a sensor.

As discussed above, microphone arrays can be employed to obtain acoustic wave direction information. These arrays are composed of multiple microphones grouped to be a single sensor. Their approaches can locate a source by using time of flight measurements. Disadvantages, however, are obvious because the arrangement of a large number of sensors is very tedious and inaccuracies can result from background noise disturbance and possible reflections from nearby structures. At the same time, large footprints are required for these arrays. As a result, there is a need to develop a compact or single sensor to detect acoustic wave direction with a wide frequency range.

Attempts above have been made to develop methods for measuring wave propagation direction and locating noise sources, but no ideal solution has been found. Although it is currently not feasible to measure the continuous response of a traveling wave, it is possible to characterize continuous mechanical vibration of a continuous structure, such as beam or plate

vibrations resulting from an acoustic excitation. From this point, we realize that continuous structures have the potential to identify the direction of propagation of an impinging acoustic wave, which can subsequently be used to locate a source of noise. Because of the availability of methods for characterizing the response of beams and plates produced by traveling loads [2], these structures make good candidates for the development of an acoustic sensor. The goal of this work is to examine the configuration requirements for a continuous acoustic wave sensor as well as develop the numerical methods needed to implement such a sensor.

There are many challenges that must be addressed when configuring a continuous structure as a new acoustic sensor. First, the structure must be sensitive enough to respond to passing acoustic loads. Because many materials, such as steel, are relatively stiff and heavy, there are potential issues associated with the small response when using these materials. It is equally important that the dynamic response of the structure should be sufficiently rich. A dynamically rich response, as illustrated in Figure 1.1, is more likely to be able to provide information about the impinging traveling acoustic wave. The manner in which the structure is mounted can also be a concern. For example, using simple supports at the edges of the structure is a very convenient method of support. Unfortunately, information provided at the instant when the acoustic load moves onto the structure may be lost due to the restraints present at those edges. As a result, alternative means of supporting the structure should be considered. One of the most important considerations in configuring such a sensor, though, is the manner in which the impinging acoustic wave loading is going to be measured from the structure's response.

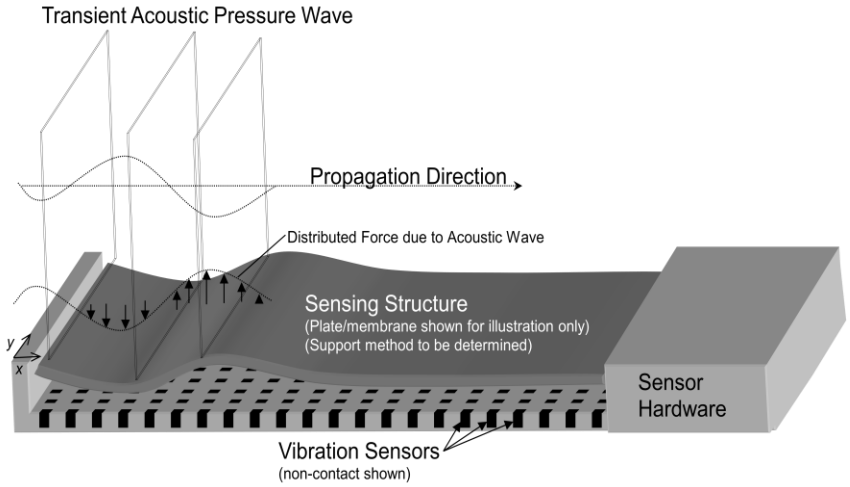

Figure 1.1 Acoustic sensor prototype expected

By measuring one or more types of mechanical response from the structure, it is possible to use inverse methods to reconstruct the forces causing that response. These inverse methods are often referred to as force reconstruction. There have been many developments and applications of force reconstruction in engineering, particularly in civil and structural engineering. S. S. Law [3], Tommy Chan [4] and L. Yu [5], for example, each used force identification on a continuous bridge structure in an attempt to identify the presence and characteristics of vehicles moving across a bridge. These studies were conducted in the time- and frequency-domains. Although traveling like an acoustic wave, moving vehicles load the structure at discrete points, identifying a distributed load, such as that caused by an acoustic wave, provides additional challenges. While measuring the location and direction of travel of the acoustic loading is certainly of interest, the general shape of the wave is also of interest. While previous research has been conducted on the reconstruction of spatially distributed loads [6], there has been no work to date on the development of distributed force reconstruction for

traveling loads. Furthermore, the accuracy of any reconstruction method can be particularly sensitive to the presence of errors. These errors may arise from inaccuracies in the description of the dynamic characteristics of the structure. Equally common are the errors that arise from errors in the measurement of the structural response. Both of these errors must be considered before an effective sensor used to reconstruct a traveling acoustic load can be implemented.

In order to evaluate potential structural configurations for such a sensor and methods for reconstructing the transient and distributed forcing function, the proposed research will first examine the response for a simple beam configuration using various simulation approaches. This response can then be used as the input to the methods developed for traveling-wave force reconstruction**.** Since the reconstructed forces may include large errors through the inversion of an ill-conditioned matrix, regularization methods such as Tikhonov regularization and L-Curve methods, as discussed previously by Liu [6], are considered in order to improve the extraction of the sinusoidally-shaped wave loads from the beam's response. The L-Curve method is an approach which is used to select the regularization parameter at its curve corner. Various levels of random noise are also considered to simulate issues associated with actually measuring a response to examine the stability of this force inverse process. Once the analytical tools have been developed, various structural parameters of interest like the beam dimensions, beam material, and support conditions are studied in an attempt to develop a configuration suitable to the problem being addressed.

Following the literature review chapter, a detailed description of the analytical tools developed and utilized in the research will be presented. To predict the sensor's response for a given configuration, the classical Bernoulli-Euler theory is first applied to predict the response for a beam with simple-supports. Note that this theory has some limitations when the frequency increases and the wavelength in the structure decreases. These limitations are being overlooked in this study as the goal here is to gauge the relative response of a structure. Also, with the use of an inverse method, methods that include shear effects become more cumbersome. As such, these shear effects will be neglected here.

In later sections of this dissertation, the force reconstruction methods and sample analytical results are discussed. Then two alternative support conditions, intermediate supports and an elastic foundation are discussed. The motivation for considering these configurations will become more apparent in those sections. Conclusions that can be drawn from the present study are also provided along with plans for future work, which will include an experimental examination of a prototype structure.

To develop a beam structure suitable for use as a sensor, the proposed research will involve the study of: 1) simple-supported beam structure subjected to moving wave loads, and associated force inverse process 2) intermediate supported beam under moving loads excitation, and 3) beam structure with elastic foundation and the associated force identification by using a force reconstruction method. The remaining portions of this dissertation are organized as follows: Chapter 2 provides a literature review of previous beam modeling as well as techniques for

identifying moving forces, which will be extended for use in sensor excitation identification. Both analytical and experimental methods are discussed. Chapter 3 presents the development of a simply-supported beam model, and then derives the formulation of a moving sine wave loads based model on extensions of a previous model developed to solve bridge structure response under the excitation of moving vehicle loads. In the development of the beam model, continuous sinusoidal wave loads with a speed equal to the sound speed in air are taken into account. Such moving load speeds have not been considered before. Chapter 4 examines the dynamic characteristics of beams with intermediate supports under moving wave loads to ensure that it is possible to determine traveling sound waves by using force reconstruction methods. By applying the assumed-modes method, and relying on clamped-free beam vibration mode functions, the vibration response of the intermediate supported beam subjected to various moving wave loads is analyzed. By applying the assumed modes method, modified beam vibration functions will satisfy the constraint conditions at the two intermediate supports as well as free boundary conditions at both ends of the beam. Numerical results are given and then verified by comparing special cases with simulation results in Fryba's book [7] and newly obtained Finite Element results. Chapter 5 discusses the responses of a free-free beam on an elastic foundation subjected to various moving loads by the application of finite element method. The Newmark integration method is used for numerical simulation. Results are verified by using commercial ANSYS package through modeling the beam with elastic foundation supports excited by moving point load at a constant speed. Chapter 6 discusses displacement and velocity response for a beam

with an elastic foundation support and the associated inverse methods. Random noise is added to the displacement and velocity responses to examine the stability of the reconstruction methods. In order to optimize the design of this new acoustic sensor, some parameters of interests such as material properties and geometry dimensions are also evaluated. Chapter 7 provides a summary of the proposed work and future plans. This future work includes using basic functions to replace traditional modal functions to describe the beam response, and then extending the modeling from beam structures to plate structures. Future plan is that the establishment of prototype model testing is needed in order to verify the force reconstruction tools developed for acoustic wave load identification.

Chapter 2 Literature review

In this chapter, force reconstruction methods available for use in developing a new acoustic sensor for predicting moving acoustic wave loads will be reviewed. Until now, most spatial acoustic sensors have been chemical based acoustic sensors which measure wave loads from chemical principles rather than from vibration mechanisms. No current acoustic sensor determines acoustic wave loads by using spatial force reconstruction methods. The goal of this research is to explore a method for determining acoustic wave loads indirectly by using force reconstruction methods with the mechanical vibration responses of a continuous sensor subjected to wave loads that travel along the structure. A review of the published literature related to moving load identification methods is presented. This review is useful in gauging the complexity of the tasks at hand.

In force reconstruction, unlike direct force measurement, externally applied force loads are identified from measured structural responses through a suitable inverse process [8]. The method is useful to find the force load when this load is unknown. A brief review of the force inverse process is presented here for completeness. As shown in Fig. 2.1, which is from Liu's work [6], $F(x, y, z, t)$ represents an initially unknown time-dependent spatial force load which acts on the 3-D structure. The response $V(x, y, z, t)$ can be expressed by

$$[D][F(x,y,z,t)] = [V(x,y,z,t)], \tag{2.1}$$

where $[D]$ represents the structural operator. If the resulting responses $V(x,y,z,t)$ is measured, the force load $F(x,y,z,t)$ can be mathematically obtained through a process which initially appears to be a simple backward calculation process

$$[F(x,y,z,t)] = [D]^{-1}[V(x,y,z,t)]. \tag{2.2}$$

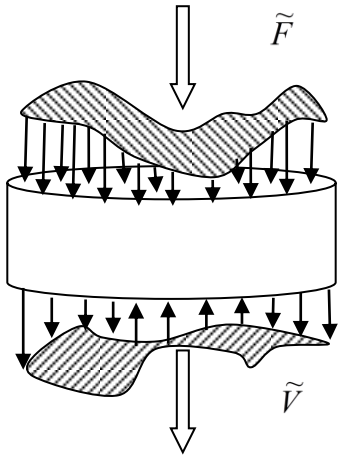

Figure 2.1 Structures excited under distributed force

Although this process seems simple, there are many issues that must be addressed if an accurate prediction of the input force is to be obtained. One issue relates to the uniqueness of the prediction of the input force. Other issues arise if $[D]$ is a severely ill-conditioned matrix due to complicated structure effects. Besides, the measured response $V(x,y,z,t)$ may be polluted with various levels of background noise δ. If the polluted $\tilde{V}(x,y,z,t)$ is applied in the inverse, the resulting inverse force $F(x,y,z,t)$ can differ dramatically from the true value even if the noise level δ is small. Many previous studies have been performed to deal with force reconstruction and inversion issues.

Historically, inverse problems first appeared in the mid-19th century for use in railroad design and building. Railway roadbed is a complicated structure which is subjected to train loading. Vibration responses are generated by passing train loads. These responses can easily be measured, but the force acting on the rail by the moving train load is more complicated and sometimes different from the train weight itself. For example, a train may be moving on a railway road with a slope through the mountains. Using the method for inferring moving loads from railway road responses, the moving force on the railway can be predicted accurately. This information is so important that railway road design criteria are based upon it.

As noted above, problems can occur when the force is calculated from backward process due to the inverse of a matrix being severely ill-conditioned. In these cases, the backward calculation does not provide accurate results. Inverse problems lead to the mathematic model establishment and improved solution methods have been developed. The first person who defined it in a mathematical sense was J.Madhard [9] in 1902. According to his view, if the solution to the mathematic model is unique in any continuous set, this model will be considered as a well-posed problem. Otherwise, if the solution is not unique for arbitrary input sets, this problem will be ill-posed. Ill-posed problems have been studied for more than a century. Many methods have been proposed to solve these problems, which have made very good progress in this area. Initially, the least square method was applied to address this problem [10]. Because the least square approach does not always provide satisfactory results, the Tikhonov regularization method was then applied to better regularize the output through the selection of regularization

parameters. Various other methods, such as generalized cross validation [11] and L-curve [12], can be applied to compute regularization parameters through numerical calculation to solve the inverse problem. It should be noted that in the L-curve method, the optimized parameter is chosen from the plot of the regularized solution against the squared norm of the regularized residual [13]. Despite its severe limitation in solving large matrix ill-conditioned problems, the method has received much attention in solving ill-posed problems. It is a simple method to use and regularization results are normally accurate.

More progress has been recently made in the inverse problem area. For example, D. Calvetti [14] applied the GMRES, RRGMRES and LSQR methods to solve large linear discrete ill-posed problems. These methods might be a good application in solving the problems of moving acoustic loads on beam structures, like the problem at hand. Yimin Wei [15] proposed a weighted Tikhonov filter method to solve discrete ill-posed and rank-deficient linear problems. Ailin Qian [16] tried to use a wavelet method to theoretically solve the ill-posed problem for an elliptic equation, while J.F. Doyle [17] applied a wavelet reconvolution method to identify an impact force using the measured responses. As can be seen, much work has been conducted in the area of regularizing inverse problems with ill conditioning. All these methods are conducted in either the time domain or the frequency domain.

A brief review of some of these reconstruction methods described above offers a good opportunity to understand engineering inverse problems. An overview of force identification problems on structures can be seen in [17]. The moving vehicle loads identification problem was

solved by using the approximated method of treating the vehicle load as simple moving-force problem [18]. Continuing in this problem, researchers [19] gave four methods, one of which is the interpretive method [19] used to obtain the moving forces directly by establishing a model with lumped masses and massless elastic beam elements. The second method is a time domain method [20] which identifies forces by using responses from a simply-supported Euler beam under an external moving load. The equations of motion of the beam are obtained through a modal coordinate transformation, and the resulting set of equations relating the Fourier transforms of the responses and the moving forces are converted into time domain by a new method proposed by the authors. The third method is a frequency-time domain method which is the same as above, that is, the modal assume method is employed to decouple the beam partial difference equation. The difference is that through the Fourier transformation approach, the moving force in frequency domain is converted into time domain by the least-squares method [21]. Another method is the Second Interpretive method [22], which reveals two-axle vehicle loads completely based on the Euler beam theory and mode assume method. All methods above could solve point load problems with generally reasonable acceptance.

But further research work in [23–25] indicated that although previous methods above could identify moving point loads effectively, limits still existed. In particular, poor results or incorrect estimations happened when these methods tried to identify force at certain time point or certain excitation frequency. Main reasons for these issues were the measured response data errors and matrix ill-conditioning problems [26]. In addition, different accuracies were obtained

due to different approaches to solve the equation [27]. The reason was that the structure inverse matrix is a pseudo-inverse (PI) matrix whose elements are sensitive to small perturbations of input responses. For example, small noise pollutions in the response can yield output data with large perturbations from the PI matrix. In this sense, by using the method of Singular Value Decomposition (SVD), one can filter errors in the PI matrix and then reasonable estimate results can be obtained [28]. The SVD technique, the common numerical inverse method within the last 35 years [29–31], is widely used in structural identification problems [32]. Hillary and Edwins [33] studied beam structure inverse problems to find a reasonable force identification method. Recently S.S. Law and Chan [34] applied Tikhonov and L-curve methods to identify single or two vehicle loads moving on single span or multi-span bridges in the time and frequency domains. Random noise of different levels was added to evaluate the stability of identification methods. Yu and Chan [35] proposed the Single Value Decomposition (SVD) technique in the frequency domain to identify single moving vehicle loads on the bridge. However, that method involved a significant computational cost. Choi et.al.[36] found that the L-curve method is better than ordinary cross validation and general cross validation methods even when background noise was present in the measured responses. Huang [37] used CGM to predict the external force in a damped system from measured responses. Chih-Kao Ma [38] extended the combined methods of the Kalman filter and a recursive least-squares estimator, which was originally applied to the linear system to identify the input forces in a nonlinear system. Dobson and Rider [39] summarized previous works about force identification and pointed out further work.

Olsson [40] tried to reveal moving load identification problem just by measuring static loads. Other force identification problems through static equivalent axle loads could be found [41–45]. Heavier vehicle static loads will increase damage to the road surface through repeated application of vehicle static loads on the road [46], this will reduce the road use life. In order to identify vehicle loads, Whittemore et al. [47] and Cantieni [48] both used instrumented vehicle loads to determine dynamic loads on bridge structures.

Although the applications above have made great progress in force identification, problems still exist. Namely, initial conditions should be known. For example, initial displacement should be given to determine time-dependent response, which is taken as the input variable to the inverse process for force reconstruction. But the problem is that in some cases, initial conditions might be unknown. Sometimes, complicated structures are found to be difficult in being represented by a definitive matrix in mathematic sense even when this matrix is severely ill-conditioned.

In this work, force reconstruction methods will be developed and applied in order to develop a new acoustic sensor for predicting moving acoustic wave loads based on a beam structure. A comprehensive review of moving loads traveling on beam structures can be found in Fyba's book: Vibration of Solids and Structures Under Moving Loads [7], which mainly dealt with vehicle loads moving on structural components representing bridges. In his book, he described the theoretical formulations of the structural response under various kinds of moving loads. The work in that book belongs to the forward problem. By extending the work described

in Fyba's book to obtain beam responses under moving loads, and applying force reconstruction methods to the simulated response to infer force loads through the inverse process, a new acoustic load sensor principle will be developed. The approach taken here will also allow the effects of ill-conditioned and noise to be examined in detail.

It is quite challenging when moving force identification methods are applied to develop an acoustic wave sensor. As it is well known, sound propagating onto a structure will generate a vibration response in that structure. Differences from common moving loads are that sound waves travel at a much higher speed. In addition, sound wave can propagate through air media while common moving loads cannot. Finally, once the sound wave traveling along the structure of a certain length touches the end with boundary constraints, it will generate a reflection wave which will superimpose with incident waves, and make the problem solution more complex. Some inverse methods above cannot filter background noise effectively. Besides, times of wave load arrival and departure are uncertain. To examine this problem, sinusoidal loads moving at sound speed will be used to mimic acoustic wave loads, then responses of the beam with different boundary conditions subjected to these wave loads will be evaluated. Therefore, the ability of inverse methods to reconstruct the forcing excitation can be examined.

To help understand the complexity of the acoustic wave load reconstruction method, various methods for force identification used in structural engineering were briefly reviewed. Recent development of inverse methods in mathematic field was also presented. These methods can be extended to develop a method for determining acoustic load through a sensor structure.

However, due to some limits, such as material properties and structural design parameters, not all materials are suitable for an effective sensor structure. The following chapters provide a detailed description of initial developments with regard to problems that will be addressed in this research work. First, a beam with simple supports subjected to moving loads will be evaluated. Then, responses of a beam with intermediate supports under moving loads will be determined. Finally in Chapter 6, the reconstruction process for an elastic foundation beam will be developed to make a basis for model prototype establishment.

Chapter 3 Simple supported beam acoustic wave propagation

In this chapter, a description of the analytical tools needed to predict the response of a simply supported beam sensor is provided. This is the forward problem which is an extension of the work of Fryba [7]. Transient responses are obtained by using analytical solutions under moving sinusoidal wave loads and they are verified by a finite element model excited by the same moving wave loads. In addition, the assessment tools are discussed along with some sample results. One of the primary goals is to examine changes to the responses of the beam as various parameters are adjusted. In using this approach, a better beam configuration for use as an acoustic sensor will be sought.

3.1 Simply supported beam model

In this section, an overview of the methods used to predict the sensor candidate structure's response when subjected to various transient pressure waves is presented. Because the initial configuration considered here is one-dimensional, the pressure wave can be treated as a distributed force. For a general transient force wave $F(x,t)$ traveling across a simply supported beam at speed c, the response will be denoted as $W(x,t)$. This dynamic deflection of the beam is a

function of position *x* and time *t*, as illustrated in Figure 3.1 for a beam of length *L*.

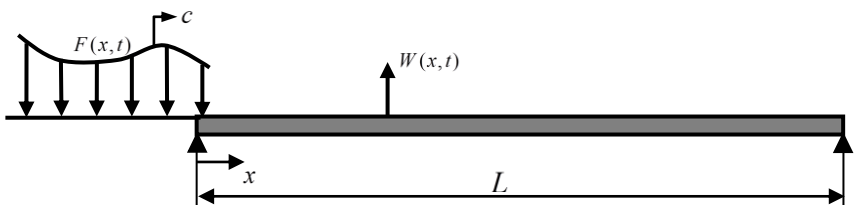

Figure 3.1 Arbitrary transient load F moving on to simply supported beam

3.2 Governing equation of a simple-supported beam under moving loads

The partial differential equation of a simply-supported beam under moving loads and its analytical solutions are detailed in the work of Fryba [7]. Those results are summarized here. Assuming a beam with small deformation is subjected to the moving loads which are parallel to the symmetrical axis of the cross-section, the governing equation is

$$EI\frac{\partial W^4(x,t)}{\partial x^4}+\mu\frac{\partial W^2(x,t)}{\partial t^2}+2\mu\omega_b\frac{\partial W(x,t)}{\partial t}=F(x,t), \tag{3.1}$$

where E is Young's modulus of the beam, I is the constant moment of inertia of the cross section, μ is the constant mass per unit length, ω_b is the circular frequency of damping for the beam, and $F(x,t)$ is the wave force. The boundary conditions are given by $W(0,t)=0$ and $W(L,t)=0$ for no motion at the ends and

$$\left.\frac{\partial^2 W(x,t)}{\partial x^2}\right|_{x=0}=0,\ \left.\frac{\partial^2 W(x,t)}{\partial x^2}\right|_{x=L}=0\ , \tag{3.2}$$

for no moment at the ends. The initial conditions are given by $W(x,0)=0$and $\left.\frac{\partial W(x,t)}{\partial t}\right|_{t=0}=0$, where $t = 0$ is the instant just before the force moves onto the beam. Considering Eq.(3.1) and

Eq.(3.2), and using a series-based solution with the *j*th mode shape of the beam, the response can be expressed as

$$W(x,t) = \sum_{j=1}^{\infty} \frac{2}{L} sin\left(\frac{j\pi x}{L}\right) V_j(t), \quad (3.3)$$

where $V_j(t), (j = 1,2,3 \ldots.)$ are the presently unknown modal displacements. After substituting Eq.(3.3) into Eq.(3.1), multiplying the resulting expression by the mode shape function $sin\left(\frac{j\pi x}{L}\right)$, $(j = 1,2,3 \ldots.)$, and then integrating with respect to *x* between 0 and *L*, the resulting equation is

$$V_j(t)\omega^2(j) + V_j''(t) + 2\omega_b V_j'(t) = \frac{1}{\mu}\int_0^L F(x,t) sin\frac{j\pi x}{L} dx \; (j = 1,2,3 \ldots. \infty), \quad (3.4)$$

where $\omega(j) = \frac{j^4\pi^4}{L^4}\frac{EI}{\mu}$, with $\omega(j)$ representing the circular frequency of the jth mode. For Eq. (3.4), when the right hand side is equal to zero, the homogenous solution (free response) is given by

$$V_j^*(t) = e^{-\omega_b t}\left\{C_{1j} sin\left(t\sqrt{\omega_j^2 - \omega_b^2}\right) + C_{2j} cos\left(t\sqrt{\omega_j^2 - \omega_b^2}\right)\right\}, \quad (3.5)$$

where C_{1j} and C_{2j} are presently unknown constants. The desired solution for Eq. (3.4) will be this homogenous solution plus the particular solution $V_j^F(x,t)$ caused by the applied transient wave load. The response for this load will now be discussed. Since any applied force function can be separated into a series of harmonic force functions, the forced vibration equation in Eq.(3.4) can be expressed as

$$V_j(t)\omega^2(j) + V_j''(t) + 2\omega_b V_j'(t) = \sum_{i=1}^{M} B_i sin(\beta_i t + \varphi_i), \quad (3.6)$$

where B_i is the force series amplitude, β_i is the circular frequency and φ_i is phase. The size of *M* is completely dependent on the nature of the term on the right hand side of Eq.(3.4). For the

harmonic force term $\sum_{i=1}^{M} B_i sin(\beta_i t + \varphi_i)_i$, the beam response that satisfies Eq. (3.6) is given by

$$V_j^F(t) = \sum_{i=1}^{M} [a_i cos(\beta_i t + \varphi_i) + b_i sin(\beta_i t + \varphi_i)], \quad (3.7)$$

where a_i and b_i are found by substituting Eq.(3.7) into Eq.(3.6) to get

$$a_i = \frac{-2\omega_b \beta_i}{(\omega^2(j) - \beta_i^2)^2 + 4(\omega_b \beta_i)^2} B_i \quad (3.8a)$$

and

$$b_i = \frac{\omega^2(j) - \beta_i^2}{(\omega^2(j) - \beta_i^2)^2 + 4(\omega_b \beta_i)^2} B_i. \quad (3.8b)$$

By combining the homogenous solution from Eq.(3.5) with the particular solution from Eq.(3.7), the general solution to Eq. (3.4) is

$$V_j(t) = e^{-\omega_b t}\left(C_{1j} sin\left(t\sqrt{\omega_j^2 - \omega_b^2}\right) + C_{2j} cos\left(t\sqrt{\omega_j^2 - \omega_b^2}\right)\right) + V_j^F(t). \quad (3.9)$$

Therefore, by substituting the coefficients found in Eq.(3.9) into Eq.(3.3), the beam structure's displacement response function under a moving sinusoidal load is

$$W(x,t) = \frac{2}{L}\sum_{j=1}^{\infty} e^{-\omega_b t} sin\frac{j\pi x}{L}\left(C_{1j} sin\left(t\sqrt{\omega_j^2 - \omega_b^2}\right) + C_{2j} cos\left(t\sqrt{\omega_j^2 - \omega_b^2}\right)\right) + V_j^F(t) sin\frac{j\pi x}{L}. \quad (3.10)$$

To complete the solution, it is necessary to utilize the forcing function and initial conditions, both when the force enters and leaves the beam, to determine the unknown coefficients in Eq.(3.10). Depending on its position, the specific motion caused by the distributed wave must be determined by using one of four distinctly different regions. These regions are: 1) the load stepping onto the beam, 2) the load completely on the beam, 3) the load stepping off the beam,

and 4) the load entirely off the beam. The motion equations of these four regions are applied to obtain the time dependent beam displacement. These analysis tools will now be used to solve the forward problem, in which the structure's response is computed for a known force input. Sample results are shown in the following section. This predicted response will be used in the inverse methods to determine the feasibility of using such a structure as an acoustic sensor.

3.3 Free response

The final region that needs to be considered is the free response when $L/c + NT < t$ denoted above as region 4. During this time period, there is no force load applied to the beam structure, so $F(x,t) = 0$. Since only the free response occurs, there is no associated forcing function or forced response. The motivation for using the analytical solution presented above is the ability to change various parameters and yet also to obtain a solution quickly. For example, the equations are not affected when L, N or T are changed.

3.4 Finite element method

In order to verify the results from this analysis, it is useful to compare the results to a finite element solution. One might initially perceive the use of this alterative solution as entirely redundant. However, use of FEM to provide an alternative solution approach serves two purposes. First, it enables verification of the analytical approach, which is used for the initial configuration study. Second, and possibly more important, is that the FEM can be used in later research for more complex configurations that cannot be conveniently solved in the manner

presented above. For example, the FEM is well suited to handling other boundary conditions as well as two dimensional structures. To that end, the FEM used to verify the analytical solution is presented. Then, some sample results for both the analytical and FEM are presented and discussed. Finite element models of time-dependent problems can be developed in two alternate ways: (a) a coupled formulation in which the time *t* is treated as an additional coordinate along with the spatial coordinate *x* and (b) a decoupled formulation where time and spatial variations are assumed to be separable. In the present work, the latter is used to solve this time-dependent problem as previously described by Reddy [52].

To solve the problem by the finite element method, the governing equation should be semi-discretized. In this issue, our beam problem is discretized into 32 nodal points and interpolated by means of the shape functions and the weight functions, respectively. First of all, local shape and weight functions are obtained from each element, then they will be assembled into global shape and weight functions. So for the present structure, the beam is discretized into 15 elements, by assuming that beam damping is negligible, therefore the beam equation is

$$[M][\ddot{q}] + [K][q] = \{F\}, \tag{3.15}$$

where $[q]$ denotes the system displacement vector, which contains all beam degrees of freedom, $[F]$ is the corresponding force vector, and $[M]$and $[K]$ represent the mass and stiffness matrices of the system, respectively.

The system equations as given in Eq.(3.15) can be solved by the Newmark β method of direct integration [52]. Consider a typical time step from t to $t+\Delta t$ in the time-history, these equations are

$$\{\ddot{q}\}_{t+\Delta t} = a_0(\{q\}_{t+\Delta t} - \{q\}_t) - a_2\{\dot{q}\}_t - a_3\{\ddot{q}\}_t, \tag{3.16}$$

and

$$\{\dot{q}\}_{t+\Delta t} = \{\dot{q}\}_t + a_6\{\ddot{q}\}_t + a_7\{\ddot{q}\}_{t+\Delta t}, \tag{3.17}$$

where the coefficients are given by

$a_0 = \frac{1}{\beta\Delta t^2}$, $a_1 = \frac{\gamma}{\beta\Delta t}$, $a_2 = \frac{1}{\beta\Delta t}$, $a_2 = \frac{1}{2\beta} - 1$,$a_6 = \Delta t(1-\gamma)$ and $a_7 = \gamma\Delta t$.

In this study, $\beta = 0.25$ and $\gamma = 0.5$ are selected, which implies a constant average acceleration with unconditional numerical stability. Substituting Eq.(3.16) and Eq.(3.17) into the system in Eq.(3.15), the following equivalent linear equation can be obtained

$$\left[\tilde{K}\right]_t\{q\}_{t+\Delta t} = \{\tilde{F}\}_{t+\Delta t}, \tag{3.18}$$

where $\left[\tilde{K}\right]_t$represents the effective stiffness matrix and $\{\tilde{F}\}_t$is the effective load vector, defined as following

$$\left[\tilde{K}\right]_t = [K]_t + a_0[M]_t, \tag{3.19}$$

$$\{\tilde{F}\}_{t+\Delta t} = \{F\}_{t+\Delta t} + [M]_t(a_0\{q\}_t + a_2\{\dot{q}\}_t + a_3\{\ddot{q}\}_t), \tag{3.20}$$

where $[K]_t$ and $[M]_t$ represent the effective stiffness matrix and mass matrix of the system evaluated at time t. $\{\tilde{F}\}_{\Delta t+t}$ denotes the external loads on the system at time $t+\Delta t$.This term is used to describe wave load with constant speed c moving along the beam. The approach to solve the system Eq.(3.15) at each time step $t+\Delta t$ is as follows: 1) Use the system matrices

$[K]_t$ and $[M]_t$ at time step t to compute the effective stiffness matrix $[K]_t$, 2) Calculate the external force vector $\{\tilde{F}\}_{\Delta t+t}$ and effective load vector $\{F\}_{t+\Delta t}$, 3) Solve the equivalent system Eq.(3.16) for the displacement $\{q\}_{t+\Delta t}$, 4) Update the system matrices $[K]_t$ and $[M]_t$ for the next time step and repeat the procedure. Results from an FE approach will be compared later to the analytical results for a few sample configurations which are now discussed.

3.5 Numerical analysis

The initial parameters of the beam structure used for the sample numeric study and finite element analysis verification to be described here are listed in Table 3.1. The purpose of these simulations is to examine the nature of the response in order to gauge if it is rich enough to work as a sensor. As such, these parameter values can be modified to determine their effects on the beam response. Some of these values will be modified later. When values are not specifically provided, the values listed in Table 3.1 can be assumed. In this work, the damping ratio is assumed to be 0.1 unless otherwise noted. Other material parameters to be considered will be described later. The numeric analysis and finite element analysis were conducted using Matlab®.

Table 3.1 Parameter definitions

Item	Value	Units	Description
L	0.75	m	Beam length
B	0.05	m	Beam width
h	0.05	m	Beam thickness

c	343	m/s	Wave speed
T	0.001	Sec	Half-cycle duration
ρ	7800	kg/m^3	Steel density
E	2.068e+11	N/ m^2	Steel Young's modulus
υ	0.29	-	Steel Poisson's ratio
N	1		Number of half-cycles

3.5.1 Waveform effects

Figure 3.2 shows the beam structure response for different kinds of wave loads $N = 1$ to $N = 4$ with a fixed T. T represents the time period of a single half wave load and N is the integer number of half-cycles as shown in Figure 3.2(a). As a result, the total time period for the excitation is NT. The forced and resulting free vibration responses are shown in each of the plots. It is not difficult to recognize that there are several peaks in each of the four figures. The first peak represents the displacement of the beam for Regions 1 through 3. The remaining peaks in all the figures are for the free vibration once the wave load has left the beam. The damping effects for the beam can clearly be seen. It is worth noting that the response as a function of position does vary for each of the four wave loads considered. Generally speaking, when the nature of the wave becomes more complicated for a higher N, the nature of the response as a function of x also becomes more complicated. This behavior is certainly desirable if there is any hope of eventually obtaining information about the incident acoustic wave. While the overall

magnitude of the response does decrease as the negative force cycles are added onto the transient excitation, the response is still in the same order of magnitude as for the purely positive $N = 1$ case. Such behavior will be important when it is desired to determine information about the excitation, as the response will not have significantly decreased.

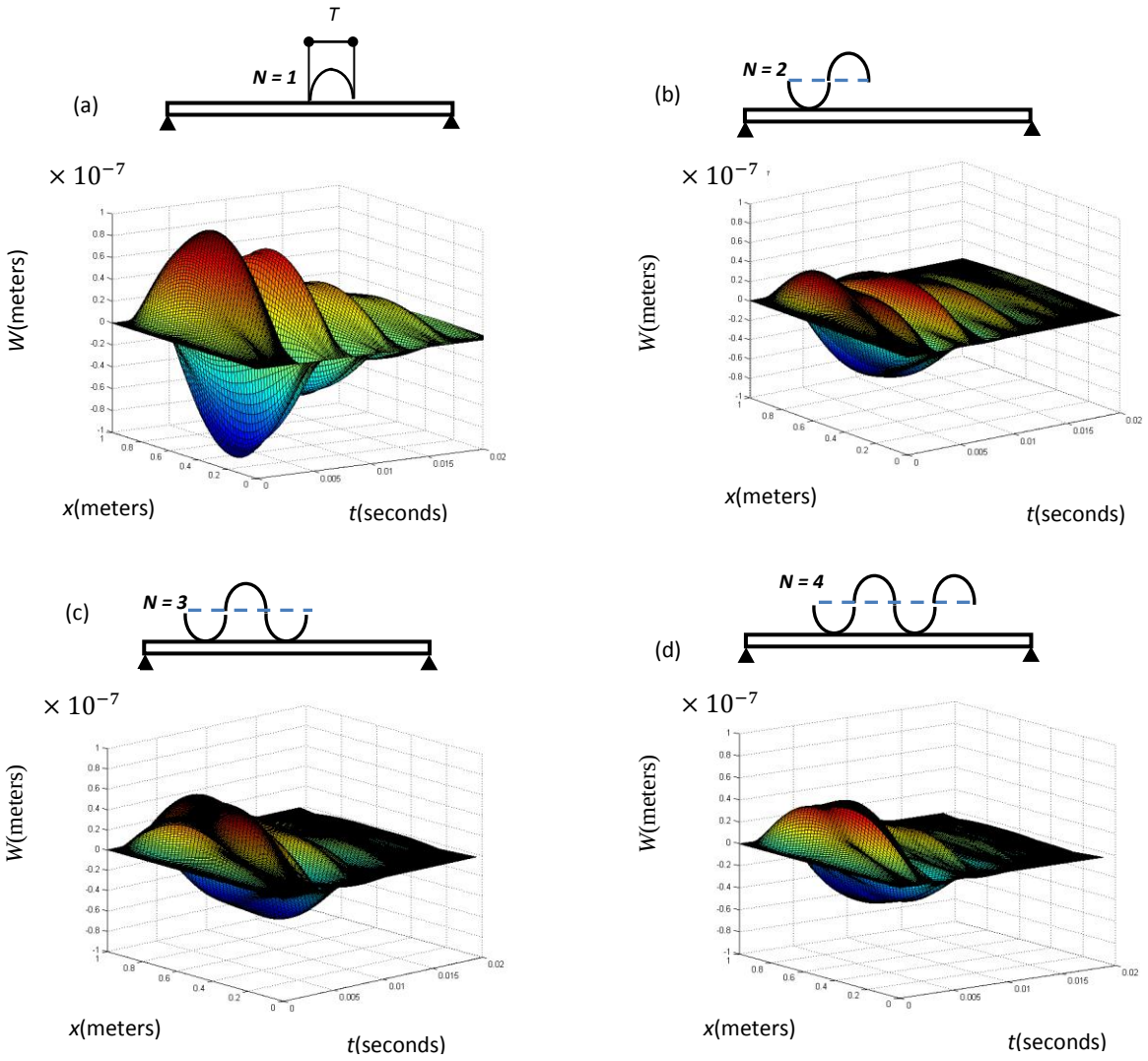

Figure 3. 2 shows structure response for different kinds of wave loads $N = 1$ to $N = 4$ with a fixed T

3.5.2 Thickness and length effects

Figure 3.3 shows a comparison of three beams with different thicknesses, h = 0.1 m, 0.05 m and 0.005 m, for a single half-cycle excitation (N = 1). As indicated in the plots, the thinner beam responds much more readily to the transient wave. This behavior is not surprising as the decreased mass of the beam enables it to respond more quickly.

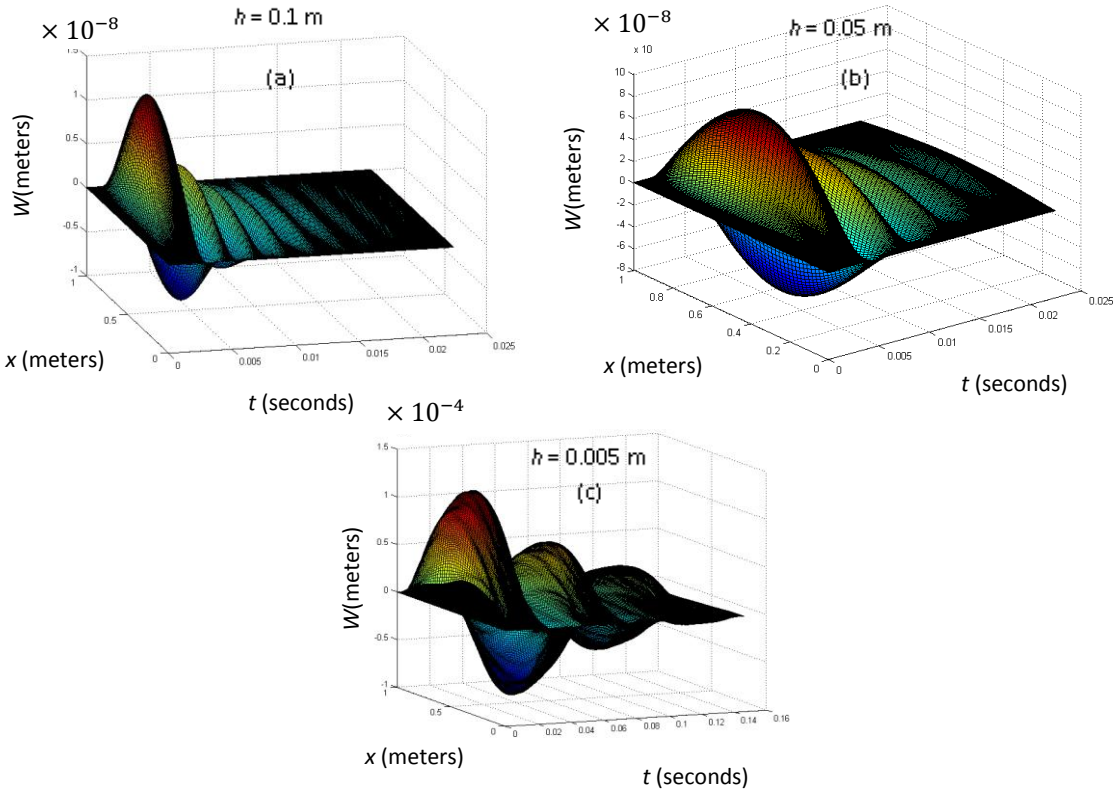

Figure 3. 3 Beam displacement influenced by different thicknesses, N = 1, L = 0.75

The ripples in Fig.3.3(c) for the thin beam indicate that the response for this beam contains more dynamic information as the response is not as uniform over the width of the beam. Obviously, focus on the further examination of a thinner beam is warranted.

In considering the sensitivity of the beam, it is useful to consider the response that occurs for each configuration after some fixed amount of time. By fixing T at 0.001 seconds, the half-cycle of $N = 1$ load will just become entirely on the beam when $ct = 0.343$ m, which corresponds to $t=T$. This case will be true regardless of the length and thickness of the beam. Figure 3.4 shows the normalized beam displacement for a range of beam thicknesses and lengths at this fixed point in time. The response is normalized to a value of unity by its maximum value for each individual configuration. Note also that the position along the beam length is normalized via the length. This normalization allows different length beams to be compared more easily. The presence of an inverted frontal wave also disappears quickly as the thickness decreases. While the response is more localized for very long beams, there is still a reasonable degree of localization even for some of the shorter beam lengths. It is also worth examining the directionality of the beam response. A plot of the difference in the response of the beam for waves coming from either end is shown in Fig.3.5. Although the thickness is relatively large for this case, it is still apparent that at reasonable lengths it would be possible to determine the end from which this wave load was entering the beam.

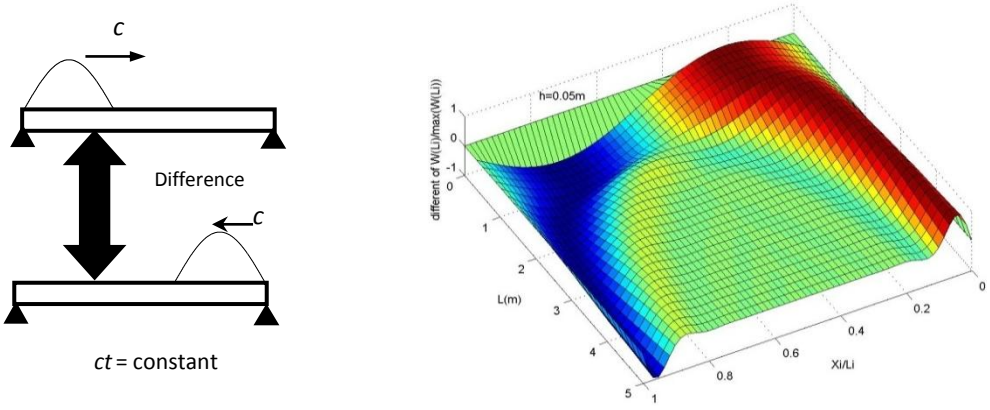

Figure 3. 4 Impact of wave load direction of travel

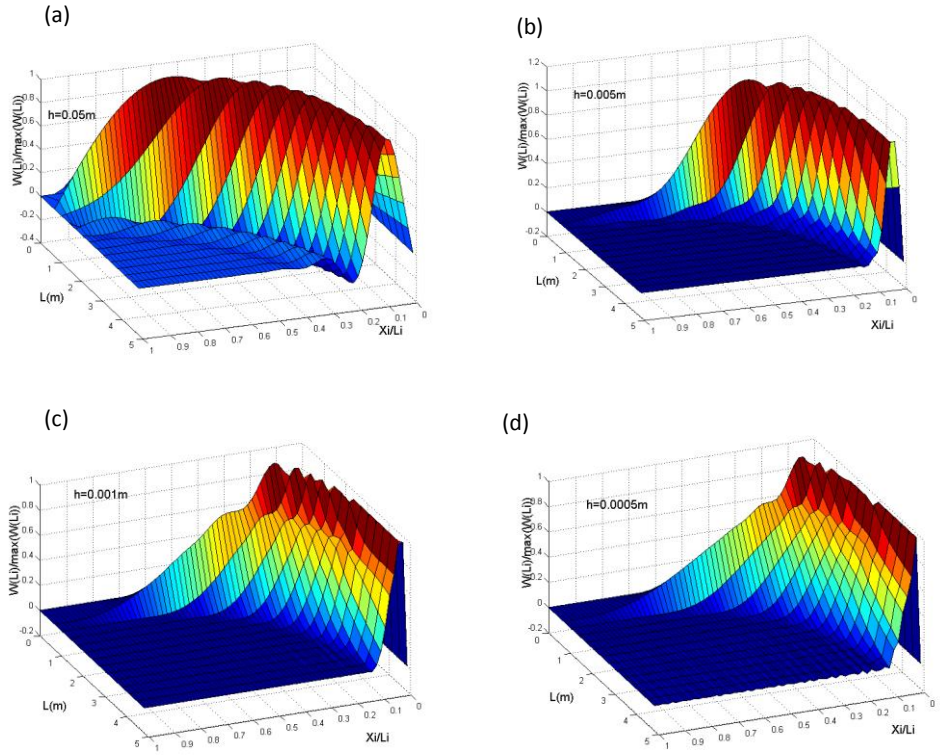

Figure 3. 5 Normalized displacement of beam structure under different thicknesses for a range of length

3.5.3 Wavenumber spectrum

The wavenumber spectrum [53] is utilized here to gather information regarding the

spatial content of the sensor's response. For the simply-supported beam structure, the velocity distribution can be expressed in terms of its spatial content [53] as

$$V(k) = V_n \int_0^L sin(n\pi x/L)\, exp(-jkx)\, dx, \tag{3.21}$$

where k is acoustic wave number and V_n represents beam structure vibration velocity amplitude for each mode. This equation represents the transverse velocity of the finite length beam in terms of infinitely long waves each with a corresponding wavenumber k. This relationship is analogous to expressing a transient time wave in terms of a continuous spectrum of various frequency components via the Fourier spectrum. By examining the wavenumber spectrum, it is possible to

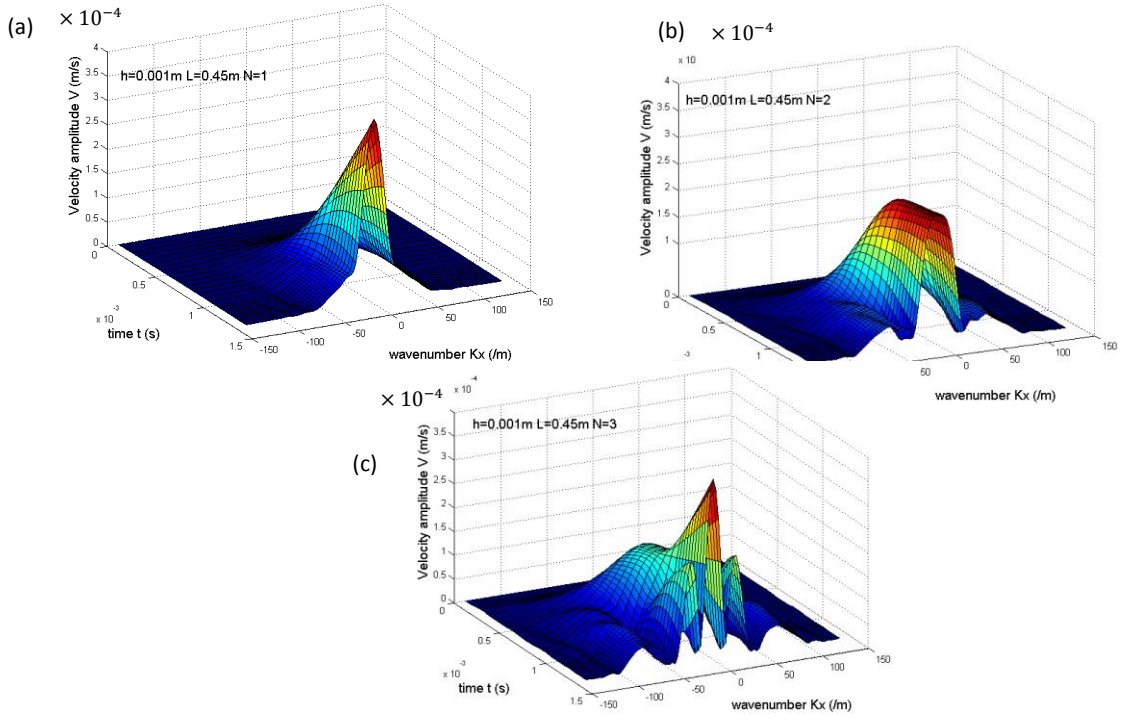

Figure 3. 6 Wavenumber spectrum under different wave loads N

obtain further insight into the spectral content of the response via these spatial terms. This information supplements simply visualizing the response in three dimensions. Figure 3.6 shows the wavenumber spectra for three identical beam sensors subject to a transient wave with increasing numbers of half cycles N. The nature of the spectra as a function of time can clearly be seen. For the $N = 1$ case of Fig.3.6(a), the beam velocity amplitude always increases and is confined to a limited region of wavenumbers. Furthermore, the spectral content does not appear to vary with time, at least for the range of time considered. When the number of half-cycles in the transient wave load is increased to $N = 2$, the long-wavelength components (low wavenumber) reach some value and then maintain a reasonably constant amplitude. As time increases, the spectrum does start to become richer with a peak and a valley. As the number of half-cycles increases further to $N = 3$, the spectrum appears to be a somewhat combined case for the first $N = 1$ and $N = 2$ cases, though the spectrum is clearly not just a simple summation of the previous two cases. The response appears to be spread out over a larger range of wavenumbers than in the previous two cases, although the difference in that range is not clearly significant. Still the presence of more peaks and valleys indicate that the energy is not as evenly distributed over the range of wavenumbers. The impact of beam length on the resulting wavenumber spectrum is shown in Fig.3.7, for $0 \leq L \leq 10$ m. Each plot is for a different thickness for the case of a half-cycle load ($N = 1$). From these results, it can be seen that velocity amplitude becomes larger with the increases of the beam length. At the same time, it can be seen that the velocity amplitude range also varies with thickness. That is, when the thickness is $h = 0.05$ m, the

velocity amplitude variance range is primarily between wavenumbers -15 m^{-1} and 15 m^{-1}. As thickness is reduced to 0.001 m, the velocity amplitude expands to a larger range of wavenumbers between -30 m^{-1} and 30 m^{-1}. Furthermore, the spectrum shape for the thinner beam sensor is more complicated than for the thicker case. Obviously, the thin beam structure is more easily excited by the transient moving wave. In comparing Fig.3.6(a) to the other figures, it is also clear that the amplitude of the spectrum increases significantly as the thickness decreases.

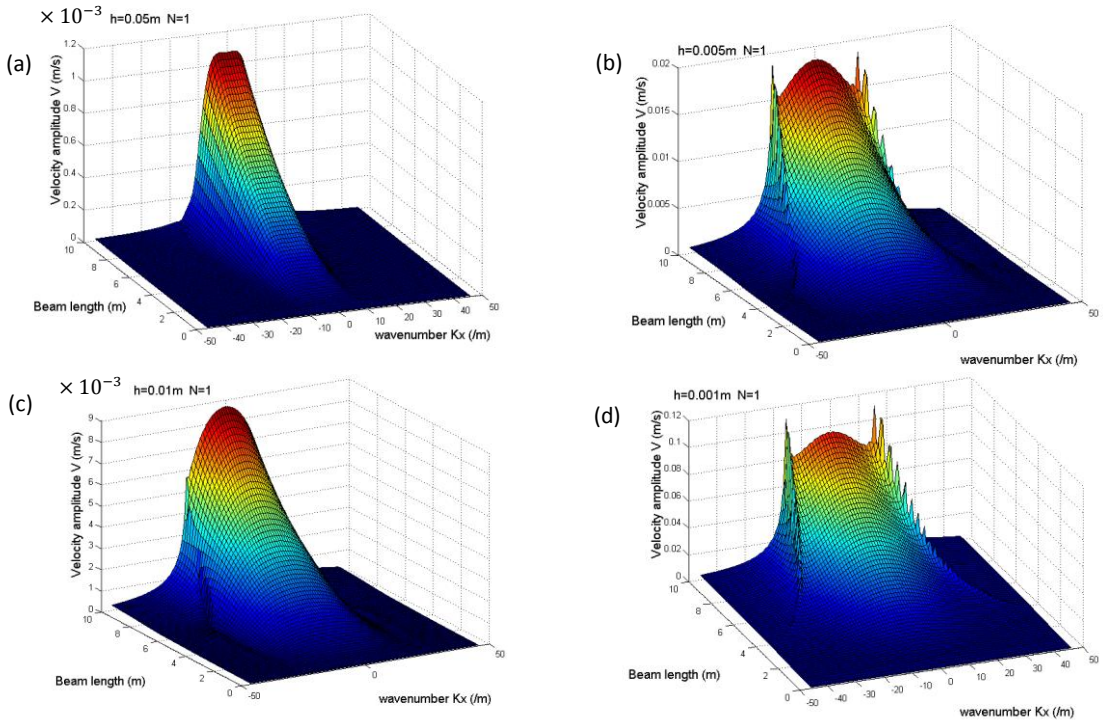

Figure 3. 7 Wavenumber spectrum for various beam sensor thicknesses

Again, this result is not surprising.

3.5.4 Material effects

Thus far, the beam has been assumed to be made of steel. Depending on the thickness desired, configuration and mounting requirements, it may be determined that steel does not provide the best response for determining the nature of the incident pressure wave. As a result, it is important to be able to consider alternative materials. Figure 3.8 shows two sets of wavenumber spectrum. One set is for a steel beam and the other set is for a beam constructed of

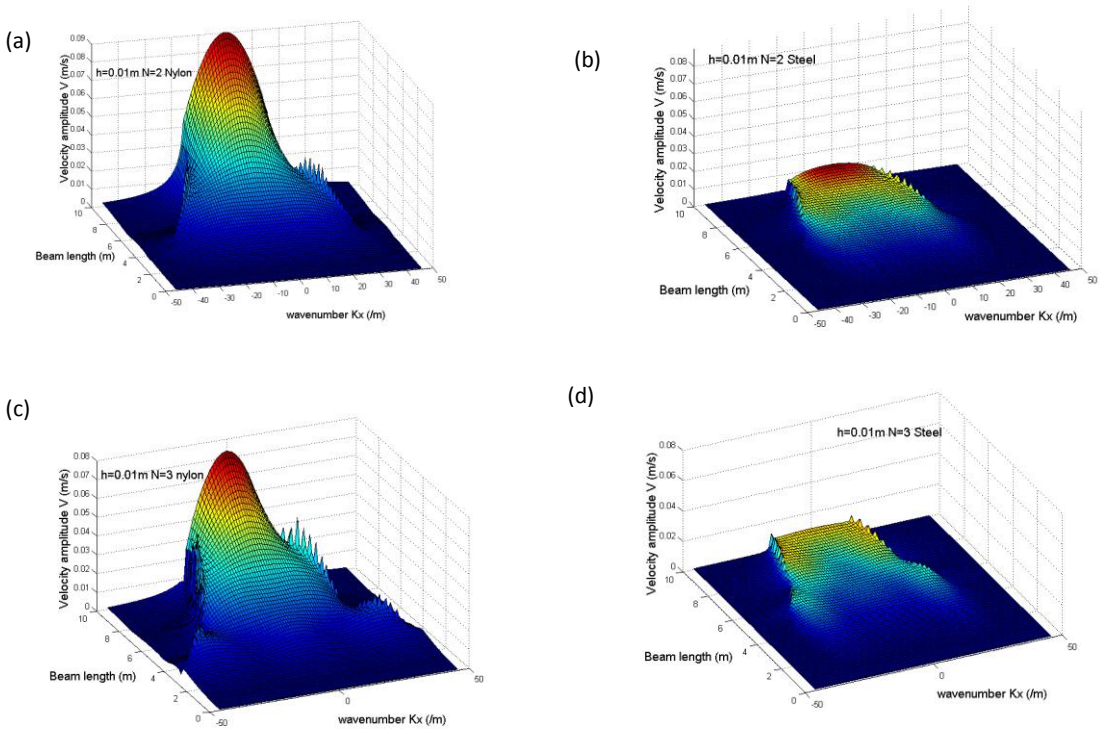

Figure 3. 8 Wavenumber spectrum for different materials

Nylon material. When constructed of Nylon, the amplitude of the spectrum is clearly larger. The approach outline here and other approaches will be used in the future to further assess Nylon and other materials to determine their effectiveness in use as a sensor structure. In next section, the transient-wave beam response for a simply-supported condition will be verified by a finite

element solution obtained using the solution approach described above. Due to the fact that FEM model ignored damping effects, damping will also be neglected in the analytical solution for the purposes of the verification. Some of the analysis conditions used here will enable comparison with Fryba's results as well.

3.6 Verification of analytical solutions by FEM

Figure 3.9 shows point load static displacements obtained from the finite element method, the current analytical method, and Fryba's results in [7]. It can be seen that the curves are all similar to Fryba's results. Despite slight deviations near the top of the curves, the errors

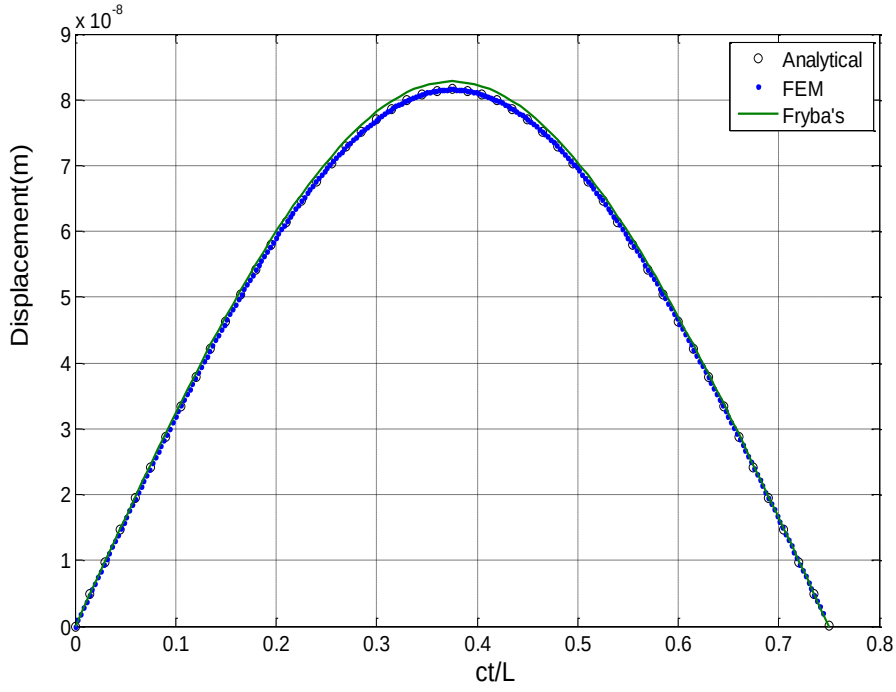

Figure 3.9 Mid-beam displacements comparison for all three methods approximating static conditions

are quite small. Therefore, the analytical results agree reasonably well with other methods when used under the conditions for which those methods were developed.

If the load now traverses the beam with speed $c = 343m/s$, the displacement for the beam at mid-position under various wave loads are plotted in Fig.3.10. Figure 3.10(a) shows the mid-beam displacement under a travelling half-cycle sine wave load. In comparing the results from the analytical method with those from the FE method, it can be seen that only very small errors exist during the time region when the load is leaving the beam. Those errors are on the order of one percent or so. In the other time regions, the results are almost identical. Figure

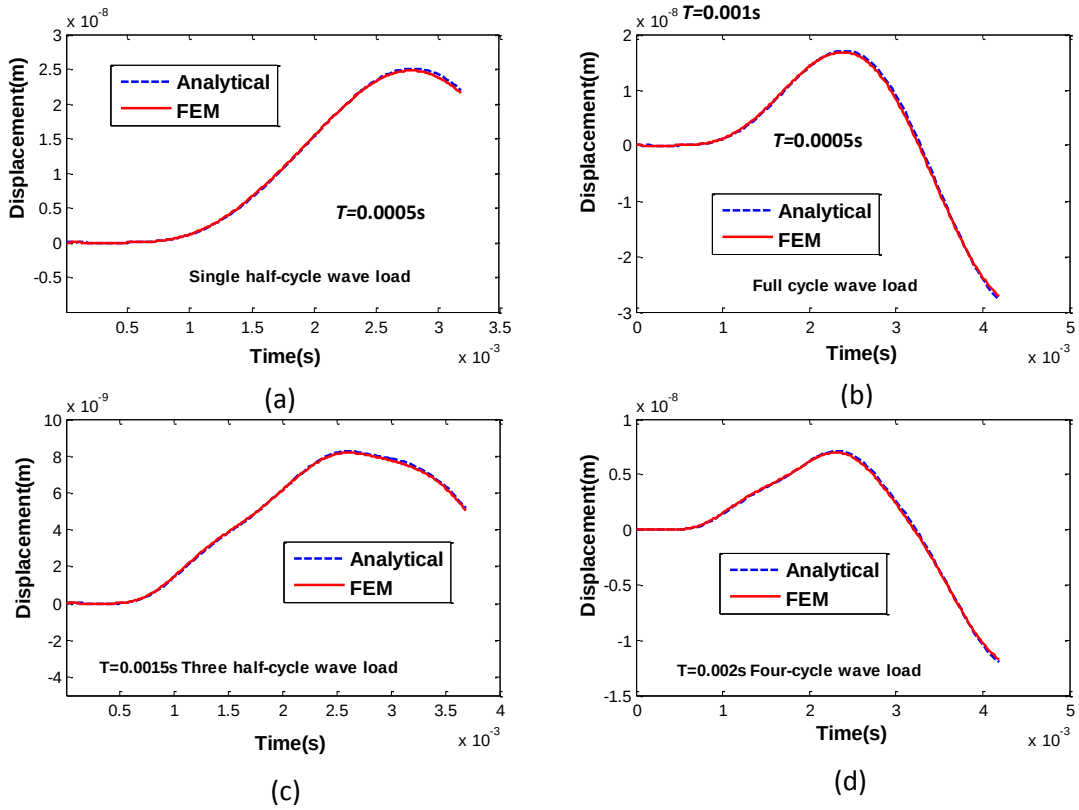

Figure 3. 10 Comparison of analytical and finite element solutions for mid-beam displacement with various wave loads

3.10(b) shows mid-beam displacement for a full-cycle sine wave load excitation. Again, the results are almost identical. Figures 3.10(c) and 3.10(d) show mid-beam displacement for a three half-cycle sine wave load and a four half-cycle wave load, respectively. Although it is clear that the displacement matches well for both solution techniques, it is also beneficial to compare the velocities for these same cases.

Velocities for the beam at mid-position under various types of wave loads are shown in Fig.3.11. The mid-beam velocity under the same loading conditions as those used for Fig.3.11 are presented in the same order presented in Fig.3.10. It can be seen that all the solutions from

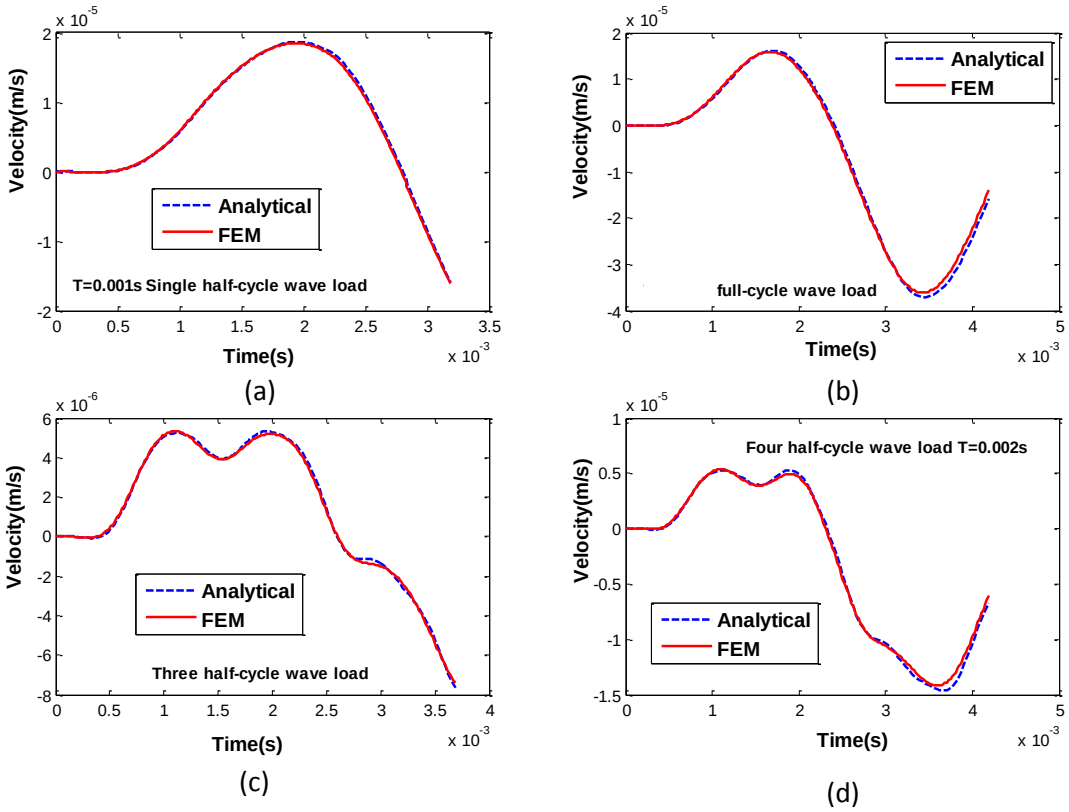

Figure 3. 11 Comparison of analytical and finite element solution for transient wave load mid-beam velocity with various wave loads

analytical method agree very well with the velocities found using the FEM solution approach. Based on these results, there is a strong confidence that the analytical method used for the initial configuration study is accurate. Furthermore, the FE method seems suitable for use in future research where more complex configurations and alternative support conditions might be considered.

From the figure showing the velocities response on the beam, it can be observed that the velocity curves under full wave loads seem to be like a sine curve when compared with other figures. Besides, velocities under full cycle wave loads are lower than those under a half-cycle wave load. The reason for this difference is that for a full cycle wave load, the pressure loads positive and negative values changing with time reduce forced response values on the beam. Furthermore, by comparison, velocity values under single half-cycle wave load are larger than in the other three plots. It should be pointed out that all solutions from the analytical method show high coincidence with FEM results for the beam response. Although there are slight deviations between the two solutions obtained, the analytical results are considered acceptable for the purpose to prove that the analytical method provides an accurate prediction of the beam response. Figure 3.12 shows the beam forced response acceleration under a single half cycle sine wave load, which will be used for force inverse together with velocity and displacement as the inputs.

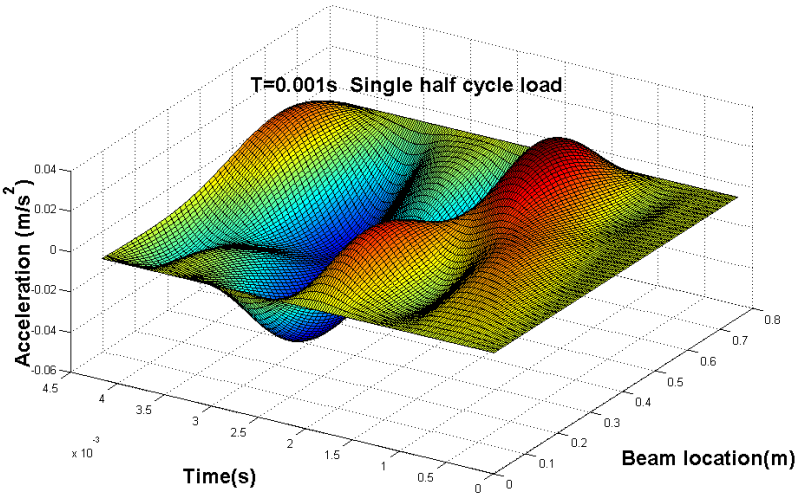

Figure 3. 12 Beam forced response acceleration under single half cycle sine wave load

3.7 Force inverse results

By referring to Eq.(3.4), since displacement amplitude $V_j(t)$, velocity amplitude $V_j'(t)$ and acceleration amplitude $V_j''(t)$ at each j $(j = 1,2,3 \dots .)$ are known from analytical results, these can now be used as inputs to the force reconstruction method in order to find the value $F(x,t)$ by using numerical terms in the right,

$$V_j(t)\omega^2(j) + V_j''(t) + 2\omega_b V_j'(t) = \frac{1}{\mu}\sum_{i=1}^{\infty} F(i,t) sin(j\pi i)\,\Delta x \;(j = 1,2,3 \dots . \infty). \quad (3.22)$$

Note that this approach is analogous to the experimental method that would be utilized for a real sensor. Here, that approach is being mimicked using simulated responses, as opposed to measured values. The approach of an analytical evaluation greatly simplifies the design approach. More detailed procedures will be presented in Chapter 6.

3.8 Summary

This chapter outlined the development of analytical tools to be used in the initial configuration study for an acoustic sensor. In examining the response of the sensor to various forms of transient excitations, the goal is to develop a continuous sensor that can be used to determine the direction of an acoustic source. This study presented here considered a simply-supported beam-like configuration. The response to various transient sinusoidal pressure waves was determined for the Euler-Bernoulli beam through the extension of Fryba's work. Various configuration aspects, such as the wave load characteristics, simple supports, sensor thickness, aperture (beam length), and material were examined, although results for each of these was not presented for the sake of brevity. To gain additional insight, the wavenumber spectrum was also utilized to decompose the response into spatial information. Results indicated that a thinner beam made of a lighter material provides a response with a larger amplitude and greater spectral content. It is also shown that with a relatively thin structure, it is possible to determine the direction from which the wave is approaching without requiring a very long sensor. The analytical solution was also verified by comparing it to a time-based finite element solution. These results will be useful when more realistic two-dimensional structures are considered. The following chapter will consider a beam with intermediate supports which seems more appropriate for an acoustic sensor.

Chapter 4 Intermediate supported beam acoustic wave propagation

In this chapter, a new beam shape function configuration method for determining transient responses of the finite Euler-Bernoulli beam with two intermediate supports excited by moving pressure wave loads is developed. To clarify this method, this beam structure is excited by moving sinusoidal loads representing a moving pressure wave load. Relative transient responses are investigated and verified by results obtained from the traditional finite element method. This method can be used to solve transient response problems of any kind of moving pressure load exciting the beam structure with two intermediate supports. The motivation for considering this configuration is to speed the rate at which information is available from the structure. By moving the supports inward, the beam responds more quickly when the excitation enters the structure. As a result, a structure with intermediate supports may be a better candidate for use as an acoustic sensor.

4.1. Introduction

Wide application of beams with various boundary conditions can be found in many branches of engineering such as in bridge and railway design. Research work on these problems has been ongoing for many years. In order to achieve a deep understanding of the dynamic response of

these structures, it is necessary for us to first review previous publications in the literature. Specifically, Frýba [7] contributed his initial work by studying transient responses of simply-supported beams under a moving load or continuous random load with a constant velocity. H.P.Lee [55] established the intermediate supported beam model through setting point constraints to be linear springs of large stiffness. He applied the assumed mode method to approximate the beam structure displacement solutions and then used these solutions to decouple the beam partial differential equation established by the Euler beam theory. Finally, he obtained transverse vibration response of the beam subjected to a moving load. Zhu and Law [56] applied Hamilton's principle to study the vibration behavior of the Timoshenko beam with non-uniform cross-section subjected to moving loads. The beam structure had multi-span supports with the intermediate point constraints being simplified with very stiff linear springs. Hilal and Zibdeh[57] studied the transverse vibration of an Euler-Bernoulli beam under different classical boundary conditions excited by a constant force in various motions including acceleration, deceleration, and constant velocity movement. Yu Tang [58] used hyperbolic sine and cosine functions as base functions to model free-vibration normal modes of a uniform beam. Good accuracy of calculated normal modes was achieved up to at least the 100th mode.

To investigate the dynamic behavior of a multi-span non-uniform bridge excited by a moving vehicle, Law and Zhu’s efforts [59] were to model the bridge structure as a continuous Euler-Bernoulli beam with multi-span linear large stiffness spring supports. Chan and Ashebo [60] tried to identify moving forces on a continuous bridge through using the singular value

decomposition method, assuming the bridge as an Euler-Bernoulli beam. In that model, exact mode shape functions of the vibrating beam were obtained from the boundary conditions. Stăn cioiu et.al.[61] theoretically and experimentally investigated the dynamic characteristics of a four-span continuous beam under a moving mass. Good agreement between the theoretical and experimental results was obtained. Francesco Ricciardelli and Carmelo Briatico [62] studied the case of a supported beam excited by a sinusoidal harmonic load moving at a constant speed. The approximated responses at and away from resonance were presented.

In this chapter, the configuration of shape functions for a beam with two intermediate points is examined by adding a polynomial function to the mode functions of the assumed constrained-free beam. The transverse vibration response of this intermediate- supported beam subjected to moving sinusoidal loads, used to represent a moving pressure wave load, is obtained by using the Lagrangian formulation to establish the structural dynamic equations first and then it is solved with the help of the Newmark integration scheme. Results from the new method are compared to those obtained using the transient finite element solution for a beam with intermediate supports.

4.2. Theoretical model

Consider a finite-length Euler-Bernoulli beam with two intermediate supports under a moving transient sinusoidal wave load as a moving pressure wave load. Illustrated in Fig.4.1, $F(x,t)$ represents two half-cycle sinusoidal wave loads and T is the single half-cycle period. $w(x,t)$ is the displacement from this beam structure and parameters a and b are distances

from the two supports to both ends of the beam structure of L length, respectively. The pressure load is moving across the beam at constant speed c.

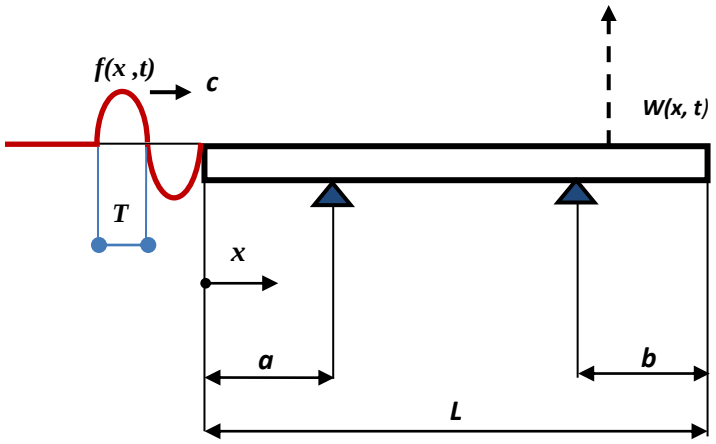

Figure 4.1 Beam with intermediate supports under moving load

For the beam with two free ends and two intermediate constraints, its boundary conditions are

$$\frac{\partial^2 W(0,t)}{\partial x^2} = \frac{\partial^2 W(L,t)}{\partial x^2} = 0, \tag{4.1a}$$

$$\frac{\partial^3 W(0,t)}{\partial x^3} = \frac{\partial^3 W(L,t)}{\partial x^3} = 0, \tag{4.1b}$$

and

$$w(a,t) = w(L-b,t) = 0. \tag{4.1c}$$

To solve the dynamic response of a beam with intermediate constraints under moving wave loads, the shape functions of this beam structure are configured based on mode functions of the clamp-free beam structure. However the clamped-free beam's boundary conditions are quite different from a beam with intermediate supported conditions shown above. To that end, the boundary constraints at the Euler-Bernoulli beam's clamped end need to be released. Furthermore, two constraint points need to be added to the initial clamped-free beam to simulate

a beam with intermediate support conditions. To do this, a linear polynomial function is added to the basis shape functions obtained from an initial beam with clamped-free boundary conditions so that new intermediate supported beam shape functions can be realized. For a clamped–free beam structure, its shape function [49] is

$$\emptyset_n(x) = cosh\beta_n x - cos\beta_n x - \frac{sinh\beta_n L - sin\beta_n L}{cosh\beta_n L + cos\beta_n L}(sinh\beta_n x - sin\beta_n x)$$

$$(n = 1,2 \dots). \quad (4.2)$$

Based on the mode shape functions shown in Eq.(4.2), by adding a linear polynomial function, the new shape function for beam with two intermediate constraints is

$$u(x) \approx \sum_{n=1}^{N+2} A_n \emptyset_n(x) + B_1 x + B_0, \quad (4.3)$$

where $A_n, B_1$and B_0 are initial unknown constants, and $N + 2$ is the total number of truncated terms. Suppose that the dynamic deflection of the intermediate-supported beam structure in free vibration state can be expressed as

$$W(x,t) = u(x)q(t), \quad (4.4)$$

where $q_n(t)$ is the generalized coordinate. Based on Eq.(4.1c) and Eq.(4.4), the constraint equations are

$$u(a) = \sum_{n=1}^{N+2} A_n \emptyset_n(a) + B_1 a + B_0 = 0, \quad (4.5a)$$

and

$$u(L-b) = \sum_{n=1}^{N+2} A_n \emptyset_n(L-b) + B_1(L-b) + B_0 = 0. \quad (4.5b)$$

By rearranging Eq.(4.5a) and Eq.(4.5b), constants $B_1$and B_0 can be represented as

$$B_1 = \frac{-1}{L-b-a}\left(\sum_{n=1}^{N+2} A_n \emptyset_n(L-b) - \sum_{n=1}^{N+2} A_n \emptyset_n(a)\right), \quad (4.6a)$$

and

$$B_0 = -\sum_{n=1}^{N+2} A_n \emptyset_n(a) + \frac{a}{L-b-a}\left(\sum_{n=1}^{N+2} A_n \emptyset_n(L-b) - \sum_{n=1}^{N+2} A_n \emptyset_n(a)\right). \quad (4.6b)$$

By substituting Eq.(4.6a) and Eq.(4.6b) into Eq.(4.3), we get

$$u(x) = \sum_{n=1}^{N+2} A_n \left\{\emptyset_n(x) + \frac{-x}{L-b-a}\left(\emptyset_n(L-b) - \emptyset_n(a)\right) + \frac{a}{L-b-a}\left(\emptyset_n(L-b) - \emptyset_n(a)\right)\right\}. \quad (4.7)$$

The boundary conditions at both ends are free for the beam structure with intermediate supports as indicated in Eq.(4.1a~b). From these conditions, we obtain

$$\begin{cases} \sum_{n=1}^{N+2} A_n \emptyset_n''(0) = 0 \\ \sum_{n=1}^{N+2} A_n \emptyset_n''(L) = 0 \end{cases}, \quad (4.8a)$$

and

$$\begin{cases} \sum_{n=1}^{N+2} A_n \emptyset_n'''(0) = 0 \\ \sum_{n=1}^{N+2} A_n \emptyset_n'''(L) = 0 \end{cases}. \quad (4.8b)$$

Due to the fact that $\emptyset_n(x)$ satisfies with the clamped–free conditions, it is not necessary to consider the free end at $x = L$ again. Besides, it is suitable to choose $N + 2$, provided that convergence in the dynamic response calculation is ensured. From Eqs.(4.8a~b) above, constants A_1 and A_2 can be represented by other constants, based on the consideration that $\emptyset_1$ and $\emptyset_2$'s second and third derivatives are not zeros, such that

$$\begin{cases} A_1 = \frac{A_3(\emptyset_3'''\emptyset_2'' - \emptyset_3''\emptyset_2''') + \cdots + A_{N+2}(\emptyset_2''\emptyset_{N+2}''' - \emptyset_2'''\emptyset_{N+2}'')}{\emptyset_2'''\emptyset_1'' - \emptyset_2''\emptyset_1'''} \\ A_2 = \frac{A_3(\emptyset_1''\emptyset_3''' - \emptyset_3''\emptyset_1''') + \cdots + A_{N+2}(\emptyset_1''\emptyset_{N+2}''' - \emptyset_1'''\emptyset_{N+2}'')}{\emptyset_2'''\emptyset_1'' - \emptyset_2''\emptyset_1'''} \end{cases}. \quad (4.8c)$$

By substituting Eq.(4.8c) into Eq.(4.3), we get

$$u(x) \approx \sum_{n=3}^{N+2} A_n \Phi_n(x), \quad (4.9)$$

where

$$\Phi_n(x) = \emptyset_n(x) + \frac{-x}{L-b-a}\left(\emptyset_n(L-b) - \emptyset_n(a)\right) + \frac{a}{L-b-a}\left(\emptyset_n(L-b) - \emptyset_n(a)\right)$$

$$+ \frac{\emptyset_2''\emptyset_n''' - \emptyset_2'''\emptyset_n''}{\emptyset_2'''\emptyset_1'' - \emptyset_2''\emptyset_1'''}\left(\emptyset_n(x) + \frac{-x}{L-b-a}\left(\emptyset_n(L-b) - \emptyset_n(a)\right)\right.$$

$$\left. + \frac{a}{L-b-a}\left(\emptyset_n(L-b) - \emptyset_n(a)\right)\right)$$

$$+ \frac{\emptyset_1''\emptyset_n''' - \emptyset_1'''\emptyset_n''}{\emptyset_2'''\emptyset_1'' - \emptyset_2''\emptyset_1'''}\left(\emptyset_n(x) + \frac{-x}{L-b-a}\left(\emptyset_n(L-b) - \emptyset_n(a)\right)\right.$$

$$\left. + \frac{a}{L-b-a}\left(\emptyset_n(L-b) - \emptyset_n(a)\right)\right).$$

For the beam with two intermediate supports, strain energy U and kinetic energy T of an Euler beam are obtained as

$$U = \frac{1}{2}\int_0^l EIW_{xx}^2 dx, \tag{4.10a}$$

and

$$T = \frac{1}{2}\int_0^l \mu W_t^2 dx, \tag{4.10b}$$

where subscripts x and t denote differentiation with respect to location and time, respectively. In order to find natural frequencies ω and mode shapes, a periodic transverse motion function is assumed

$$W(x,t) = u(x)sin\omega t. \tag{4.11}$$

By substituting Eq.(4.11) into Eq. (4.10b), one can obtain an expression for kinetic energy as

$$T = \frac{1}{2}\int_0^L \omega^2\, \mu u^2(x)cos^2(\omega t)dx = \frac{1}{2}\int_0^L \rho A\omega^2 u^2(x)\frac{1+cos(2\omega t)}{2}dx. \tag{4.12a}$$

Therefore, the maximum kinetic energy is

$$T_{max} = \frac{\rho A\omega^2}{2}\int_0^L (\sum_{n=3}^{N+2} A_n\Phi_n(x))^2\, dx\,. \tag{4.12b}$$

Similarly, the potential energy is

$$U = \frac{EI}{2}\int_0^L (\sum_{n=3}^{N+2} A_n \Phi_n^{"}(x) sin\omega t)^2 dx\,, \tag{4.12c}$$

and the maximum potential energy is

$$U_{max} = \frac{EI}{2}\int_0^L (\sum_{n=3}^{N+2} A_n \Phi_n^{"}(x))^2 dx\,. \tag{4.12d}$$

Finally

$$\Theta = (U_{max} - T_{max})\,. \tag{4.13}$$

According to Eq.(4.12b), Eq.(4.12d) and Eq.(4.13), Θ can be represented by $A_n: n = 3,4 \ldots N+2$. Applying stationary conditions of Θ with regard to A_n (let partial derivatives to be zero), then an explicit relation for $\mathrm{A_n}$ will be expressed as

$$\frac{\partial \Theta}{\partial A_n} = \frac{EI}{2}\int_0^L 2\left(\sum_{n=3}^{N+2} A_n \Phi_n^{"}(x)\right)\Phi_n^{"}(x)dx - \frac{\rho A\omega^2}{2}\int_0^L 2(\sum_{n=3}^{N+2} A_n \Phi_n(x))\,\Phi_n(x)dx = 0. \tag{4.14a}$$

By appropriately grouping terms and using matrix relation

$$EI\begin{bmatrix} \int_0^L \Phi_3''\Phi_3''dx - \rho A\omega^2\int_0^L \Phi_3\Phi_3 dx & \cdots & \int_0^L \Phi_{N+2}''\Phi_3''dx - \rho A\omega^2\int_0^L \Phi_{N+2}\Phi_3 dx \\ \vdots & \ddots & \vdots \\ \int_0^L \Phi_3''\Phi_{N+2}''dx - \rho A\omega^2\int_0^L \Phi_3\Phi_{N+2}dx & \cdots & \int_0^L \Phi_{N+2}''\Phi_{N+2}''dx - \rho A\omega^2\int_0^L \Phi_{N+2}\Phi_{N+2}dx \end{bmatrix} \times \begin{bmatrix} A_3 \\ \ldots \\ A_{N+2} \end{bmatrix} = 0. \tag{4.14b}$$

This equation can be summarized as

$$(K_\alpha - \omega^2 M_\alpha)\psi = 0. \tag{4.15}$$

The structure's with natural frequency of ω can be therefore obtained, using

$$K_\alpha = EI\begin{pmatrix} \int_0^L \ddot{\Phi}_3(x)\,\ddot{\Phi}_3(x)dx & \cdots & \int_0^L \ddot{\Phi}_3(x)\,\ddot{\Phi}_{N+2}(x)dx \\ \vdots & \ddots & \vdots \\ \int_0^L \ddot{\Phi}_{N+2}(x)\,\ddot{\Phi}_3(x)dx & \cdots & \int_0^L \ddot{\Phi}_{N+2}(x)\,\ddot{\Phi}_{N+2}(x)dx \end{pmatrix},$$

$$M_\alpha = \rho A \begin{pmatrix} \int_0^L \Phi_3(x)\,\Phi_3(x)dx & \cdots & \int_0^L \Phi_3(x)\,\Phi_{N+2}(x)dx \\ \vdots & \ddots & \vdots \\ \int_0^L \Phi_{N+2}(x)\,\Phi_3(x)dx & \cdots & \int_0^L \Phi_{N+2}(x)\,\Phi_{N+2}(x)dx \end{pmatrix}, \qquad (4.16)$$

and

$$\Psi = \begin{bmatrix} A_3 \\ A_4 \\ .. \\ A_{N+1} \\ A_{N+2} \end{bmatrix}.$$

In the following section, the dynamic equation of a beam with intermediate supports will be established with the help of the Lagrangian formulation, based on the assumed beam shape functions developed above.

4.3. Forced response of the beam structure with intermediate supports

The assumed basis function approach employed in this section is to determine the forced response of the beam with intermediate supports. So the dynamic deflection of the beam structure can be expressed as

$$W(x,t) \approx \sum_{n=3}^{N+2} u_n(x) q_n(t), \qquad (4.17)$$

where N is the total number of truncated terms, $q_n(t)$ is the generalized coordinate, and $u_n(x)$ represents shape functions of the beam. Note that $u_n(x) = A_n \Phi_n(x)$ is obtained in Eq.(4.9). The kinetic energy T_E, the bending potential energy V_E are obtained respectively, as

$$T_E = \frac{1}{2}\int_0^L \mu \left(\frac{\partial W(x,t)}{\partial t}\right)^2 dx = \frac{1}{2}\sum_{i=3}^{N+2}\sum_{j=3}^{N+2}\int_0^L A_i A_j \mu \dot{q}_i(t)\Phi_i(x)\,\Phi_j(x)\dot{q}_j(t)dx$$

$$= \frac{1}{2}\sum_{i=3}^{N+2}\sum_{j=3}^{N+2} m_{i,j}\dot{q}_i(t)\dot{q}_j(t), \qquad (4.18)$$

where $m_{i,j} = \int_0^L A_i A_j \mu \Phi_i(x)\Phi_j(x)dx$,and

$$V_E = \frac{1}{2}\int_0^L EI\left(\frac{\partial^2 W(x,t)}{\partial^2 x}\right)^2 dx = \frac{1}{2}\sum_{i=3}^{N+2}\sum_{j=3}^{N+2}\int_0^L A_i A_j EI\Phi_j^{"}(x)\Phi_j^{"}(x)q_i(t)q_j(t)dx$$

$$= \frac{1}{2}\sum_{i=3}^{N+2}\sum_{j=3}^{N+2} k_{i,j}q_i(t)q_j(t), \qquad (4.19)$$

where $k_{i,j} = \int_0^L EIA_iA_j\Phi_j^{"}(x)\Phi_j^{"}(x)dx$.

The external force work W_E is

$$W_E = \sum_{i=3}^{N+2} q_i(t)\int_0^L f(x,t)\Phi_i(x)dx. \qquad (4.20)$$

The beam Lagrangian function L_E is $T_E - V_E + W_E$, where $V_E - W_E$ is the total potential energy. It should be pointed out that in order to clarify our new analytical method, damping is ignored in this work for equation simplification. Therefore the Euler-Lagrange equation is expressed

$$\frac{d}{dt}\left(\frac{\partial L_E}{\partial \dot{q}_i}\right) - \frac{\partial L_E}{\partial q_i} = 0. \qquad (4.21)$$

Substituting Eq. (4.18~4.20) into Eq. (4.21)

$$\sum_{j=3}^{N+2} m_{ij}\ddot{q}_j(t) + \sum_{j=3}^{N+2} k_{ij}q_j(t) = Q_i(i = 3, \dots N+2), \qquad (4.22)$$

where $Q_i = \int_0^L f(x,t)\Phi_i(x)dx$.

Using matrix form for Eq. (4.22),

$$\begin{pmatrix} m_{3,3} & \cdots & m_{3,N+2} \\ \vdots & \ddots & \vdots \\ m_{N+2,3} & \cdots & m_{N+2,N+2} \end{pmatrix}\begin{bmatrix} \ddot{q}_3 \\ \dots \\ \ddot{q}_{N+2} \end{bmatrix} + \begin{pmatrix} k_{3,3} & \cdots & k_{3,N+2} \\ \vdots & \ddots & \vdots \\ k_{N+2,3} & \cdots & k_{N+2,N+2} \end{pmatrix}\begin{bmatrix} q_3 \\ \dots \\ q_{N+2} \end{bmatrix}$$

$$= \begin{bmatrix} Q_3 \\ \dots \\ Q_{N+2} \end{bmatrix}. \qquad (4.23)$$

Equation (4.23) can be summarized as,

$$[M][\ddot{q}] + [K][q] = [Q], \qquad (4.24)$$

where, $[M] = \begin{pmatrix} m_{3,3} & \cdots & m_{3,N+2} \\ \vdots & \ddots & \vdots \\ m_{N+2,3} & \cdots & m_{N+2,N+2} \end{pmatrix}, [\ddot{q}] = \begin{bmatrix} \ddot{q}_3 \\ \dots \\ \ddot{q}_{N+2} \end{bmatrix}, [K] = \begin{pmatrix} k_{3,3} & \cdots & k_{3,N+2} \\ \vdots & \ddots & \vdots \\ k_{N+2,3} & \cdots & k_{N+2,N+2} \end{pmatrix},$

$$[q] = \begin{bmatrix} q_3 \\ \dots \\ q_{N+2} \end{bmatrix}, [Q] = \begin{bmatrix} Q_3 \\ \dots \\ Q_{N+2} \end{bmatrix}.$$

Transient responses can be calculated numerically in the time domain by using Newmark's integration scheme [52], used with the integration parameters $\alpha = 0.25$ and $\beta = 0.5$ which lead to the constant-average acceleration approximation. Here parameters α and β are used to control the stability and accuracy of the Newmark method. By using this approach in Eq.(4.24), the beam response displacement and velocity at each position for any time can be obtained.

4.4. Numerical example

In this study, a finite set of traveling sinusoidal half-cycles as the force load to represent a transient moving pressure wave load is considered. To explain this continuous wave load $f(x,t)$ traveling over the beam structure, three different time stages are described [51]. When this distributed force load begins to progressively step on the beam until it is entirely on the beam, it is expressed by

$$f(x,t) = -sin\left\{\frac{2\pi}{cT}(x-ct)\right\}\{1-H(x-ct)\}, (0 \le t \le NT), \quad (4.25a)$$

where N is the number of half-cycles, T is single half-cycle time period as shown in Fig.4.1, and H is the Heaviside step function. The speed of the wave is denoted by c. Once the load is completely on the beam, the force is expressed as

$$f(x,t) = sin\left\{\frac{2\pi}{cT}(x-ct)\right\}\{H(x-c(t-NT)) - H(x-ct)\}, \left(NT \le t \le \frac{L}{c}\right)$$

(4.25b)

until it reaches the other end of the beam. Finally, the load begins to leave the beam as

$$f(x,t) = sin\left\{\frac{2\pi}{cT}(x-ct)\right\}\{H(x-c(t-NT)) - H(x-L)\}. \left(\frac{L}{c} \le t \le \frac{L}{c} + NT\right) \qquad (4.25c)$$

Initial parameters of the beam structure used for numeric study to be described below are listed in Table 4.1.

Table 4.1 Parameter Definitions

Item	Value	Units	Description
L	0.75	m	Beam length
B	0.05	m	Beam width
H	0.05	m	Beam thickness
C	343	m/s	Wave speed
N	1		Number of half-cycles
T	0.002	sec	Half-cycle duration
ρ	7820	kg/m^3	Beam density
E	2.068e+11	N/ m^2	Beam Young's modulus
N	0.29		Beam Poisson's ratio
A	0.15	m	Left constraint
B	0.25	m	Right constraint

In this work, the aim is to exploit the general method for solving the transient response of an intermediate supported beam subjected to various types of moving pressure wave loads. To

simplify our problem, damping will be ignored. The analytical analysis and finite element method are both conducted by using Matlab®.

4.4.1 Natural frequencies comparison

Table 4.2 shows the comparison results of first ten natural frequencies for an intermediate supported beam between the finite element method (FEM) and the analytical method. Relative errors of natural frequencies are based on FEM results. It can be noticed that relative error is well less than one percent, and is therefore quite reasonable.

Table 4.2 Natural frequencies comparison (Hz)

No.	FEM results	Analytical results	Error(%)
1	370.2	370.0	-0.062
2	863.4	863.4	0.0055
3	1798.0	1797.2	-0.044
4	3402.1	3401.3	-0.0235
5	4981.3	4981.4	0.002
6	8626.1	8624.0	-0.0243
7	10219	10254	0.34
8	11686	11750	0.54
9	17187	17167	-0.116
10	21473	21321	-0.70

Comparisons of the first eight mode shapes found using each method are shown in Figure 4.2 and Figure 4.3. It can be seen that there is excellent agreement in the first four mode shapes. While there are some slight differences in the higher mode shapes of Fig.4.3,the

agreement is still good.

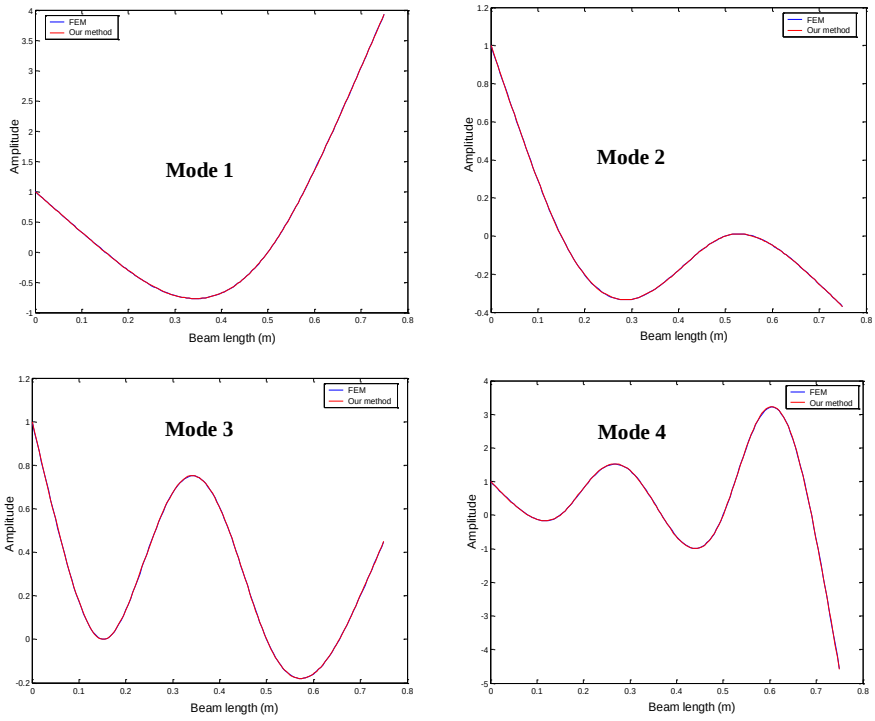

Figure 4.2 First four mode shapes for corresponding frequencies in Table 4.2.

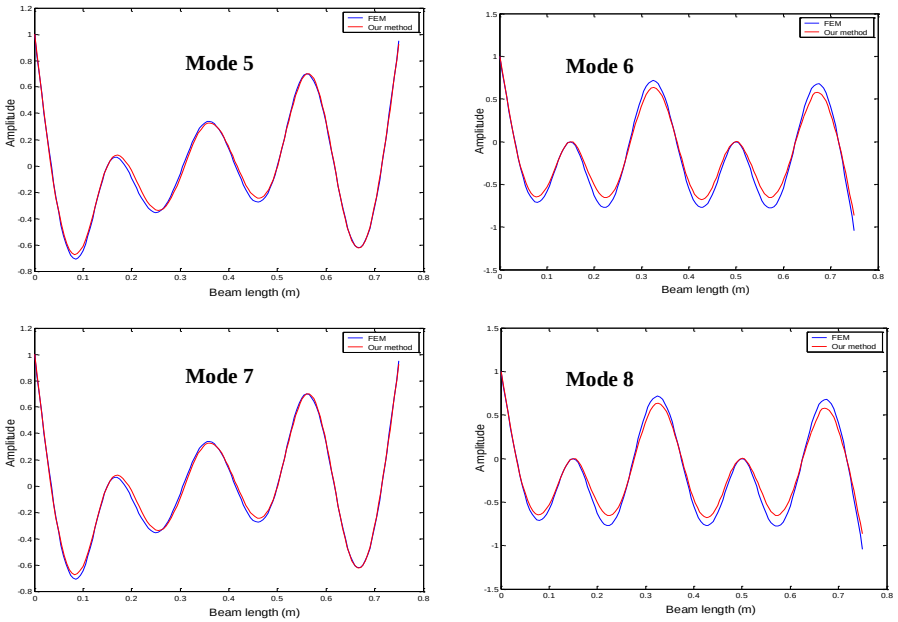

Figure 4.3 Higher mode shapes for corresponding frequencies in Table 4.2.

4.4.2 Transient response analytical solutions verification by FEM

In this section, transient responses are calculated numerically in the time domain by using the Newmark's integration scheme [52]. The beam response with intermediate supports is verified by the finite element solutions with the same parameters. In the case, the transient load moves along the beam with speed $c = 343m/s$. Displacements of the beam at mid-position are obtained by using analytical and finite element methods. As seen in Fig.4.4~4.6 for displacement, velocity, and acceleration respectively. These response solutions show high coincidence. Despite very slight deviations, both solution results representing the beam response are almost the same. Although not shown, transient responses from other beam locations show the same correlation as at the mid-location. So the analytical results are considered acceptable to represent beam transient responses under moving pressure wave load. This fact draws the conclusion that the new analytical method based on this intermediate support model can be used to simulate beam transient response with two intermediate supports under moving load excitation.

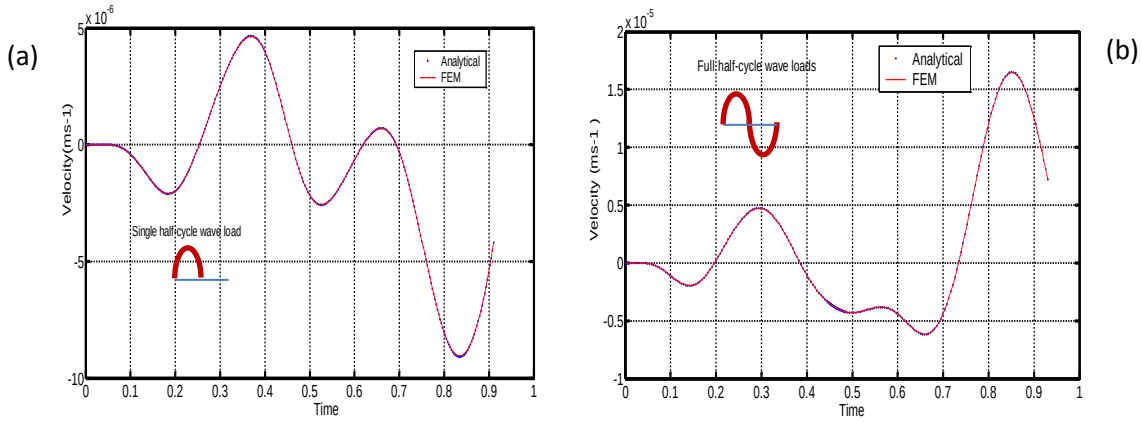

Figure 4.4 Mid-beam location forced displacement vs time under sine wave loads

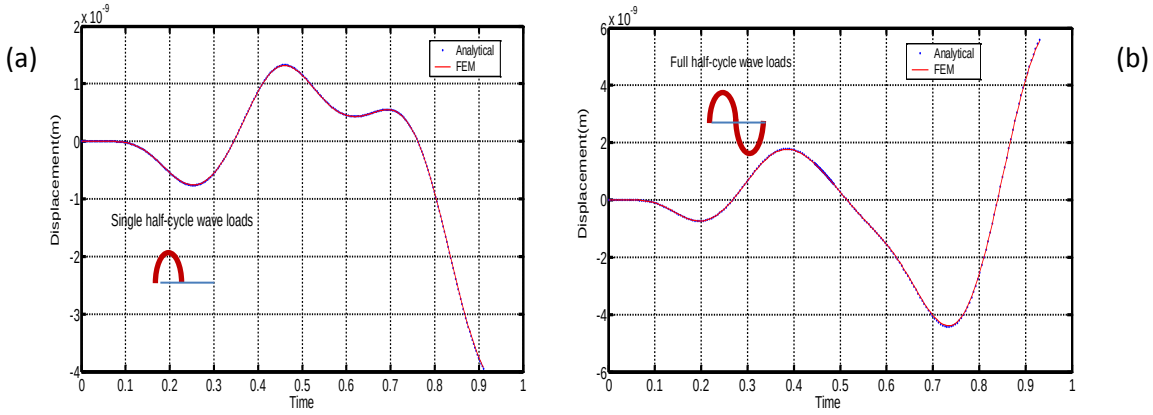

Figure 4.5 Mid-beam location forced velocity vs time under sine wave loads

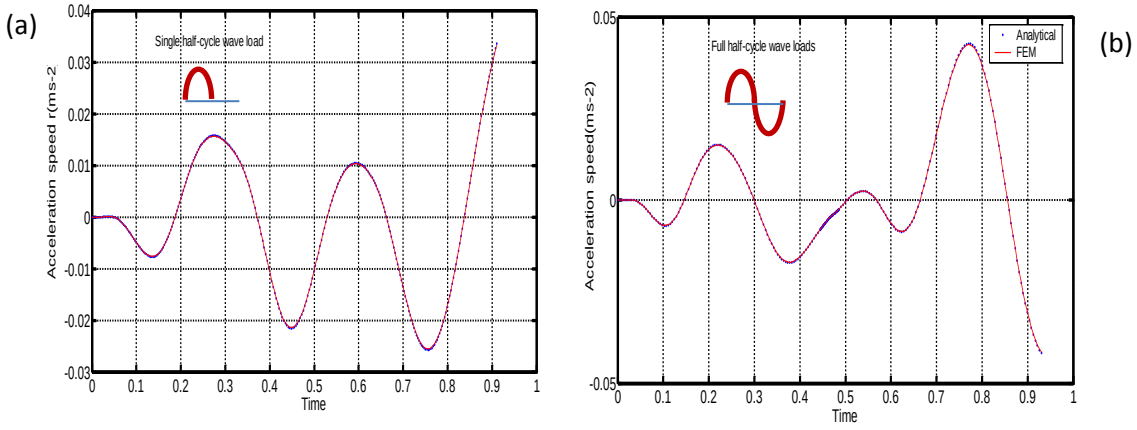

Figure 4.6 Mid-beam location forced acceleration vs time under sine wave loads

4.5. Summary

This chapter focused on the development of analytical tools to be used in the shape functions configuration study for transient responses of the beam with intermediate supports under moving pressure wave loads. The responses to transient sinusoidal pressure wave as a moving pressure wave load example are determined through shape function configuration method based on clamped-free beam mode functions and a polynomial function. Analytical

results obtained from the new method are well verified by the finite element method when the beam is subjected to the same loads. The analytical method presented in this work can be useful in application to solve the transient response of intermediate beam under any type of moving pressure wave loads. These response values will be useful as input parameters in force loads inverse process when considering intermediate beam as an acoustic sensor candidate. Although the intermediate supported beam has the potential to provide more dynamic information for use in the inverse process, there are still some potential issues. The main issue has to do with the lack of dynamic information of the support locations. As a result, a beam that has no constrained points seems a better candidate for an acoustic sensor, so such a configuration will be examined in the next chapter. Although the development of inverse methods for the intermediate supported beam will not be provided, the insight gained in considering this configuration was useful in the research progress. Furthermore, the configuration may be reconsidered in the future research.

Chapter 5 Transient responses of finite beam with elastic foundation supports under moving wave load excitation

Based on the analysis of the two configurations under a sinusoidal moving load excitation shown in previous chapters, the simple supported beam and the intermediate supported beam are less than ideal when used for force inverse to predict acoustic wave loads. This limitation is primarily due to the information that is removed at the locations of the constraint points. In order to remove the constraints, a continuous beam supported by an elastic foundation will be considered as an alternative candidate sensor structure. By using an elastic foundation, it is expected that the structural response, which will be examined through modeling, will be rich enough to provide more information about the impinging wave.

In this chapter, the responses of a beam supported on an elastic foundation when subjected to various moving loads are studied by the application of finite element method. We apply the Newmark integration method for numerical simulation. Results are verified by using commercial ANSYS package through modeling the beam with elastic foundation supports excited by moving point load at the constant speed. The effects of the following parameters on the dynamic behavior of the beam under both moving point load and pressure wave load are evaluated, the

traveling load speed, stiffness of the elastic foundation base, and viscous damping. This study offers a good basis for research work on the beam sensor for identifying moving acoustic wave loads in Chapter 6.

5.1 Introduction

Beam structures with elastic foundation supports have seen wide applications in mechanical and aerospace engineering. Historical research work in these fields can be seen in the literature of engineering mechanics. Most of these beam problems discussed issues about time and space varying loads. Actually moving loads have considerable effects on the dynamic behavior of the structures. In order to obtain a better understanding of dynamic responses from moving loads on beam structure, it is necessary for us to review previous works from the literature. Jaiswal and Iyengar [63] revealed the dynamics characteristics of the infinite beam on a finite elastic foundation base when it was subjected to a moving load. Effects of loads, beam structure parameters, and material properties on structure responses were evaluated. Thambiratnam and Zhuge [64] conducted the dynamic analysis of beams on an elastic foundation when subjected to moving point loads through simplifying the foundation with springs of variable stiffness. The authors also investigated effects of some parameters the response of the beam such as the speed of the moving load, the foundation stiffness and the length of the beam. Chen et al. [65] studied the response of an infinite Timoshenko beam on a viscoelastic foundation under a harmonic moving load. Kim, and Roesset [66] analyzed dynamic response of an infinitely long beam on the frequency-independent linear hysteretic damping

foundation base by using the constant amplitude or a harmonic moving load as an excitation force. In the model developed by Kim [67], the vibration and stability of an infinite Euler - Bernoulli beam on a Winkler foundation were investigated through applying a static axial force and a moving load with either constant or harmonic amplitude variations to excite the system. Some important results were obtained from the process of changing relative parameters. Roman Bogacz et.al.[68] studied dynamical problems caused by a distributed load which was acting on a beam on an elastic foundation at a moving velocity. The load was represented by the Heaviside function(or its linear superposition) and by a moving load harmonically distributed in space. Lei Shi et.al[69] established the mathematic model which was used to describe elastic foundation beam with cantilevered support excited by the moving load speed. The transient response under the moving load speed was obtained. Shahin and Mbakisya [70] studied the problem of a simply-supported beam on an elastic foundation to repeated moving concentrated loads by means of the Fourier sine transformation method in order to obtain the analytical forced responses.

The objective of this chapter is to develop a numerical procedure for evaluating the dynamic response of the elastic foundation beam when subjected to transient sinusoidal moving loads. Such a study has not been conducted before. The finite element method is used for modeling beam elements. The Newmark integration method is used to obtain the dynamic response. Effects of the following parameters on the dynamic behavior of the beam are evaluated: the traveling speed of the load; the stiffness of the elastic foundation base and viscous damping. This will make a good basis for developing a beam acoustic sensor with the help of a distributed

force reconstruction method, which is used to identify moving acoustic loads through their excitation process on the beam structure. The latter will be discussed in the next chapter.

5.2 Theoretical model

Consider a finite-length Bernoulli–Euler beam resting on an elastic foundation under moving sinusoidal loads as illustrated in Fig. 5.1.

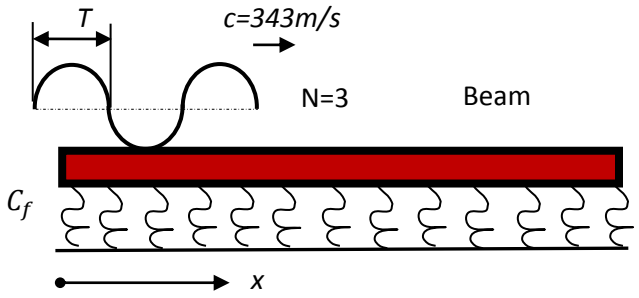

Figure 5.1 Elastic foundation beam subjected to moving wav**e** loads

The equation of motion is [49]

$$\mu \frac{\partial^2 W(x,t)}{\partial t^2} + 2\mu\omega_b \frac{\partial W(x,t)}{\partial t} + EI \frac{\partial W^4(x,t)}{\partial x^4} + C_f W(x,t) = f(x,t), \tag{5.1}$$

where the beam flexural rigidity is EI, the beam mass density is μ, the foundation elasticity constant is C_f, ω_b is the damping circular modal frequency, and $f(x,t)$ represents moving loads. Note that the mass and bending stiffness of the elastic foundation are being neglected. For an elastically supported free-free beam illustrated in Fig.5.1 above, its boundary conditions are

$$\frac{\partial^2 W(0,t)}{\partial x^2} = \frac{\partial^2 W(L,t)}{\partial x^2} = 0, \tag{5.2a}$$

and

$$\frac{\partial^3 W(0,t)}{\partial x^3} = \frac{\partial^3 W(L,t)}{\partial x^3} = 0. \tag{5.2b}$$

5.3. FE formulation for the beam under the moving point load

The Euler-Bernoulli beam theory is used for constituting the finite element matrices. The beam illustrated in Fig.5.1 is modeled with 15 equally sized elements. A straight beam element i with uniform cross section under a moving point load is shown in Fig.5.2

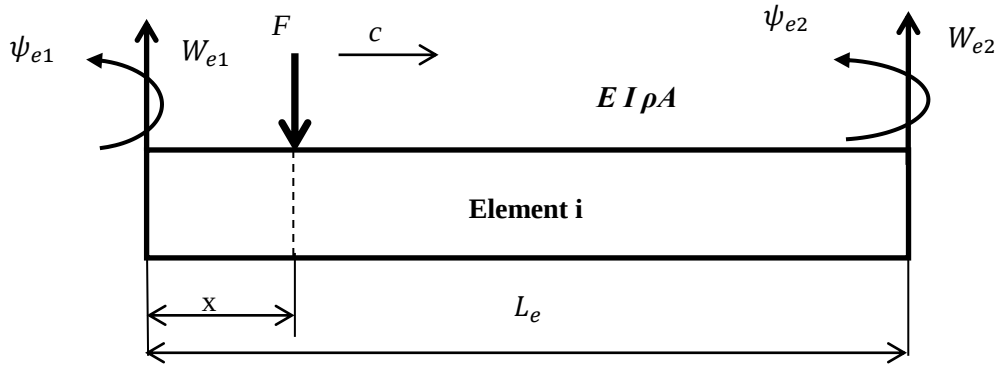

Figure 5.2 Moving load on a straight beam element

The shape functions of element i are represented [52] as

$$\begin{cases} N_{e1}(x) = 1 - 3\left(\frac{x}{L_e}\right)^2 + 2\left(\frac{x}{L_e}\right)^3 \\ N_{e2}(x) = x - 2L_e\left(\frac{x}{L_e}\right)^2 + L_e\left(\frac{x}{L_e}\right)^3 \\ Ne_3(x) = 3\left(\frac{x}{L_e}\right)^2 - 2\left(\frac{x}{L_e}\right)^3 \\ N_{e4}(x) = -L_e\left(\frac{x}{L_e}\right)^2 + L_e\left(\frac{x}{L_e}\right)^3 \end{cases}. \tag{5.3}$$

Mass matrix of this beam element is

$$M = \frac{\rho A L_e}{420}\begin{bmatrix} 156 & 22L_e & 54 & -13L_e \\ 22L_e & 4{L_e}^2 & 13L_e & -3{L_e}^2 \\ 54 & 13L_e & 156 & -22L_e \\ -13L_e & -3{L_e}^2 & -22L_e & 4{L_e}^2 \end{bmatrix}. \tag{5.4}$$

Stiffness matrix of the beam element is

$$K = \frac{EI}{{L_e}^3}\begin{bmatrix} 12 & 6L_e & -12 & 6L_e \\ 6L_e & 4{L_e}^2 & -6L_e & 2{L_e}^2 \\ -12 & -6L_e & 12 & -4L_e \\ 6L_e & 2{L_e}^2 & -6L_e & 4{L_e}^2 \end{bmatrix}. \tag{5.5}$$

Supposing that the beam structure is on the Winkler's foundation base, the Winkler's foundation stiffness matrix for the element [52] is

$$K_f = \begin{bmatrix} \frac{13bL_eC_f}{35} & \frac{11bL_e{}^2C_f}{210} & \frac{9bL_eC_f}{70} & \frac{-13bL_e{}^2C_f}{420} \\ \frac{11bL_e{}^2C_f}{210} & \frac{bL_e{}^3C_f}{105} & \frac{13bL_e{}^2C_f}{420} & \frac{-bL_e{}^3C_f}{140} \\ \frac{9bL_eC_f}{70} & \frac{13bL_e{}^2C_f}{420} & \frac{13bL_eC_f}{35} & \frac{-11bL_e{}^2C_f}{210} \\ \frac{-13bL_e{}^2C_f}{420} & \frac{-bL_e{}^3C_f}{140} & \frac{-11bL_e{}^2C_f}{210} & \frac{bL_e{}^3C_f}{105} \end{bmatrix}. \tag{5.6}$$

The expression of the beam element deflection is

$$W_e(x) = N_{e1}(x)W_{e1} + N_{e2}(x)\psi_{e1} + N_{e3}(x)W_{e2} + N_{e4}(x)\psi_{e2}, \tag{5.7}$$

where $N_{ei}(x)$, *(i=1,2,3,4)* are the interpolation functions shown in Eq. (5.3). After decouping Eq.(5.1) by using Eq.(5.7), the equation of motion for a multiple degree of freedom damped structural system is represented

$$[M]\{\ddot{y}\} + [C][\dot{y}] + \left[K + K_f\right]\{y\} = \{F(t)\}, \tag{5.8}$$

where $\ddot{y}$,$\dot{y}$ and y are the respective acceleration, velocity and displacement vectors for the whole structure and $\{F(t)\}$ is the external force vector, which is depended on the moving point load. For the case that the moving load is the pressure wave load rather than point load, the

problem will be more complicated, but the solution procedure is similar.

5.4. Results and Discussion

5.4.1 Moving point load at a constant speed

Table 5.1 provides a list of the initial modeling parameters, including the geometry and material properties for both the beam and elastic foundation. Here, E is the Young's modulus of beam material and E_F is the Young's modulus of foundation material. The foundation elasticity constant can be obtained from $C_f = E_F \frac{B}{TH}$, where B is width of the beam and TH is the thickness of the foundation base.

Table 5.1 Parameter Definition

Item	Description	Units	Value
L	Beam length	m	0.5
B	Beam width	m	0.03
h	Beam thickness	m	0.001
c	Moving load speed	ms^{-1}	343
ρ	Beam density	kgm^{-3}	2700
E	Beam young's modulus	Nm^{-2}	70GPa
ν	Poisson's ratio	-	0.33
TH	Foundation thickness	m	1
E_F	Foundation Young's modulus	Nm^{-2}	33.1MPa

The transverse point load F travels with a constant velocity c. In the forced vibration analysis, the constant-average acceleration approximation is needed for the implicit Newmark

integration method [52] through setting the integration parameters$\alpha = 1/4$ andβ =1/2. Here the time step Δt is $\Delta t = \frac{T_{20}}{20}$ during the transient response analysis, and T_{20} is the period of the 20th natural mode of the structure to ensure that all top 20 modes contribute to the dynamic response. Response of the beam with elastic foundation under the moving point load is obtained using Matlab software package and ANSYS simulation results. As shown in Fig.5.3 and Fig.5.4, Matlab results show high agreement with ANSYS results.

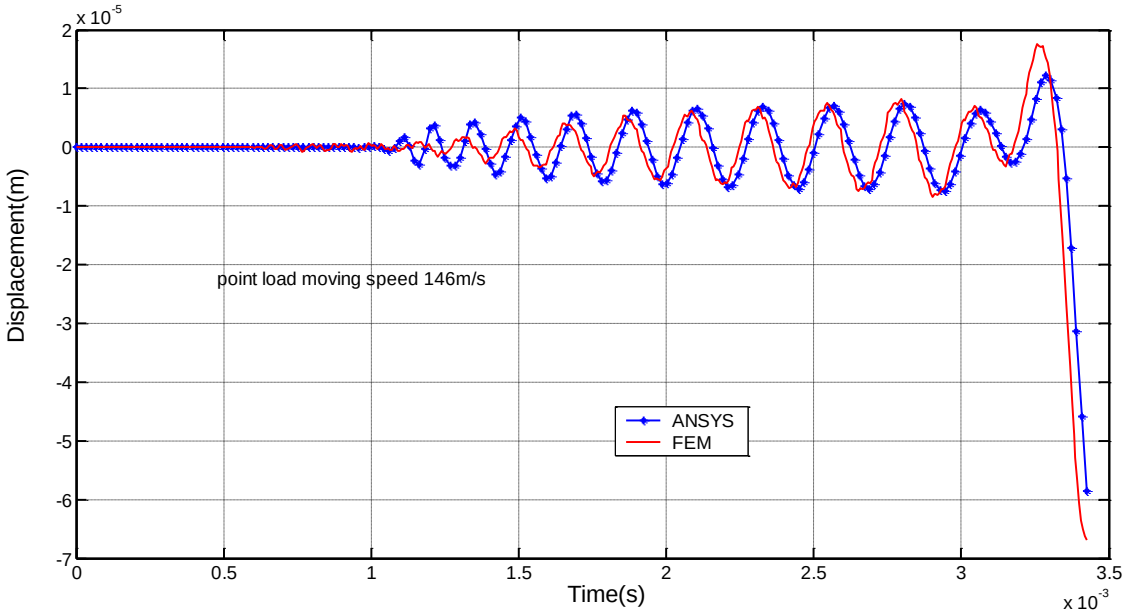

Figure 5.3 Response of beam end point when the moving load is leaving at 146m/s

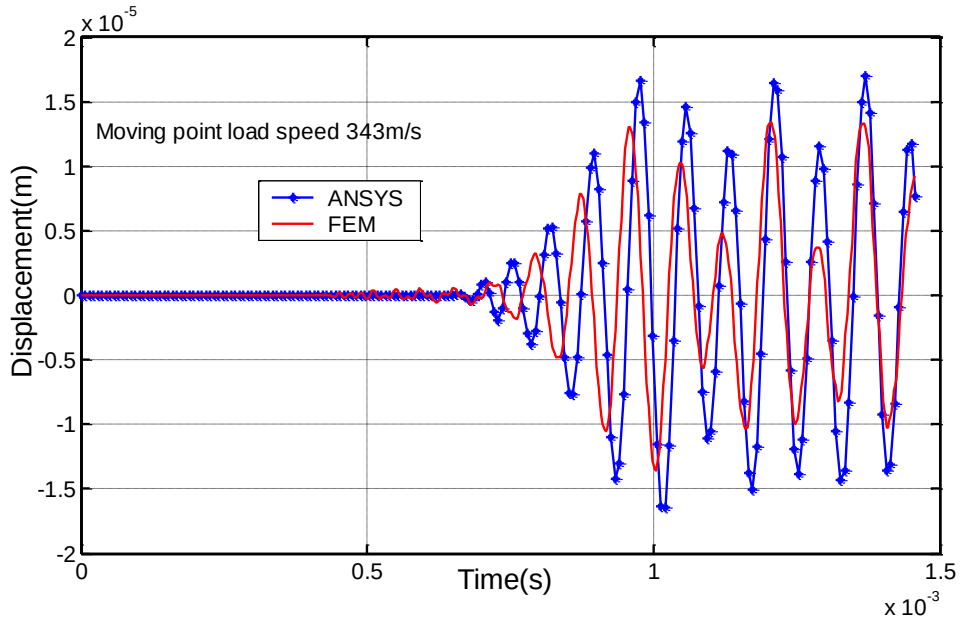

Figure 5.4 Response of beam end point when the moving load is leaving at 343m/s

For the beam with finite length under the static load, its displacement at the middle location can be calculated as [72]

$$W_0 = \frac{\beta F}{2K_f}\frac{2+cosh\beta L+cos\beta L}{sinh(\beta L)+sin(\beta L)}, \tag{5.9}$$

where $\beta = \left(\frac{K_f}{4EI}\right)^{0.25}$. The beam structure is under the point load of 10N, so the static displacement at mid-location is $W_0 = 2.5051 \times 10^{-05}$m under the point load moving at the speed of 343*m/s*. Figure 5.5 shows the effect of the Rayleigh damping on mid-point displacement of beam structure vs time. Displacements are decreased with increasing damping ratio. It should be noted that D_d represents transient response at mid-point divided by the static displacement W_0mid-location. In this figure, we can find that with the decrease of foundation stiffness value, the maximum transient displacement is increased.

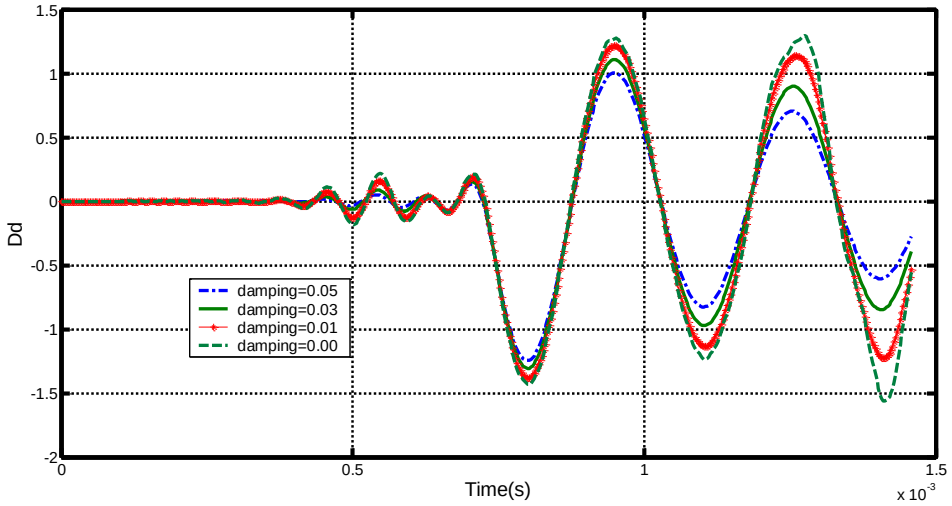

Figure 5.5 Rayleigh damping effect on transient displacement at the beam mid-location

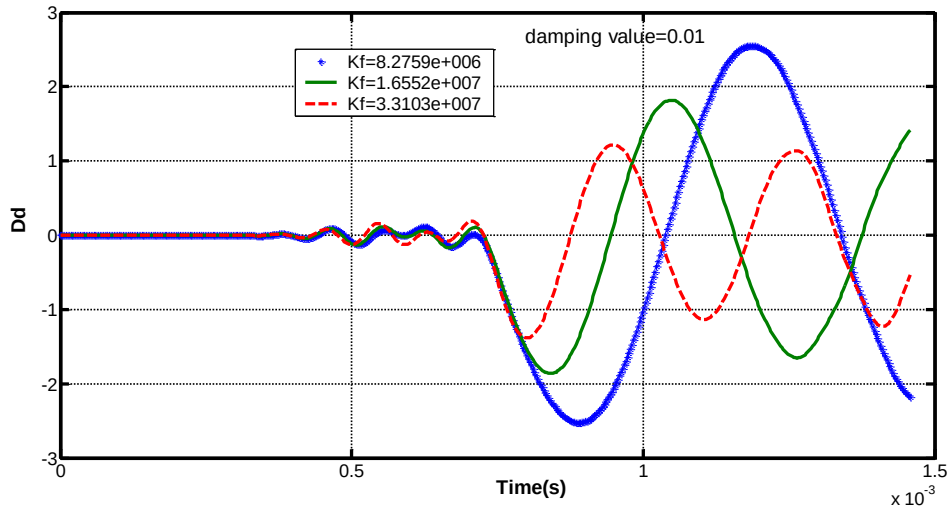

Figure 5.6 shows foundation base stiffness effect on transient displacement at the beam

Figure 5.6 Foundation base stiffness effect on transient displacement at the beam mid-location. Figure 5.7 shows the deflection of the beam mid-location under a moving load for different load speeds. With the increase of moving load speeds, the maximum deflection at the middle location has increased.

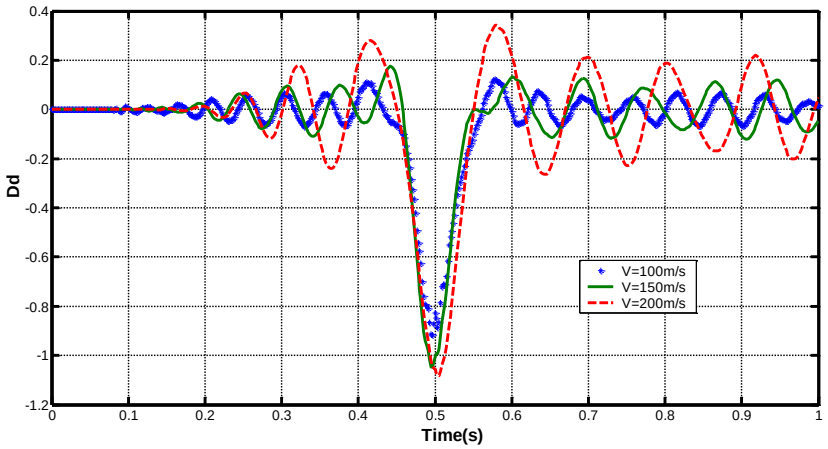

Figure 5.7 Deflection of the beam mid-location under a moving load for different load speeds

5.4.2 Moving sinusoidal load at a constant speed

In this study, a finite set of traveling sinusoidal half-cycles will be considered as the loading on the structure. Continuous wave loads $f(x,t)$ traveling over the beam sensor structure were previously described in Chapter 4 for details. By discretizing the elastically supported beam structure with the finite element method, transient responses can be calculated numerically in the time domain by using Newmark's integration scheme [52]. Specifically the elastically supported beam is discretized into 15 beam elements with 16 nodal points. Of course, the response at any point can be interpolated by using the shape functions and the weight factors. Although not specifically shown, 15 beam elements have been determined to be sufficient for convergence of the FEM transient response calculations. When increasing the number of elements from 15 to 30, no appreciable increase in the accuracy of the solution is obtained. Because of the time T chosen for the excitation force, most of the frequency content of that excitation is not that much greater than the fundamental frequency of the beam. In our work, the

beam structure damping ratio is assumed to be very small and ignored initially. Damping will be addressed in future work.

In addition to Table 5.1, Table 5.2 provides a list of the initial modeling parameters for the beam structure under wave loads excitation, including the geometry and material properties for both the beam and elastic foundation.

Table 5.2 Parameter definition

Item	Description	Units	Value
c	Moving load speed	ms^{-1}	343
T	Half-cycle duration	Sec	0.0004
A	Force amplitude	N	10
N	The number of half-cycles	---	2

Figure 5.8~5.11 show the effect of foundation stiffness on beam transient responses under sinusoidal wave loads. It can be seen that by reducing beam elastic foundation base stiffness, beam transient responses under a given wave load increases. Furthermore, the resulting wavelength within the structure appears to be shorter with lower stiffness.

$K_f = 8.27586 \times 10^6\, N/m^2$

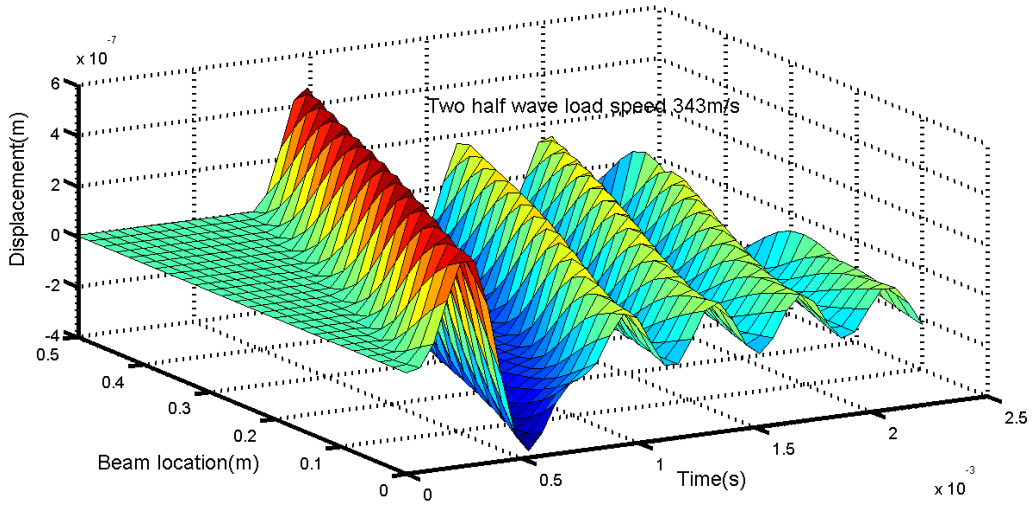

Figure 5.8 Effect of foundation stiffness on beam transient responses under half-cycle wave load

$K_f = 2.3645 \times 10^7\, N/m^2$

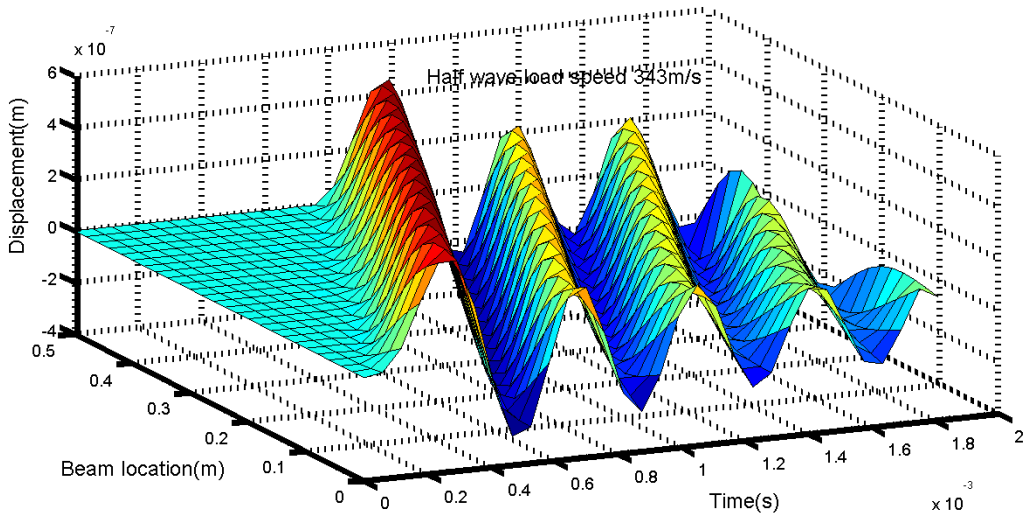

Figure 5.9 Effect of foundation stiffness on beam transient responses under full cycle wave load

$$K_f = 2.3645 \times 10^7\, N/m^2$$

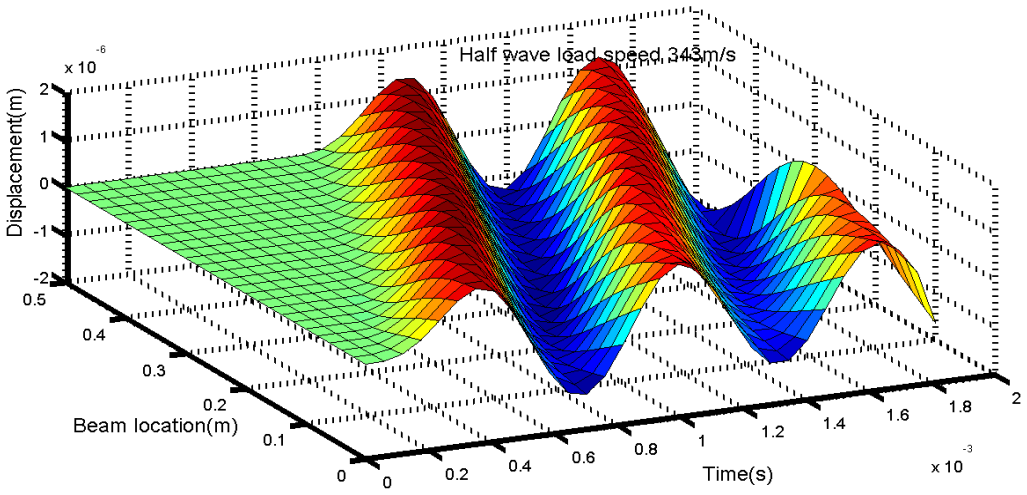

Figure 5.10 Effect of foundation stiffness on beam transient responses under half-cycle wave load.

$$K_f = 8.27586 \times 10^6\, N/m^2$$

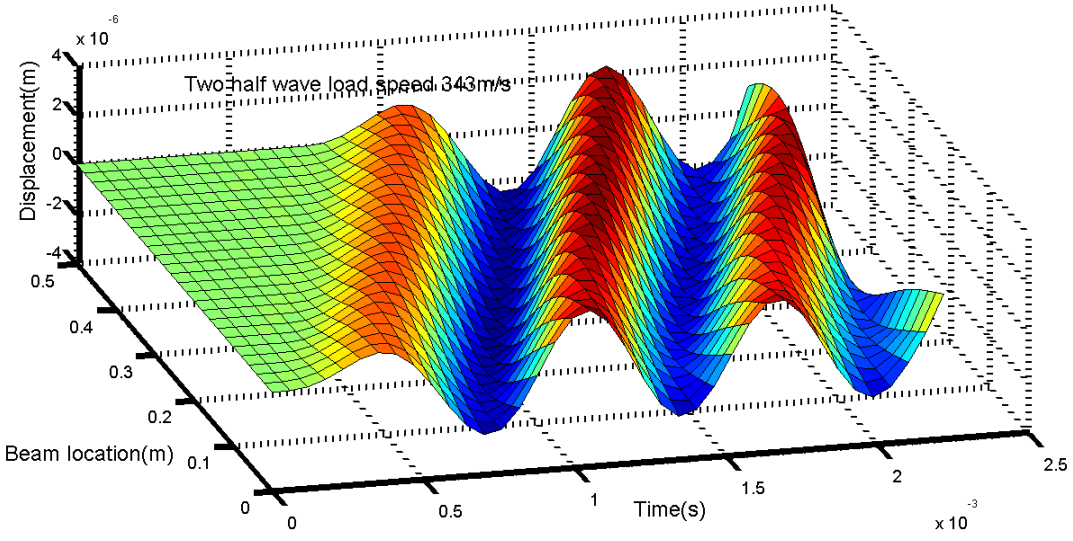

Figure 5.11 Effect of foundation stiffness on beam transient responses under full cycle wave load.

5.5. Summary

The response of a free beam on an elastic foundation to moving concentrated load and sinusoidal wave load by means of the finite element method has been presented in this chapter. Numerical results have been verified by corresponding results obtained from ANSYS commercial codes. This technique is attractive for treating the problems of beams on an elastic foundation under moving loads, which are extended to develop the acoustic wave sensor by using the force identification method. The effect of some important parameters, such as the foundation stiffness and the load travelling speed, has been studied. Numerical examples are given in order to determine the effects of various parameters on the response of the beam. Through general consideration, the conclusion can be drawn that an increase in velocity for moving loads leads to the dramatic increase in response deflections. This fact is very important because it will have useful contributions on moving loads problems regarding vehicle load design and bridge structure analysis. It was also shown, not surprisingly, that a foundation with a lower stiffness provided a greater beam response for a given excitation. The technique and the findings in this chapter can offer a good basis in practical applications such as acoustic wave beam sensor development by means of force reconstruction method, which is described next.

Chapter 6 Beam elastic foundation acoustic load reconstruction

This chapter focuses on development of the inverse methods needed to reconstruct the transient wave loads from measured vibration responses. As noted earlier, instead of using actual measurements, the response is instead found using the simulation methods developed in earlier chapters. In using such an approach, the amount of noise and errors can more easily be controlled. The latter is important in assessing the effectiveness of this method.

6.1 Introduction

To develop a new kind of acoustic sensor used to locate acoustic sources, a beam structure with elastic foundation supports acting as a sensor configuration is studied. By using an elastic foundation, it is hoped that the structural response, which will be examined through modeling, will be rich enough to provide sufficient information about the impinging wave. The novelty of the work includes the reconstruction of spatially distributed pressures traveling across a structure, and in particular a structure with elastic supports. A finite element method is applied to solve the partial differential equations for this structure when subjected to sinusoidally-shaped traveling wave loads. Velocities at the locations of interest can be obtained from this FEM time response calculation. In order to evaluate methods for reconstructing the transient and distributed

forcing function, the simulated response is then used as the input to the traveling-wave force reconstruction methods**.** Regularization methods are applied to deal with numerical issues and improve the accuracy in identifying the moving acoustic waves. Methods such as Tikhonov regularization and L-Curve methods were discussed in Liu's work [6]. Since the reconstructed forces may include large errors through the inversion of an ill-conditioned matrix, Tikhonov regularization is used to improve the conditioning of the matrix inversion. The L-Curve method is used to choose the regularization parameter. This generates reasonable and practical results. In addition, to verify results stability with these inverse methods, various levels of random noise are added to simulate issues associated with actually measuring a response in this study. Also various structural parameters of interest like the beam dimensions, beam material, and elastic foundation material are considered in an attempt to develop a configuration suitable to the problem being addressed.

In the following section, a description of the analytical tools used to predict the sensor's response for a given configuration is provided. In this study, the classical Bernoulli-Euler theory is used to predict the response for a beam on an elastic foundation. Note that this theory has some limitations when the frequency increases and the wavelength in the structure decreases. These limitations are being overlooked in this initial study as the goal here is to assess the relative response of a structure. Also, with the use of an inverse method, methods that include shear effects become more cumbersome. As such, these effects will be considered in future works where a more accurate prediction of the response is needed. Note that the intent of this

study is to demonstrate the feasibility of using such a structure for detecting the presence and direction of a wave. In the approach demonstrated here, the inverse method is performed in an offline manner in that the solution is determined after the response has been measured, not while it is being measured. In later sections, the force reconstruction method and analytical results are discussed. Conclusions that can be drawn from the present study are also provided along with plans for future work, which will include an experimental examination of a prototype structure and development of more direct online measurement and processing techniques**.**

6.2 Theoretical model

Consider a finite-length Bernoulli – Euler beam resting on an elastic foundation as illustrated in Fig. 5.1, the equation of motion is [51,52]

$$\mu \frac{\partial^2 W(x,t)}{\partial t^2} + 2\mu\omega_b \frac{\partial W(x,t)}{\partial t} + EI \frac{\partial W^4(x,t)}{\partial x^4} + C_f W(x,t) = f(x,t), \qquad (6.1)$$

where the beam flexural rigidity is EI, the beam mass density is μ, the foundation elasticity constant is C_f, ω_b is the damping circular modal frequency, and $f(x,t)$ represents moving loads. As noted in chapter 5, the mass and bending stiffness of the elastic foundation are being neglected.

For the elastically supported beam in free vibration, namely $f(x,t) = 0$, Eq.(6.1) becomes

$$\mu \frac{\partial^2 W(x,t)}{\partial t^2} + 2\mu\omega_b \frac{\partial W(x,t)}{\partial t} + EI \frac{\partial W^4(x,t)}{\partial x^4} + C_f W(x,t) = 0. \qquad (6.2)$$

By using the method of separation of variables, Eq. (6.2) can be expressed as

$$EI\frac{W^{(4)}(x)}{W} = -\frac{\mu T^{"} + 2\mu\omega_b T^{'} + C_f T}{T}, \tag{6.3}$$

where $W(x,t) = W(x)T(t)$. Since the left side of Eq. (6.3) is only the function x and the right side of this equation is only the function of t, both sides of this equation must be equal to a constant of p. This equivalence yields

$$EI\frac{dW^4}{dx^4} - pW = 0, \tag{6.4}$$

and

$$\mu T'' + 2\mu\omega_b T' + C_f T + pT = 0. \tag{6.5}$$

The solution of Eq. (6.4) is

$$W(x) = C_1\cos(\gamma x) + C_2\sin(\gamma x) + C_3\cosh(\gamma x) + C_4\sinh(\gamma x), \tag{6.6}$$

where $\gamma = \sqrt[4]{\frac{p}{EI}}$ and $C_i (i = 1,2,3,4)$ is constant. Based on Eq. (5.2), its boundary conditions are

$$x = 0 \qquad \begin{cases} W''(0) = 0 \\ W'''(0) = 0 \end{cases}, \tag{6.7a}$$

$$x = L \qquad \begin{cases} W''(L) = 0 \\ W'''(L) = 0 \end{cases}. \tag{6.7b}$$

Eq. (6.7) and Eq.(6.6) give $\cos(\gamma_n L)\cosh(\gamma_n L) = 1$, where $\gamma_{1\sim5}L = 4.730, 7.853, 10.996, 14.137,$ 17.279 and $\gamma_n L = (n + \frac{1}{2})\pi, (n > 5)$. Note that for the case $\gamma_n L = 0$, there are two shape solutions for this beam structure with elastic foundation support, the shape functions are

$$\gamma_n L = 0 \qquad \begin{cases} \phi_1 = 1 \\ \phi_2 = x - \dfrac{L}{2} \end{cases} \quad (n = 1,2)\,, \tag{6.8a}$$

and for $\gamma_n L \neq 0$ $(n = 1,2,..)$, through setting $\beta_n = \gamma_{n-2} \neq 0$ $(n = 3,4,..)$,

$$\phi_n(x) = \cosh(\beta_n x) + \cos(\beta_n x) - \frac{\cosh \beta_n L - \cos \beta_n L}{\sinh \beta_n L - \sin \beta_n L}\left(\sinh(\beta_n x) + \sin(\beta_n x)\right), \quad (n > 2)\,. \tag{6.8b}$$

It should be mentioned that the shape functions given in Eq.(6-8a~b) are not the mode shapes of the beam structure with elastic foundation support corresponding to its natural frequencies. However, these functions satisfy the boundary conditions above and they are orthogonal. As a result, solutions for the displacement and velocity in Eq. (6-1) can be found by using an assumed basis function approach, respectively, as

$$W(x,t) = \sum_{n=1}^{\infty} \phi_n(x) q_n(t)\,, \tag{6.9}$$

and

$$\dot{W}(x,t) = \sum_{n=1}^{\infty} \phi_n(x) \dot{q}_n(t)\,, \tag{6.10}$$

where $q_n(t)$ is the n th amplitude and $\phi_n(x)$ is the corresponding shape function for the beam structure given above. By applying this conventional expansion approach, the function superposition in Eq. (6.9) is substituted into Eq. (6.1), and the result is multiplied by shape functions and integrated between 0 and L. By using this set of orthogonal basis conditions, the resulting equation of motion becomes

$$\frac{d^2 q_n(t)}{dt^2} + 2\omega_b \frac{dq_n(t)}{dt} + EI \frac{\sum_{i=1}^{\infty} q_i(t) \int_0^L \phi_i^{(4)}(x)\phi_n(x)dx}{\mu \int_0^L \phi_n^2(x)dx} + \frac{C_f}{\mu} q_n(t) = \frac{\int_0^L f(x,t)\phi_n(x)dx}{\mu \int_0^L \phi_n^2(x)dx}. \tag{6.11}$$

By substituting the shape functions used in Eq. (6.8) into Eq. (6.11) and applying the orthogonality condition, the result is

$$\frac{d^2 q_n(t)}{dt^2} + 2\omega_b \frac{dq_n(t)}{dt} + EI \frac{\Lambda_n}{\mu \int_0^L \phi_n^2(x)dx} + \frac{C_f}{\mu} q_n(t) = \frac{\int_0^L f(x,t)\phi_n(x)dx}{\mu \int_0^L \phi_n^2(x)dx}, \tag{6.12}$$

where $\Lambda_n = \sum_{i=1}^{\infty} q_i(t) \int_0^L \phi_i^{(4)}(x)\phi_n(x)dx = 0$, $(n = 1,2)$ and $\Lambda_n = q_n(t)\beta_n^4 \int_0^L \phi_n^2(x)dx$, $(n > 2)$. The displacement response amplitude from Eq. (6.12) can be solved by applying the convolution integral in the following format

$$q_n(t) = \int_0^t F(\tau)h(t-\tau)d\tau, \tag{6.13}$$

where $F(\tau) = \int_0^L f(x,\tau)\phi_n(x)dx$. The displacement response can be obtained by substituting Eq.(6.13) into Eq. (6.9),

$$W(x,t) = \sum_{n=1}^{\infty} \varphi_n(x) \frac{1}{\omega_d} \int_0^t F(\tau) e^{-\zeta_n \omega_n (t-\tau)} \sin(\omega_d (t-\tau))d\tau, \tag{6.14}$$

where $\omega_d = \omega_n\sqrt{1-\zeta_n^2}$ and ζ_n is the damping ratio for n ($\zeta_n = \frac{\omega_b}{\omega_n}$). For the beam structure with elastic foundation supports, the natural frequency ω_n can be expressed as $\omega_n^2 = \frac{C_f}{\mu}$ ($n = 1,2$) and $\omega_n^2 = \frac{EI\beta_n^4}{\mu} + \frac{C_f}{\mu}$ ($n > 2$). Eq. (6.14) can be written in discrete terms as

$$W(x,t) = \sum_{n=1}^{\infty}\phi_n(x)\frac{1}{\omega_d}\sum_{j=0}^{i}\left\{e^{-\zeta_n\omega_n\Delta t(i-j)}\sin\omega_d\Delta(i-j)\right\}\Pi(j)\Delta t \quad (i = 0,1,2...,N)\,, \tag{6.15}$$

where Δt is the sampling time interval and $\Delta(i-j)$ represents the time increment of $t-\tau$. From the Composite Simpson's Rule for numerical integration, the term $\Pi(j)$ in Eq. (6.15) can be expressed as

$$\Pi(j) \cong \frac{h}{3}\left\{ f(0,j)\phi_n(0)dx + 2\sum_{i=1}^{(N/2)-1} f(x_{2i},j)\phi_n(x_{2i}) + \right.$$

$$\left. 4\sum_{i=1}^{\frac{N}{2}} f(x_{2i-1},j)\phi_n(x_{2i-1}) + f(L,j)\phi_n(x_N)\right\}. \tag{6.16}$$

This beam FEM model has 15 elements and each element is divided by 10, totaling 151 points (division N=150). Note that $h = \frac{L-0}{N}$ and $x_i = 0 + i\frac{L}{150}$. The residual error associated with the approximation in Eq.(6.16) is

$$Error = \left|\frac{Lh^4}{180}\left[f(x,t)\phi_n(x)\right]^{(4)}\right| \le 1.9879\times10^{-5}. \tag{6.17}$$

From Eq.(6.17), it can be known that the residual error is very small, so using the Composite Simpson role Eq.(6.16) to estimate the term $\Pi(j)$ is reasonable. The velocity response can be obtained from directly differentiating Eq. (6.14)

$$\dot{W}(x,t)=\sum_{n=1}^{\infty}\phi_n(x)\frac{1}{\omega_d}\int_0^t F(\tau)e^{-\zeta_n\omega_n(t-\tau)}[-\zeta_n\omega_n\sin\omega_d(t-\tau)+\omega_d\cos\omega_d(t-\tau)]d\tau\,. \tag{6.18}$$

Similarly, Eq. (6.18) can be written in discrete terms as

$$\dot{W}(x,t)=\sum_{n=1}^{\infty}\phi_n(x)\frac{1}{\omega_d}\sum_{j=0}^{i}e^{-\zeta_n\omega_n\Delta t(i-j)}\left[-\zeta_n\omega_n\sin(\omega_d\Delta(i-j))+\omega_d\cos\left(\omega_d\Delta t(i-j)\right)\right]\Pi(j)\Delta t$$

$$(i=0,1,2..N)\,. \tag{6.19}$$

Arranging Eq. (6.15) and Eq. (6.19) into matrix form

$$\left[a(0,0),a(x_1,0),...,a(x_N,0),a(0,1),a(x_1,1),...,a(x_N,1),....,a(0,N),a(x_1,N),...,a(x_N,N)\right]^T=$$

$$\sum_{n=1}^{\infty}A_n\begin{bmatrix}s_0\\s_0\\...\\s_0\\s_0\end{bmatrix}\begin{bmatrix}s_0&0&...&0\\s_0&s_1&...&0\\...&&...&\\s_0&s_1&...&s_N\end{bmatrix}\begin{bmatrix}B&0&...&0\\0&B&...&0\\...&&....&\\0&0&....&B\end{bmatrix}\times$$

$$\left[f(0,0),f(x_1,0),...,f(x_N,0),f(0,1),f(x_1,1),...,f(x_N,1,),....,f(0,N),f(x_1,N),...,f(x_N,N)\right], \tag{6.20}$$

where for displacement

$$S_j=e^{-\zeta_n\omega_n\Delta t(i-j)}\sin(\omega_d\Delta t(i-j))\,, \tag{6.21}$$

and for velocity

$$S_j = e^{-\zeta_n \omega_n \Delta t(i-j)}[-\zeta_n \omega_n \sin(\omega_d \Delta t(i-j)) + \omega_d \cos(\omega_d \Delta t(i-j))], \tag{6.22}$$

with

$$B = \left[\frac{h}{3} \quad \frac{4h}{3} \quad \frac{2h}{3} \quad \frac{4h}{3} \quad \frac{2h}{3} \quad \frac{4h}{3} \quad \frac{2h}{3} \quad \ldots \quad \ldots \quad \frac{h}{3}\right]. \tag{6.23}$$

Eq. (6.20) can be simplified as:

$$V_{[(N+1)\times(N+1)]\times 1} = G_{[(N+1)\times(N+1)]\times[(N+1)\times(N+1)]} \times F_{[(N+1)\times(N+1)]\times 1}, \tag{6.24}$$

where, $V_{[(N+1)\times(N+1)]\times 1} = \left[a(0,0), a(x_1,0), ..., a(x_N,0), a(0,1), ..., a(x_N,1), ..., a(0,N), ..., a(x_N,N)\right]$. Here $a(x_i, j)$ is used as a dummy variable to represent displacement or velocity. The computation of this $a(x_i, j)$ will depend on a specific S_j used for displacement or velocity and the other two terms in Eq. (6.20) are given by

$$G_{[(N+1)\times(N+1)]\times[(N+1)\times(N+1)]} = \sum_{n=1}^{\infty} A_n \begin{bmatrix} s_0 \\ s_0 \\ \ldots \\ s_0 \\ s_0 \end{bmatrix} \begin{bmatrix} s_0 & 0 & \ldots & 0 \\ s_0 & s_1 & \ldots & 0 \\ \ldots & & \ldots & \\ s_0 & s_1 & \ldots & s_N \end{bmatrix} \begin{bmatrix} B & 0 & \ldots & 0 \\ 0 & B & \ldots & 0 \\ \ldots & & \ldots & \\ 0 & 0 & \ldots & B \end{bmatrix}$$

and $F_{[(N+1)\times(N+1)]\times 1} = \left[f(0,0), f(x_1,0), ..., f(x_N,0), f(0,1), ..., f(x_N,1), ..., f(0,N), ..., f(x_N,N)\right]^T$.

From Eq.(6.20) and Eq.(6.24), it is apparent that by distributing *N* fixed points on the beam, the time dependent displacement or velocity at these locations can be determined. As a result, the moving force load can be described through time dependent force information at each fixed point regardless of arrival time for that wave. There is no need for *a priori* information regarding the time of arrival of the acoustic wave during the force inverse process. This method has not been seen in previous publications, but it is very practical in studying this acoustic wave sensor.

6.3. Regularization of inverse solution

Once the response of the structure is predicted using the formulations above, that response is then assumed as known and used in the inverse method to reconstruct the wave force that caused that resulting response. By using this approach, it is possible to perform various studies and quickly assess the impact of various structural configuration parameters on the performance of the system without requiring multiple prototype testing. Note that the actual means of measuring such a response will not be addressed until future work. The intent here is to simply evaluate the initial configuration requirements for a sensor of this type. The following section discusses the methods used to reconstruct the characteristics of the traveling transient wave load from the known response computed using the above analysis tools.

When Eq. (6.24) is expressed as an inverse problem, $F = G^{-1}V$ an ill- posed matrix problems may result. To solve this problem and find a useful and stable solution, a regularization method such as the Tikhonov method must be used. The goal in Tikhonov regularization is to incorporate a prior assumption about the size and smoothness of the desired solution. By applying this principle to the traveling wave load reconstruction problem, one is able to get the Tikhonov form from Eq. (6.24) as

$$F_\lambda = \left\| G \times F - V \right\|_2^2 + \lambda^2 \left\| F \right\|_2^2, \tag{6.25}$$

where the regularization parameter is λ. To select an optimum regularization parameter λ, a convenient graphical tool, the L-curve method, is applied. The L-curve method involves a plot of the norm, $\left\| F \right\|_2^2$ versus the corresponding residue norm, $\left\| G \times F - V \right\|_2^2$, on a suitable scale. For more

details on this regularization and the method in which it is applied, see the work of Liu [6] or Hansen [13].

6.4. Numerical analysis

In order to check the ability of the identification method described above to identify the shape of a distributed traveling wave load, a sample set of simulation results is provided. The goal is to identify moving acoustic wave load from the structure response by using the force reconstruction method. Since the damping ratio is very small in most materials, the damping ratio is assumed zero. The equations used for the inverse are simplified, which improves verification of the identification approach. Because most practical engineering systems have damping, those affects should be considered later. In this study, a finite set of traveling sinusoidal half-cycles will be considered as the loading on the structure. In modeling this continuous wave load $f(x,t)$ traveling over the beam sensor structure, three different time stages must be considered [51]. More details about the wave load can be seen in Chapter 4. Note that sinusoid wave loads traveling across the beam sensor structure must be at parallel direction to the beam axial direction. Because the intent here is to demonstrate the validity of the proposed approach, waves incident at oblique angles are not considered. Nevertheless, there is no restriction in the approach to parallel traveling waves. The force reconstruction method works well regardless of what angle the acoustic waves move across the beam sensor. Once demonstrated as valid, this one-dimensional approach can be extended in future work to consider

reconstruction along more than one axis. By discretizing the elastically supported beam structure with the finite element method, transient responses can be calculated numerically in the time domain by using Newmark's integration scheme [52]. Specifically the elastically supported beam is discretized into 15 beam elements with 16 nodal points. Of course, the response at any point can be interpolated by using the shape functions and the weight factors. Although not specifically shown, 15 beam elements have been determined to be sufficient for convergence of the FEM transient response calculations. When increasing the number of elements from 15 to 30, no appreciable increase in the accuracy of the solution is obtained. Because of the time T chosen for the excitation force, most of the frequency content of that excitation is not that much greater than the fundamental frequency of the beam. Note that the number of modal orthogonal functions N_f has a large effect on the accuracy of displacement calculation. In this work, it was determined that $N_f = 25$ provides accurate results.

To examine the ability to implement the force reconstruction, various sinusoidal wave loads moving across the beam structure will be studied numerically. As described above, the inverse process is ill-posed. In addition to examining the impact of the regularization on this problem, random noise will also be added to the simulated transient response to study the impact of measurement errors on the force reconstruction. Table 6-1 provides a list of the initial modeling parameters, including the geometry and material properties for both the beam and elastic foundation. Here, E is the Young's modulus of beam material and E_F is the Young's

modulus of foundation material. The foundation elasticity constant can be obtained from $C_f = E_F \frac{B}{TH}$, where B is width of the beam and TH is the thickness of the foundation base.

Table 6.1 Parameter Definition

Item	Description	Units	Value
L	Beam length	m	0.5
B	Beam width	m	0.01
h	Beam thickness	m	0.001
c	Wave speed	ms^{-1}	343
T	Half-cycle duration	sec	0.0005
ρ	Beam density	kgm^{-3}	2700
E	Beam young's modulus	Nm^{-2}	70GPa
ν	Poisson's ratio	-	0.33
TH	Foundation thickness	m	3
E_F	Foundation Young's modulus	Nm^{-2}	2.3MPa
K_E	The number of half-cycles	---	1

Figure 6.1 shows the time trace for the sinusoidal wave loads with different numbers of half-cycles used for evaluating the beam structure sensor. Figure 6.1(a) is a half-cycle wave load with a half-cycle period of 0.0005s. Figure 6.1(b) is a full-cycle wave load with a half-cycle period of 0.0005s. Figure 6.1(c) is a three half-cycle wave load with a half-cycle period of 0.0005s. The amplitude of the sinusoidal wave loads in each case is $1Nm^{-1}$. Because the actual

acoustic wave load amplitude will be smaller than the sinusoidal wave load considered here, amplitude modification will be conducted when a prototype sensor model is developed for tests in the future.

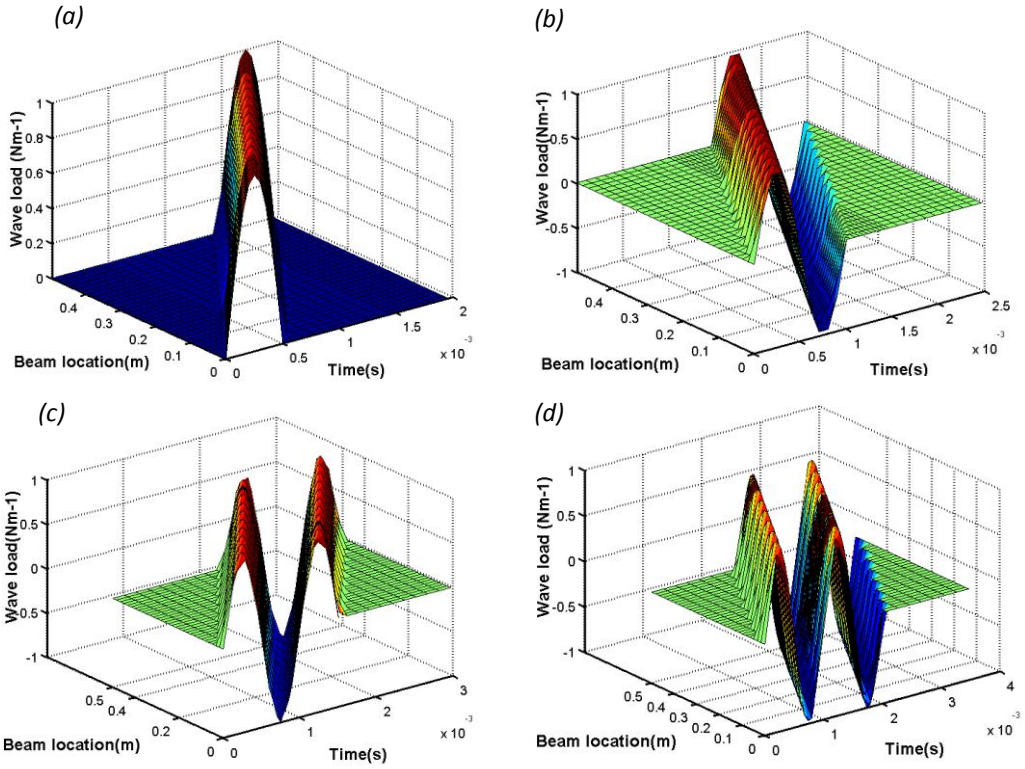

Figure 6.1 Exact wave loads on the beam with different half-cycle periods, *a) N=1, T=0.0005s b) N=2, T=0.0005s c) N=3, T=0.0005s d) N=4, T=0.0005s*

Figure 6.2 shows the transient displacement response for an aluminum beam structure with two different wave loads. These loads are a three half-cycle wave load and four half-cycle wave load, respectively. Each figure shows the response as the wave travels across the beam. Since every point on the beam with an elastic foundation support is subjected to motion, there is a potential to gain more information than say, for a simply supported beam. For simply supported beams, no information about the force can be obtained when the force is near the

restraints. This behavior is not an issue with elastic foundation support. The dynamic response from the beam contains information that will be useful when implementing the force reconstruction method.

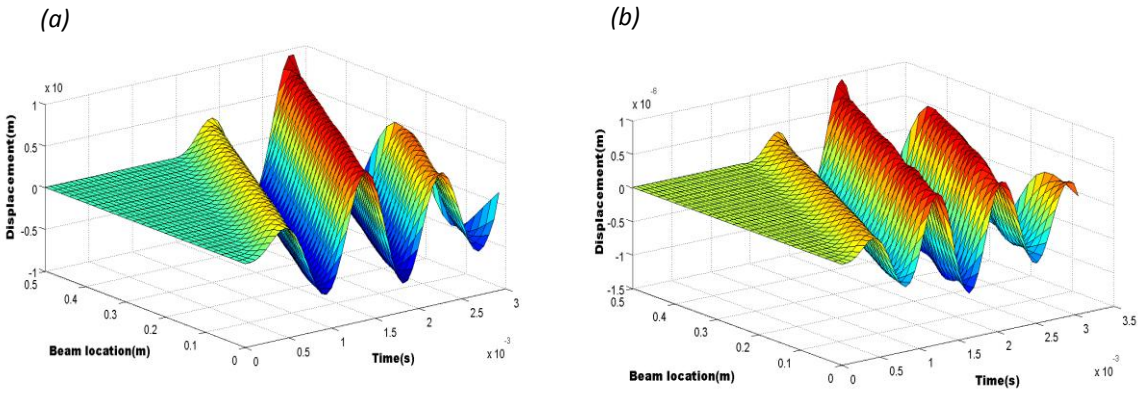

Figure 6.2 Transient beam displacements under different wave loads, *a) N=3, T=0.0005s,b) N=4, T=0.0004s*

6.4.1 Displacement-based force reconstruction

To mimic the acoustic sensor used for predicting moving acoustic loads, the displacement responses obtained above are applied as known input parameters in the inverse

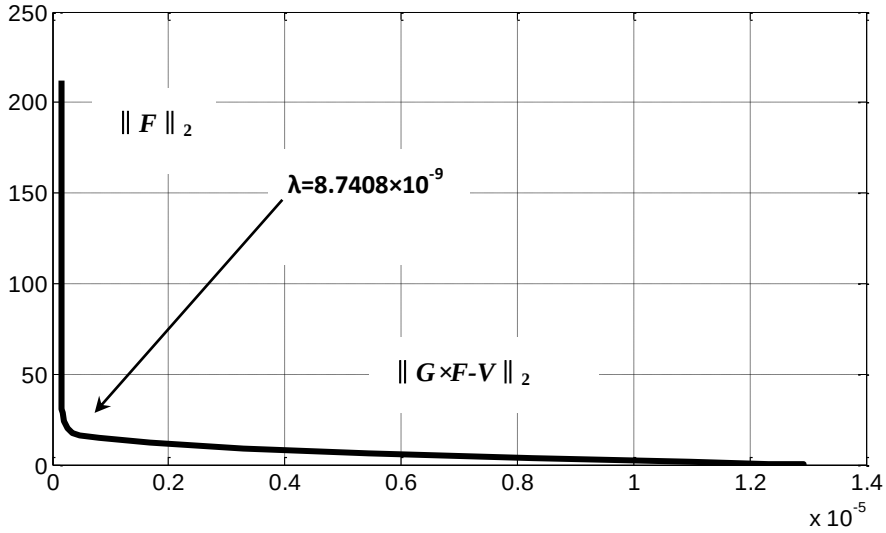

Figure 6.3 L-curve plot for selecting regularization parameter λ in displacement inverse

process. Since this inverse process is an ill-posed problem, the regularization method described above is implemented. The L-curve for Tikhonov regularization is plotted in Fig.6.3.

The optimum parameter of $\lambda=8.7408\times10^{-9}$ is computed from Eq.(6-25). Using this optimum parameter in the Tikhonov method, the reconstructed force results are obtained, as shown in Fig.6.4~Fig.6.5. These inverse results correspond to the moving three half-cycle and four half-cycle loads, with their amplitudes at $1Nm^{-1}$. The inverse results are good, illustrating that the force reconstruction method is practical and solvable.

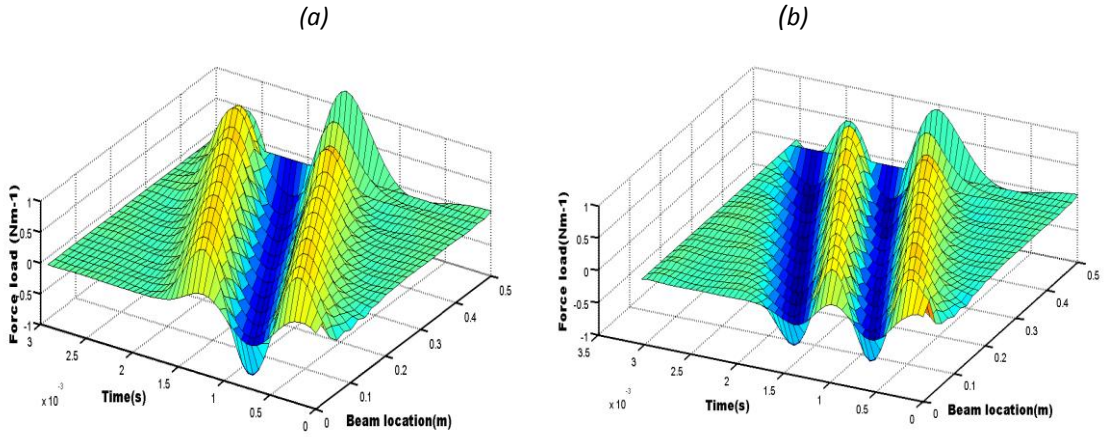

Figure 6.4 Force reconstruction with no added noise, *a) N=3 T=0.0005s δ=0.0 b) N=4 T=0.0004s δ=0.0*

In order to fully evaluate the beam structure sensor performance for predicting acoustic wave loads, random noise is added to the displacements calculated above as

$$W_{noise}(x,t)=W(x,t)_{calculated}(1+\delta)\,, \tag{6.26}$$

where δ represents the random noise amplitude. Random noise levels of 5% and 10% are added to the simulated responses and the inverse force values are obtained respectively, as illustrated in Fig.6.5. When compared to the noise-free inverse results above, it can be seen that there is not

much influence on the force load when the random noise level is very low. When the random noise level is larger than 5%, there is some influence on the reconstructed force load amplitude and wave shape. Although not shown, it was determined that if the noise level is larger than 20%, the reconstructed wave shape will be indistinguishable from the background noise. Figure 6.6 shows the exact and reconstructed time histories for a four half-cycle wave load passing the beam location at x=0.38m. Reconstructed force values are obtained for this case from displacements with no noise pollution. As mentioned above, a noise level below 5% has almost no influence on inverse results. Noise levels between 5% and 10% will have slight effects on reconstruction results. The results in the figure can be considered typical for the force reconstruction method discussed above. It can be seen that although there is some deviation between these two curves, they are almost coincident in time. Figure 6.7 shows a comparison of exact and reconstructed force values at the time $t=0.0021s$.This plot indicates that identified values have some deviations from the exact forces although the identified curve has a definite trend approaching the true curve. Now that the displacement has been considered, emphasis is shifted to the use of velocity response in the inverse problem.

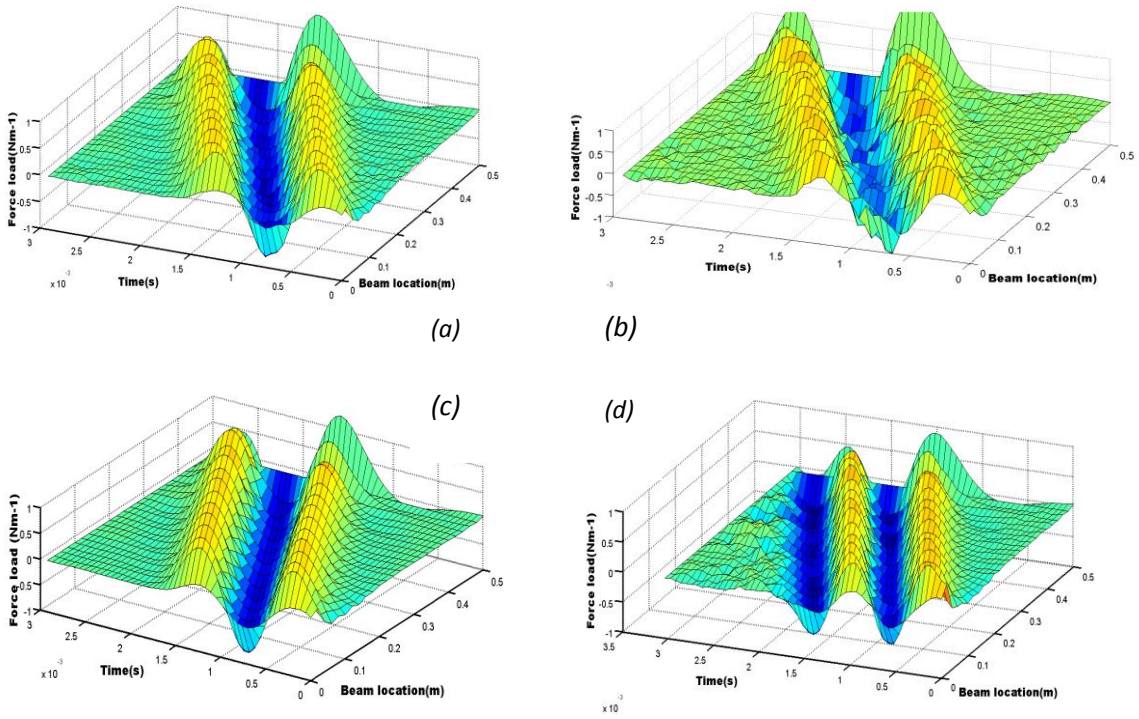

Figure 6.5 Force reconstruction with different random noise level, *a) N=3 T=0.0005s δ=0.05 b) N=3 T=0.0005s δ=0.10, c) N=4 T=0.0004s δ=0.05 d) N=3 T=0.0004s δ=0.10*

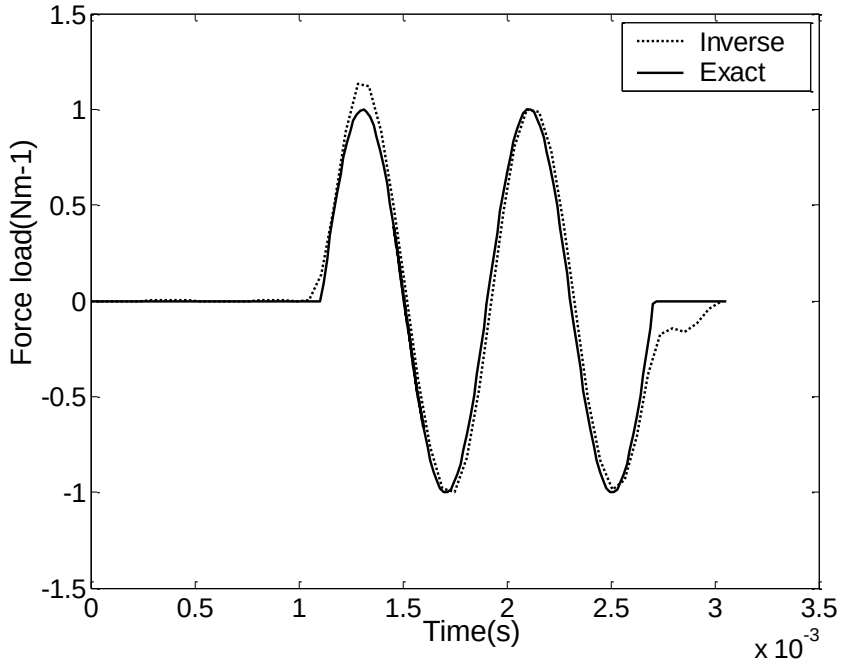

Figure 6.6 Comparison of inverse load and its exact wave load at beam location, *x=0.38m, N=4, T=0.0004s* Exact ——— Inverse ------

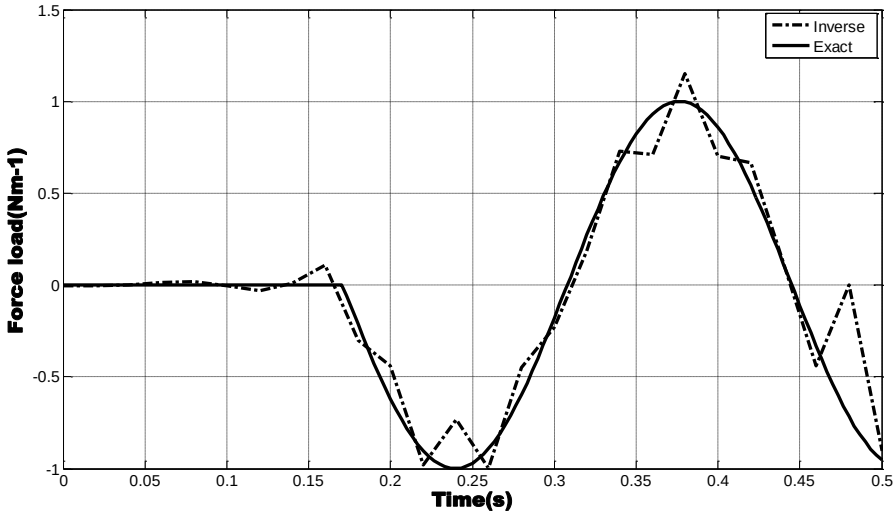

Figure 6.7 Identified and true wave load comparison at fixed time, *t=0.0021s, N=4, T=0.0004s, δ=0.0,*
Inverse – · – · Exact ——

6.4.2 Velocity based force reconstruction

Figure 6.8 shows the transient velocity response from the aluminum beam under different types of wave loads. Figure 6.9 shows the results under the same wave loads as Fig. 6.8, but replacing aluminum with steel. It is obvious that the velocity amplitude of a steel beam is smaller than that of an aluminum structure. Furthermore, an aluminum beam with a lower elastic modulus shows more variances in velocity amplitude than what the steel structure does. Therefore the trend for displacement is the same. Because of this, aluminum material appears to be a better sensor structure. The inverse problem of finding the wave load when these velocities are known is now of interest. It should first be pointed out that the displacement response inverse in Eq.6.26 is easier than the velocity response inverse, the reason is that velocity is obtained from the derivative of displacement, this will develop more ill-condition terms to the equation, and make ill-posed issue in velocity inverse equation more severe than displacement inverse equation.

Optimal regularization values obtained from L-Curve and Tikhonov methods seem to be not very effective in accuracy improvement on inverse force results for velocity inverse issue. The displacement inverse does have the disadvantage of smaller amplitudes when compared with velocity. Compared with velocity, accurate displacement amplitudes are difficult to measure with sensors. As a result, it is more practical to use the velocity inverse method when implementing an acoustic sensor, particularly when considering possible instrumentation.

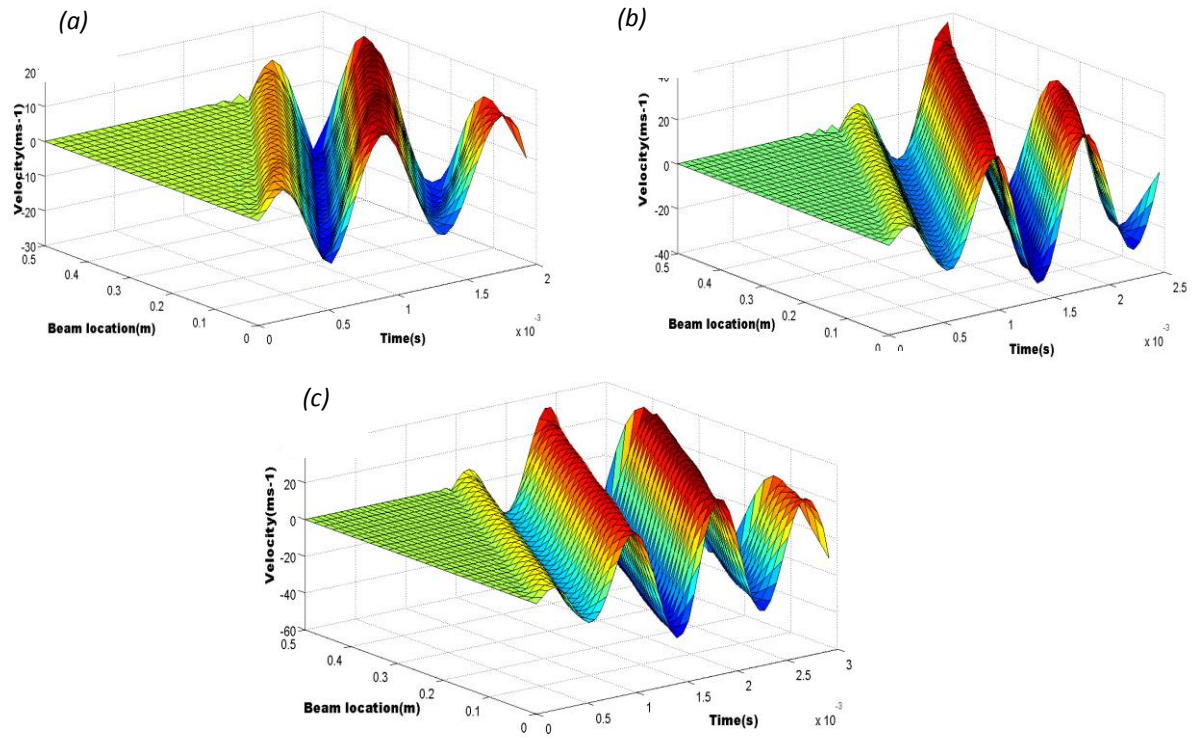

Figure 6.8 Velocities for aluminum beam under different wave loads, *N=1 T=0.0005s, b) N=2 T=0.0005s, c) N=3 T=0.0005s.*

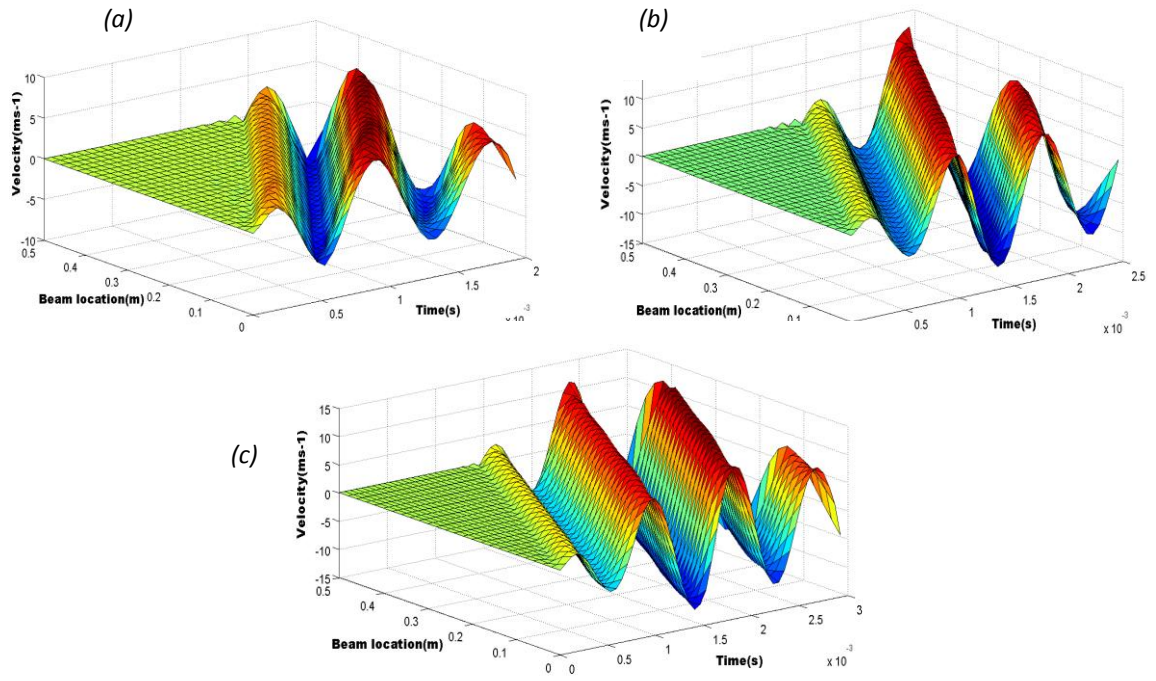

Figure 6.9 Velocities for steel beam under different wave loads, *a) N=1 T=0.0005s, b) N=2 T=0.0005s, c) N=3 T=0.0005s.*

To evaluate background noise effects on velocity inverse results, levels of random noise 2%, 5%, and 10% are added to the simulated velocity responses, and the impact on the inverse force values examined. To overcome the difficult inversion problem, the regularization method described above is again implemented. The L-curve for Tikhonov regularization is plotted in Fig. 6.10. With a noise level of 5%, the optimum parameter of $\lambda = 1.2813 \times 10^{-7}$ is computed from Eq.6.16, which is different from the optimal parameter obtained from the displacement inverse and 10% are added to the simulated velocity responses, and the impact on the inverse force values examined. To overcome the difficult inversion problem, the regularization method described above is again implemented. The L-curve for Tikhonov regularization is plotted in Fig.

6.10. With a noise level of 5%, the optimum parameter of $\lambda = 1.2813 \times 10^{-7}$ is computed from Eq.6.16, which is different from the optimal parameter obtained from the displacement inverse method discussed above. It should be mentioned that the optimum parameter in this case will not be changed with noise level variance. Using this optimum parameter in the Tikhonov-based enhanced method, the reconstructed force result with various noise levels is shown in Fig.6.11. From these results, it can be seen that there is not much influence on the force load when the

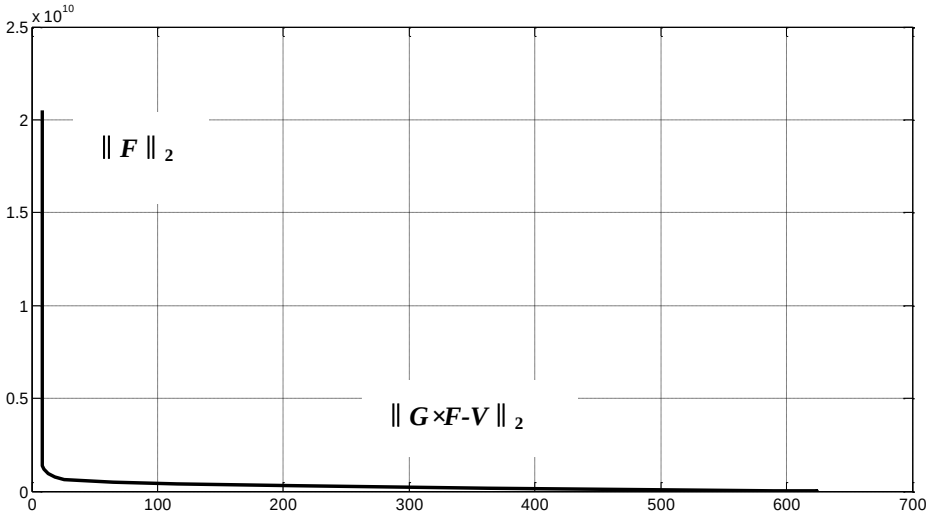

Figure 6.10 L-curve plot for selection of optimal regularization parameter λ in velocity inverse

random noise level is very low, as shown in Fig. 6.11(a) and Fig.6.11(b). When the random noise level is larger than 10%, there is some influence on force load amplitude and wave shape. Furthermore, it has been determined that if the noise level is larger than 20%, the wave shape will be poor and indistinguishable from the random noise background. The latter is illustrated in Fig.6.12, which shows that comparison of exact force value and inverse results at the beam

location 0.38m under the influence of different noise levels. Note that even if the noise level is zero, the amplitude and shape of the reconstructed wave load does not exactly correspond with the exact force. That error is primarily in the form of a phase shift with some amplitude errors. It is ultimately desirable to improve the force identification results by choosing suitable beam structure dimensions, material properties, and even elastic foundation properties.

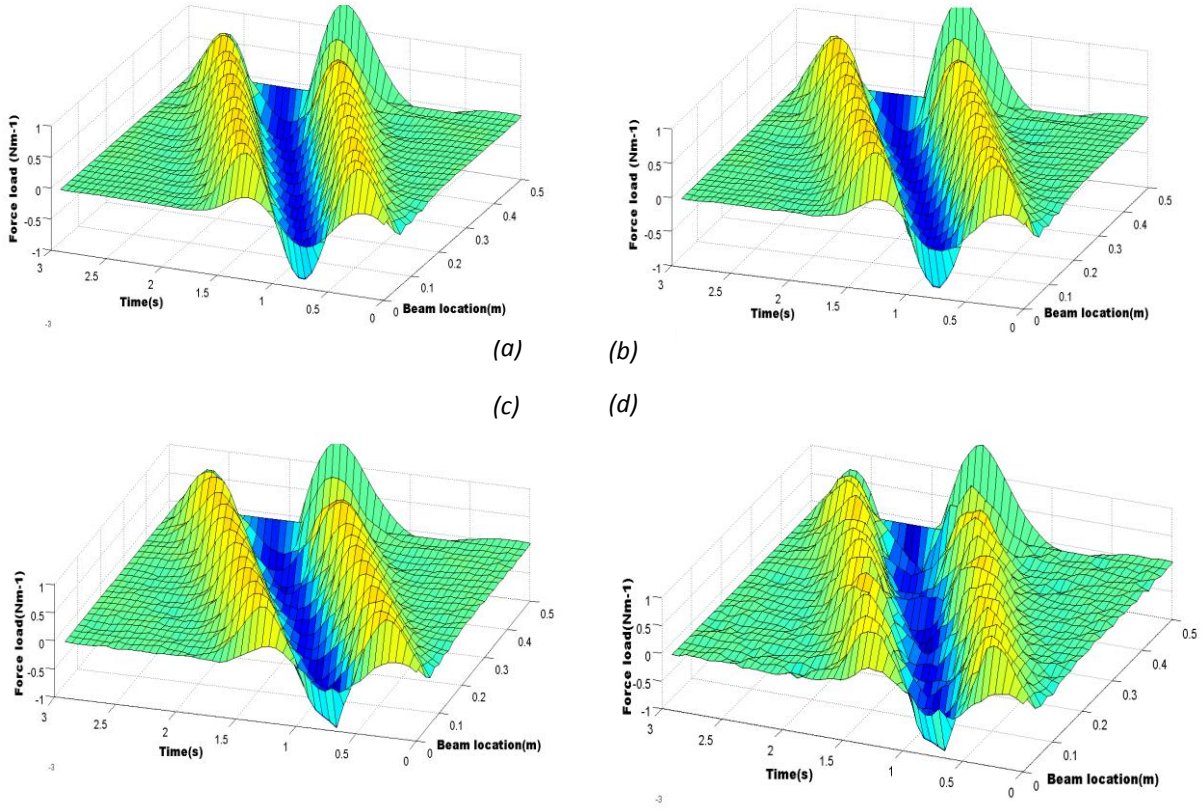

Figure 6.11 Wave load inversed results under the influence of different noise levels, aluminum beam, *N=3,T=0.0005s, a) δ=0.0 b) δ=0.02 c) δ=0.05 d) δ=0.10.*

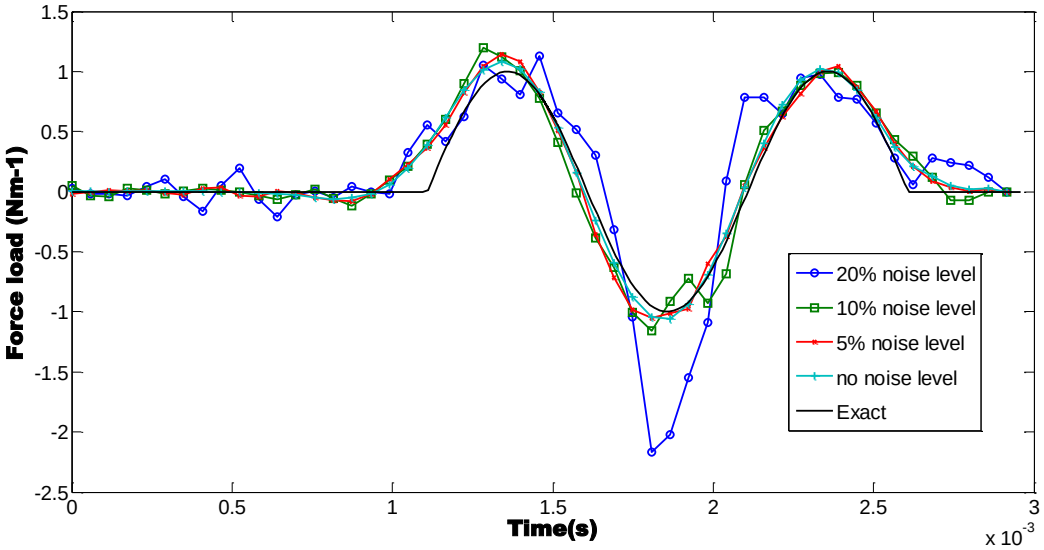

Figure 6.12 Comparison of exact and inverse results under noise levels at beam location, *x=0.38m, N=3, T=0.0005s*

The effect of beam length on the inverse results is shown in Fig. 6.13, which indicates that for some lengths, the inverse results are improved. Fig. 6.14 shows inverse results for different beam thicknesses. It can be seen that by increasing beam thickness, the wave load amplitude is close to the exact force solution in Fig. 6.1(c). Note that exact force results are obtained from Eqs.(4.25a~c). This result is not surprising.

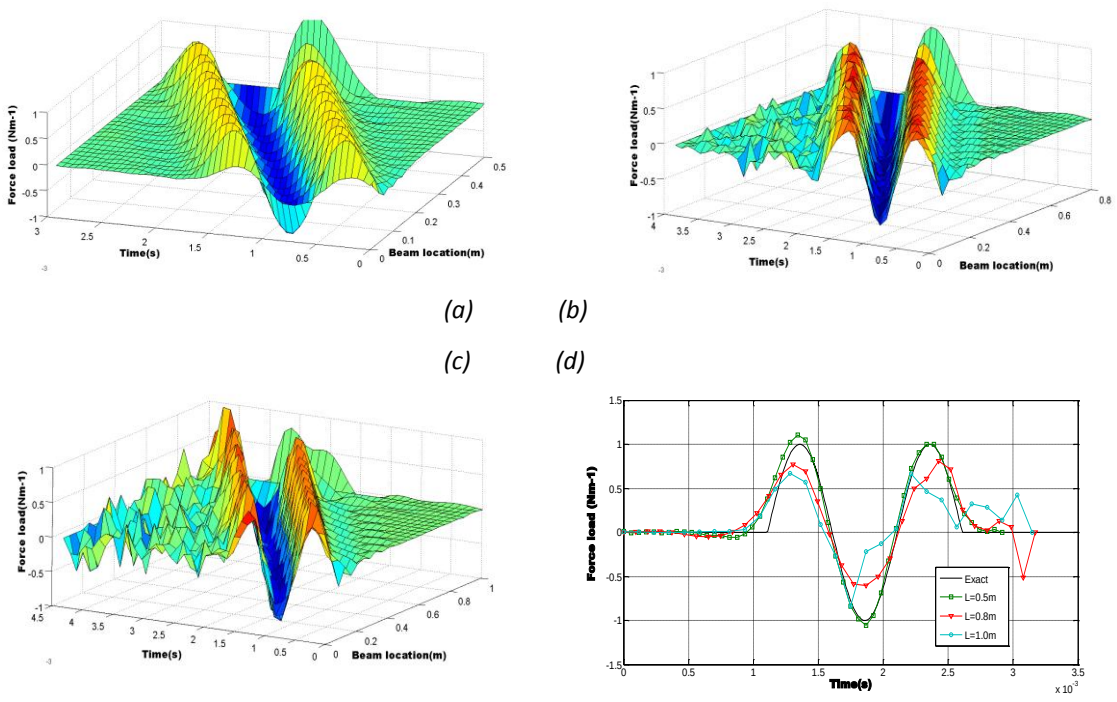

Figure 6.13 Wave load inversed values under different beam length. *a) N=3 T=0.0005s, δ=0.02 L=0.5m b) N=3 T=0.0005s, δ=0.02 L=0.8m, c) N=3 T=0.0005s,* δ=0.02 L=1.0m d) Comparison of exact and inverse results at beam location *x=0.38m.*

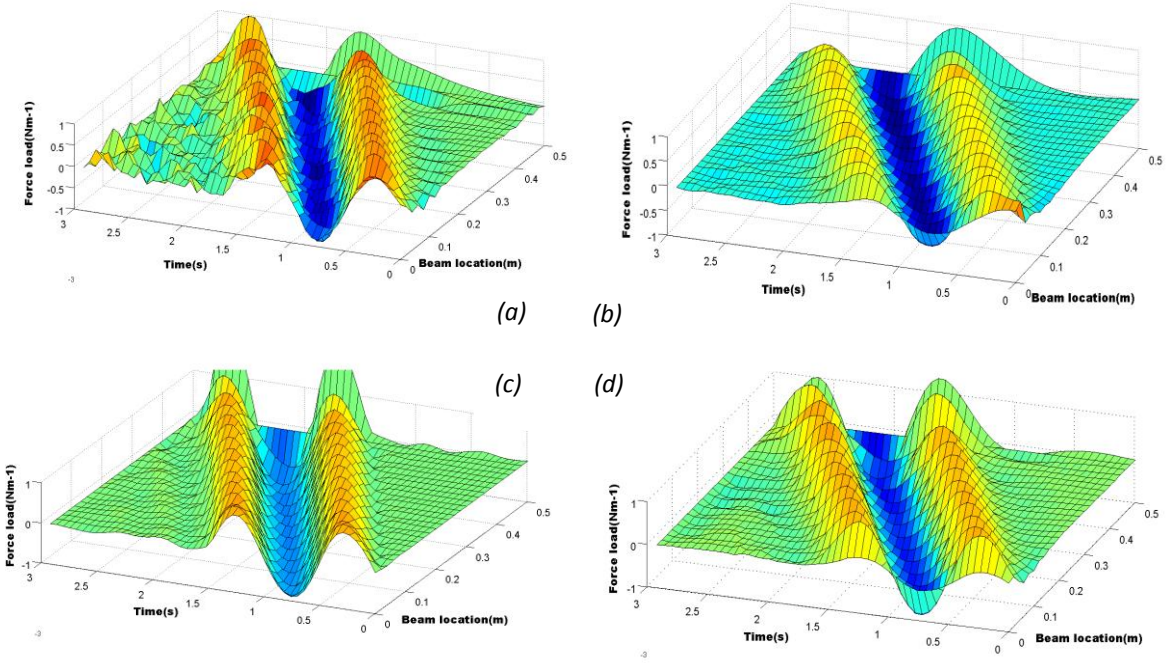

Figure 6.14 Wave load inversed values under different beam thickness *N=3, T=0.0005s, a) h= 0.2mm b) h=0.5mm c) h= 1 mm d) h= 1.5mm.*

Figure 6.15 shows inverse results for different beam widths. It can be seen that by increasing the beam width, the wave load amplitude is closer to the exact value shown in Fig. 6.1(a). It also can be seen that by reducing beam width, the wave shapes will be closer to exact ones. Figure 6.16 shows wave load inverse values for different beam materials. All these inverse results come from beam structures subjected to three half-cycle wave loads with the time period T=0.0005s and noise level of 2%. It can be seen in Fig. 6.16 that results for some soft materials which have lower Young's modulus, like nylon, are worse than results for materials like steel and Titanium. It seems that hard materials are not as sensitive to noise impact. It is obvious based on the results shown that a soft material like nylon is the not best candidate material for the sensor. Common materials such as steel and aluminum are suitable to be used for the current sensor configuration. Note that any effects of elastic foundation inertia have been neglected. These interial effects may become important with the lighter beam structures. The inverse results shown in Fig. 6.17 are obtained by taking a rubber material as the elastic foundation, and changing the Durometer parameters. From the results, it is seen that a lower Durometer material will have better amplitude inverse results. However, extremely high Durometer materials also lead to better inverse amplitudes. A Durometer material of 70A provides a case with a relatively low error. Figure 6.18 shows wave load inverse values obtained under different elastic base thickness. Obviously, inverse results remain almost the same good when elastic base thickness is changed. This illustrated that our method is stable and effective to solve inverse results in application for different base foundation structures.

It should be pointed out that there are some limitations to this research work. The optimal regularization parameter is the same for the cases with increasing noise levels. Therefore errors in the identified force increases for cases with more noise. This indicates that the optimal regularization values obtained from L-Curve and Tikhonov methods is not very effective to filter noise, although the force inverse results are robust when the noise level is lower than 10%. This behavior is indicated in Fig.6~Fig.11, where noise levels are shown to have some effects on the reconstructed force magnitude. If the beam material or the elastic foundation properties change, the regularization parameter will change.

There is one other characteristic of this study that is worth noting. Generally for the case that half-wave period T is less than the fundamental frequency period for the beam, the force identification accuracy is reduced. With T decreasing and making the force excitation frequency far above the fundamental beam natural frequency, force identification accuracy increases within some range. But to have constantly good force inverse results, other effects such as material properties and beam structure geometry parameters need to be considered together. As a result, there may not necessarily be a single optimum configuration.

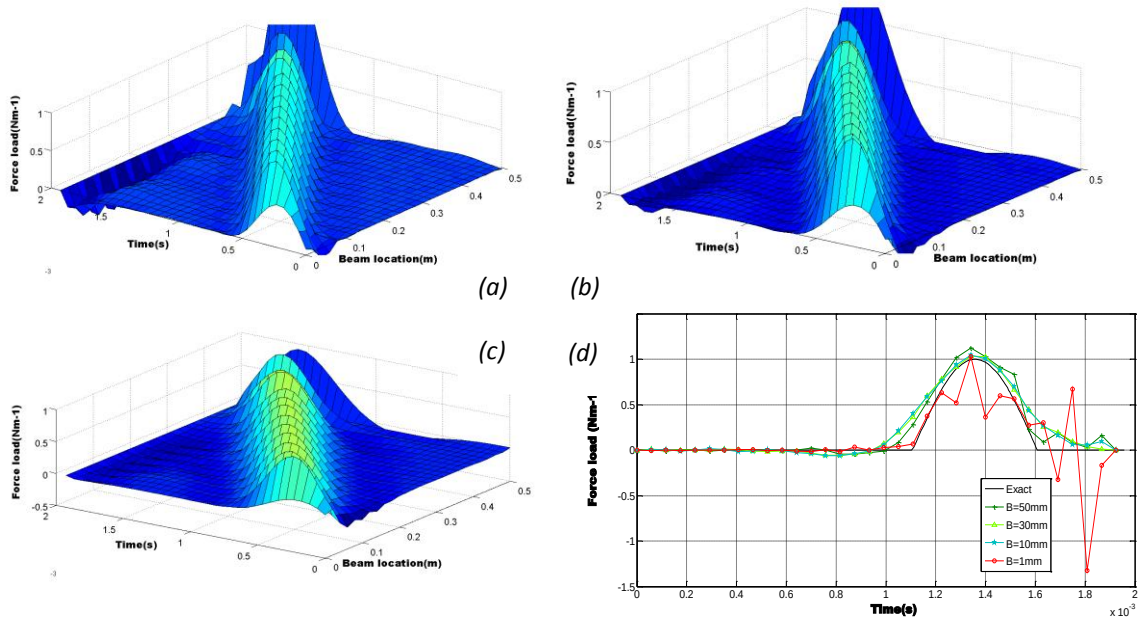

Figure 6.15 Wave load inversed values under different beam structure width, *N=1, T=0.0005s, δ=0.02, a) B=10mm b) B=30mm c) B=50mm*,Comparison of exact and inverse results at beam location *x=0.38m*.

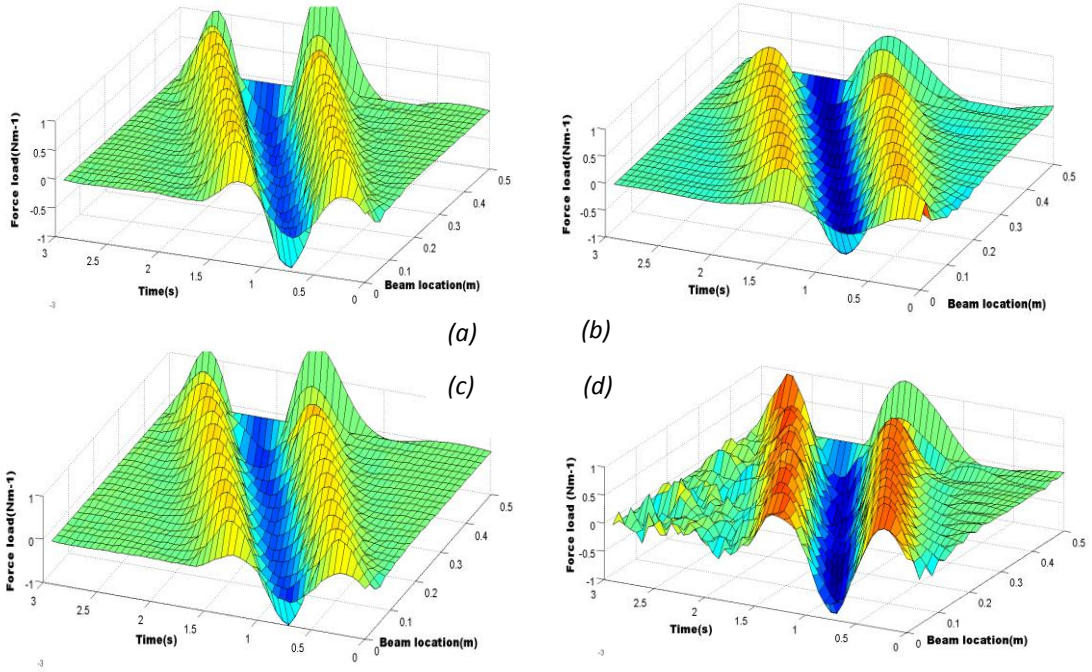

Figure 6.16 Wave load inversed values under different beam structure material *N=3 T=0.0005s, δ=0.02*, a) Titanium b) Steel c) Aluminum d) Nylon.

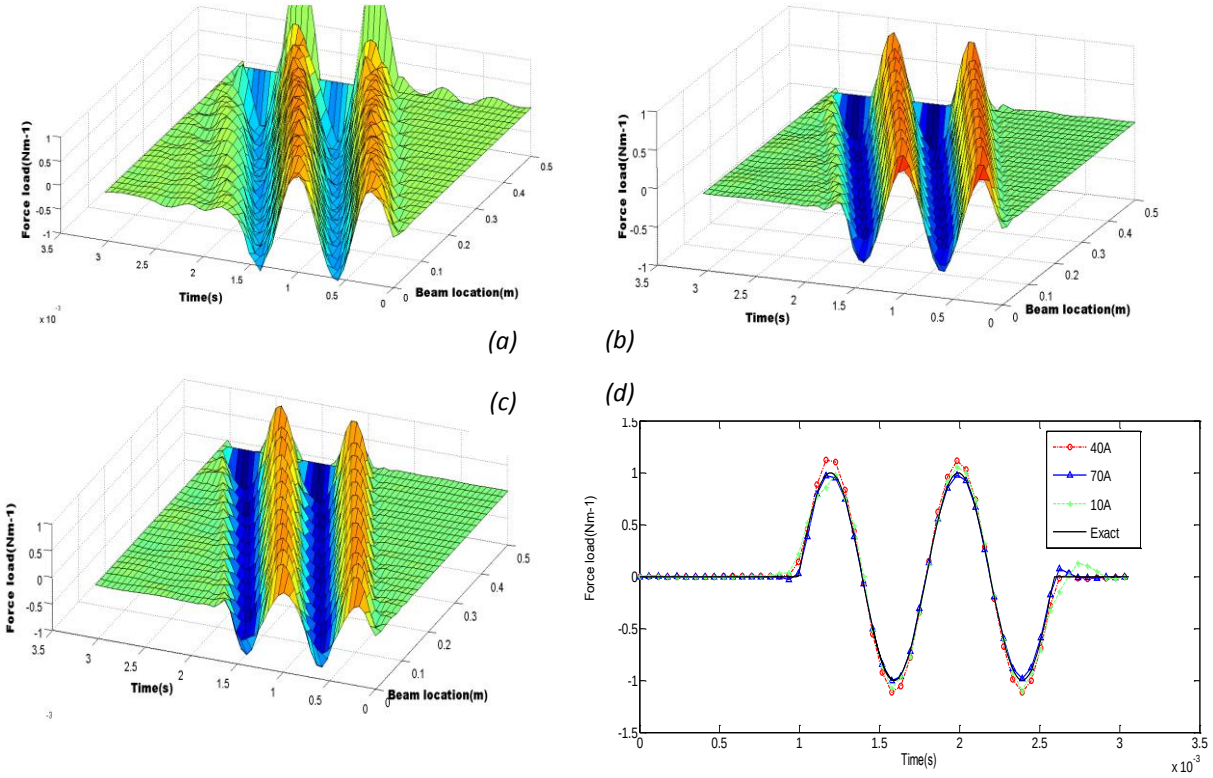

Figure 6.17 Wave load inversed values under different elastic base modulus, *N=4 T=0.0008s, δ=0.0*2 a) Durometer 10A b) Durometer 40A c) Durometer 70A d) Comparison of exact and inverse results at beam location *x=0.35m*.

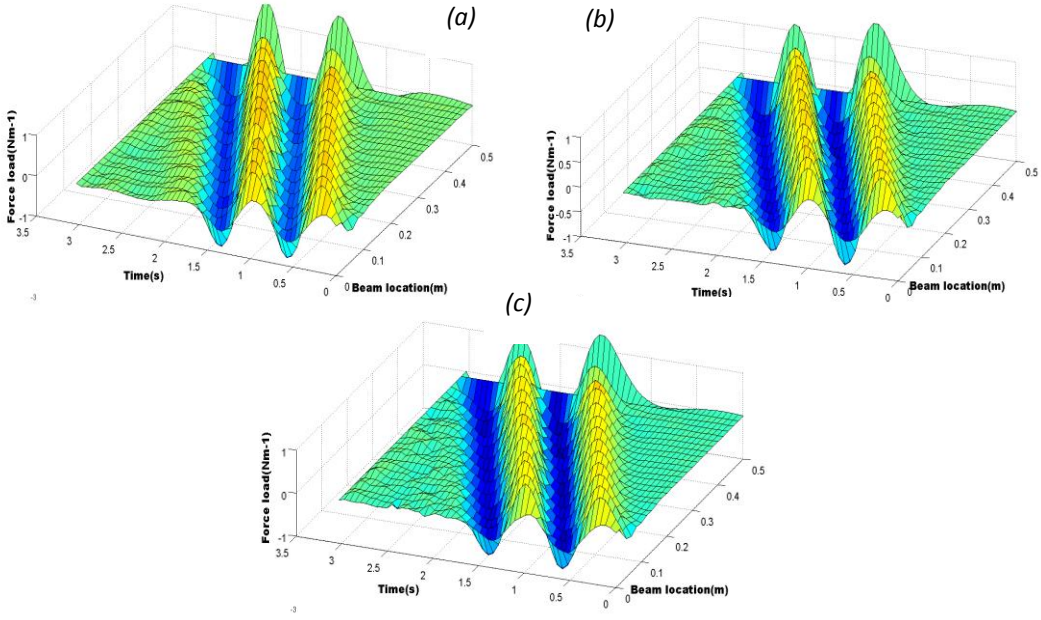

Figure 6.18 Wave load inversed values under different elastic base thickness, *N=4 T=0.0004s, δ=0.02,a) TH= 1mm b) TH=3mm c) TH= 5 mm*

6.5. Summary

To study continuous wave load reconstruction for developing a new type of acoustic sensor, the dynamic response of a one-dimensional continuous structure subjected to moving sinusoidal loads is studied. By applying the finite element method, a continuous wave load reconstruction method is proposed and applied to solve moving load identification using both clean and noise polluted displacement and velocity responses. Since inverse matrix methods can be severely ill-conditioned, the Tikhonov and L-curve method are used to find the optimized regularized parameter. Moderate noise levels, for example 10%, have a relatively small influence on force identification results. As shown in the results, reconstructed force values are in good agreement with true wave loads. In addition, beam structure dimensions and various materials are studied. The elastic foundation base material and thickness are also discussed. It appears from the results shown here that choosing a suitable elastic foundation base material and selecting a beam structure with a lower elastic modulus material will be very helpful in producing a practical sensor. It should be noted that in this research work the damping ratio is set to be zero in order to simplify this initial study, despite the fact that most materials have some damping. This research work provides a good basis for additional acoustic sensor prototype configuration studies as well as future prototype testing.

Chapter 7 Conclusions and plans

In this chapter, configuration study on acoustic sensor development based on the beam structure with various boundary conditions is summarized and the main conclusions are summarized. Recommendations for future work are also discussed. Future research work includes the extension of time domain results to the frequency domain.

7.1 Conclusions

To our knowledge, the continuous structures such as beam and plate can be a good candidate to identify moving acoustic wave loads because of their available transient responses when subjected to moving loads. In order to develop the beam structure as the sensor, responses with various boundary conditions must be examined. Some effects caused by beam structure parameters such as beam geometries and beam material have been discussed. In this dissertation, the beam theoretical models with various boundary conditions such as simple supported, intermediate supported and elastic foundation have been developed. The responses of these beams under different numbers of half-cycle sinusoidal wave loads, mimicking transient acoustic waves have been determined under a range of configuration parameters. A beam with simple

ends or intermediate supports, responses are zero at the boundary constraint points. The beam with elastic foundation model does not have this issue. In order to satisfy the sensor requirement in which the beam structure has a sufficient response for force loads to be well identified, the beam on elastic foundation seems to be a good candidate. Force reconstruction methods, originally applied to bridge structures for identifying moving vehicle loads have been discussed and reviewed as they relate to the problem at hand. These methods can be applied to identify moving acoustic wave loads in the sensor. Displacement and velocity responses will be used in the force inverse methods in order to compute information about the impinging wave loads. As stated earlier, one of the primary concerns is that the inverse matrix is normally ill-conditioned. The force cannot always be calculated from the direct inverse process. To deal with this problem, regularization methods such as Tikhonov method and L-curve method were used to find the optimized regularized parameter. In addition, to evaluate the force reconstruction method's effectiveness and stability, random noise of different levels was added to responses before being used in the inverse method. Then, the obtained force inverse values with noise input were compared with the exact force values. Developing a good sensor requires further examination of relative materials and beam sensor geometry. Their effects of these parameters on the force inverse results were examined so that the most promising sensor configuration could be identified. The inverse method in the time-domain has been well developed. The study suggests the following conclusions: It is feasible to use beam responses to identify moving acoustic like wave loads. Through using Tickhonov filtering tools, sufficient force identification results can be

obtained from input response data even with normal noise pollution. Furthermore, these inverse results are stable under the influence of noise levels of less than 20% amplitude increase in both simulated displacement and velocity responses. Such conditions for an elastically supported thin beam seem an ideal sensor structure for further consideration.

7.2 Recommendations for further studies

Naturally, such a study creates new ideas for further research. These new aspects are summarized as:

(a) Although results in the time-domain have shown much promise, a study in the frequency-domain is also warranted.

(b) The current method used to solve partial differential equation of foundation beam has not considered damping. Since all materials have damping, it is necessary to examine the effects of damping on force identified results. As a result, methods for including various levels of damping should also be considered.

(c) In this work, a moving sinusoidal wave load was used to simulate acoustics loads. This pressure wave load may be quite different from real acoustic loads as the latter has the character of incident and reflection wave propagation. Considering more realistic acoustic wave loads in the future work would improve acoustic wave sensor development.

(d) As with any development program, a suitable sensor prototype should be constructed and various measurement approaches examined to fully evaluate the performance of

the proposed approach.

References

[1] Metcalf, M. G., “Acoustics on the 21st century battlefield,” Joint Force Quarterly, Winter 1995-96, pp. 44-47.

[2] Roman Bogacz and Kurt Frischmuth, *Vibration in sets of beams and plates induced by traveling loads*, Archive of Applied Mechanics,Volume 79, Numbers 6-7, 509-516, DOI: 10.1007/s00419-008-0293-7.

[3] S.S. Law, T.H.T Chan and Q.H. Zeng 1999 American Society of Mechanical Engineers Journal of Dynamical Systems, Measurement, and Control 121.394-401.*Moving force identification-a frequency and time domains analysis.*

[4] Tommy H.T. Chan and Demeke B.Ashebo, *Theoretical study of moving force identification on continuous bridges*, Journal of Sound and Vibration, 870-883, Vol.295 (2006).

[5] L. Yu, Tommy H.T. Chan, *Recent research on identification of moving loads on bridges*, Journal of Sound and Vibration, 3-21,Vol.305 (2007).

[6] Yi Liu, W. Steve Shepard Jr, *An improved method for the reconstruction of a distributed force acting on a vibrating structure*, Journal of Sound and Vibration, 369-387,Vol.291 (2006).

[7] Fryba, L, *Vibration of Solids and Structures under Moving Loads*, Thomas Telford, London, 14 (1999).

[8] Thomas G. Carne, etc., *Reconstruction using the sum of weighted accelerations techniques Max-flat procedure*, Sandia national laboratories, Albuquerque, New Mexico, 87185.

[9] Cartwright,M. L. (1965). "Jacques Hadamard.1865-1963". *Biographical Memoirs of Fellows of the Royal Society* 11: 75–26.

[10] Jerome Idier, *Regularization tools and models for image and signal reconstruction,* Proceeding of the 3rd international conference on Inverse problems in Engineering, June 1999.

[11] Mario Bertero,Tomaso, A. Proggio and Vincent Torre, *Ill-posed problems in early version,* Proceeding of the IEEE,Vol.76,No.8,August 1988.

[12] Lenoid.I.Rudin, Stanley Osner and Emad Fatern, *Nonlinear total variation based noise removal algorithms*, proceeding of the 11th Annual International Conference of the center for nonlinear studies, physics D,Vol,60,pp-259-268,Nov.1992.

[13] P.C. Hansen Regularization tools: *A Matlab package for analysis and solution of discrete ill-posed problems* (2001).

[14] D.Calvetti, *Invertible smoothing preconditioners for linear discrete ill-posed problems,* Applied numerical mathematics,54 (2005),135-149.

[15] Yimin Wei, *Weighted Tikhonov filter matrices for ill-posed problems*, Applied mathematics and computation, 149 (2004),411-422.

[16] Ailin Qian, *A new wavelet method for solving an ill-posed problem,* Applied mathematics and computation 203 (2008) 635-640.

[17] K.K Stevens, *Force identification problems—an overview*, Proceedings of the SEM Spring Conference on Experimental Mechanics, Houston, TX, June 14-19, 1987, pp. 838–844

[18] S.P. Timoshenko, D.H. Young, W. Weaver, *Vibration Problems in Engineering*, Wiley, New York, 1974.

[19] T.H.T. Chan, C. O'Connor, *Wheel loads from highway bridge strains: field studies,* Journal of Structural Engineering, American Society of Civil Engineers 116 (1990) 1751–1771.

[20] S.S. Law, T.H.T. Chan, Q.H. Zeng, *Moving force identification: a time domain method,* Journal of Sound and Vibration 201 (1997) 1–22.

[21] S.S. Law, T.H.T. Chan, Q.H. Zeng, *Moving force identification-a frequency and time domain analysis,* Journal of Dynamic System, Measurement and Control 121 (1999) 394–401.

[22] T.H.T. Chan, S.S. Law, T.H. Yung, X.R. Yuan, *An interpretive method for moving force identification*, Journal of Sound and Vibration 219 (1999) 503–524.

[23] T.H.T. Chan, L. Yu, S.S. Law, *Comparative studies on moving force identification from bridge strains in laboratory*, Journal of Sound and Vibration 235 (1) (2000) 87–104.

[24] T.H.T. Chan, L. Yu, S.S. Law, T.H. Yung, *Moving force identification studies, I: theory*, Journal of Sound and Vibration 247 (1) (2001) 59–76.

[25] T.H.T. Chan, L. Yu, S.S. Law, T.H. Yung, *Moving force identification studies, II: comparative studies*, Journal of Sound and Vibration 247 (1) (2001) 77–95.

[26] J.A. Fabunmi, *Effects of structural modes on vibratory force determination by the pseudo-inverse technique,* American Institute of Aeronautics and Astronautics 24 (1986) 504–509.

[27] L. Yu, T.H.T. Chan, *Moving force identification from bending moment responses of bridges*, Structural Engineering and Mechanics, An International Journal 14 (2) (2002) 151–170.

[28] S. Hashemi, J.K. Hammond, *The interpretation of singular values in the inversion of minimum and non-minimum phase systems*, Mechanical Systems and Signal Processing 10 (3) (1996) 225–240.

[29] H. Gloub, W. Kahan, *Calculating the singular values and pseudo-inverse of a matrix*, SIAM Journal of Numerical Analysis Series B. 2 (1965) 48–59.

[30] T.F. Chan, *An improved algorithm for computing the singular value decomposition,* ACM Transactions on Mathematical Software 8 (1982) 72–83.

[31] J.A. Brandon, C.F. Cremona, *Singular value decomposition: sufficient but not necessary*, Proceedings of Eighth International Modal Analysis Conference, Florida, Vol. 2 (1990) 1376-1380.

[32] W.H. Press, S.A. Teukolsky, W.T. Vetteling, B.P. Flannery, Numerical Recipes in Fortran 90: The Art of Parallel Scientific Computing, 2nd Edition, Vol. 2, Fortran Numerical Recipes, Cambridge University Press, Cambridge,1995.

[33] B. Hillary, D.J. Ewins, *The use of strain gauges in force determination and frequency response function measurements*, Proceedings of Second IMAC, Orlando, Florida, USA, 1984, pp. 627–634.

[34] S.S.Law and T.H.T.Chan, *Regularization in moving force identification,* Journal of Engineering Mechanics,Vol.127,No.2, February,2001.

[35] L.Yu,Tommy H.T.Chan, *Moving force identification based on the frequency-time domain method*, Journal of Sound and Vibration 261 (2) (2003).

[36] Hyoung Gil Choi, Anand N. Thite, David J. Thompson, *Comparison of methods for parameter selection in Tikhonov regularization with application to inverse force determination*, Journal of Sound and Vibration, Volume 304, Issues 3-5, 24 July 2007, Pages 894-917

[37] C.-H. Huang, *An inverse non-linear force vibration problem of estimating the external forces in a damped system with time-dependent system parameters*, Journal of Sound and Vibration, Volume 242, Issue 5, 17 May 2001, Pages 749-765.

[38] Chih-Kao Ma, Chih-Chergn Ho, *An inverse method for the estimation of input forces acting on non-linear structural systems*, Journal of Sound and Vibration, Volume 275, Issues 3-5, 23 August 2004, Pages 953-971

[39] B.J. Dobson, E. Rider, *A review of the indirect calculation of excitation forces form measured structural response data*, Proceedings of Institution of Mechanical Engineers, Part C: Journal of Mechanical Engineering Science 204 (1990).

[40] Olsson,M., *On the fundamental moving load problem*, Journal of Sound and Vibration,145,299-307,1991.

[41] C. Koniditsiotis, R. Buckmaster, P. Fraser, *Australian highway speed weigh-in-motion—an overview, Road Transport Technology-4*, Proceedings of the Fourth International Symposium on Heavy Vehicle Weights and Dimensions, University of Michigan, Transportation Research Institute, Ann Arbor, 1995, pp. 143–151.

[42] F. Moses, *Weigh-in-motion system using instrumented bridges*, Journal of Transport Engineering, ASCE 105 (1978) 233–249.

[43] O.K. Norman, R.C. Hopkins, *Weighing vehicles in motion*, Public Road 27 (1) (1952) 1–17.

[44] R.J. Peters, Axway, *A system to obtain vehicle axle weights,* Proceedings of 12th ARRB Conference, Australia, 1984, pp. 19–29.

[45] R.J. Peters, Culway, *An unmanned and undetectable high speed vehicle weighing system,* Proceedings of 13th ARRB/Fifth REAAA Conference, Australia, 1986, pp. 70–83.

[46] D. Cebon, *Assessment of the dynamic wheel forces generated by heavy road vehicles*, Symposium on Heavy Vehicle Suspension and Characteristics, Austrian Road Research Board, 1987.

[47] A.P. Whittemore, J.R. Wiley, P.C. Schultz, D.E. Pollock, D*ynamic pavement loads of heavy highway vehicles*, Highway Research Board, National Cooperative Highway Research Program Report No. 105, 1970.

[48] R. Cantieni, *Dynamic behavior of highway bridges under the passage of heavy vehicles*, Swiss Federal Laboratories for Materials Testing and Research (EMPA) Report No. 220, 1992.

[49] Daniel J. Inman, Engineering vibration, Prentice Hall, Upper Saddle River, New Jersey, TS176.K34, 2000.

[50] Richard. L Burden and J. Douglas Faires, *Numerical analysis*, 8th edition, Thomson, 2005.

[51] W. S. Shepard, Jr., B. B. Zhang and C.-C. Chen, *Structural configuration study for an acoustic wave sensor*, in Proceedings of SPIE, 15th Annual International Symposium on Smart Structures and Materials & Nondestructive Evaluation and Health Monitoring (San Diego, CA, March 10-14, 2008) Paper No. 6932-131.

[52] J.N. Reddy, *An Introduction to the Finite Element Method* (Third Edition), McGraw-Hill Higher Education, Boston, 2006.

[53] Fahy, F., Sound and Structural Vibration: *Radiation, Transmission and Respons*e, Academic Press, Oxford, 75 (1985).

[54] L.Fryba, *Vibration of Solids and Structures under Moving Loads,* Noordhoff International Publishing, Groningen, 1972.

[55] H. P. Lee, *Dynamic Responses of a Beam with Intermediate Point Constraints Subject to a Moving Load,* Journal of Sound and Vibration, Vol. 171, 1994, pp. 361-368.

[56] X. Q. Zhu and S. S. Law, *Moving forces identification on a multi-span continuous bridge,* Journal of Sound and Vibration, Volume 228, Issue 2, 25 November 1999, Pages 377-396.

[57] M.Abu Hilal and H.S.Zibdeh, *Vibration analysis of beams with General Boundary conditions traversed by a moving force*, Journal of Sound and vibration (2000)229(2), Page 377-388.

[58] Yu Tang, *Numerical Evaluation of Uniform Beam Modes*, Journal of Engineering Mechanics, Vol. 129, No. 12, December 2003, pp. 1475-1477.

[59] S. S. Law and X. Q. Zhu, *Bridge Dynamic Responses due to Road Surface Roughness and Braking of Vehicle*, Journal of Sound and Vibration, Vol. 282, 2005, pp. 805-830.

[60] H.T. Chan and Demeke B. Ashebo, *Theoretical study of moving force identification on continuous bridges*, Journal of Sound and Vibration,Volume 295, Issues 3-5, 22 August 2006, Pages 870-883.

[61] Danut Stăncioiu, Simon James, Huajiang Ouyang, John E Mottershead, *Vibration of a continuous beam excited by a moving mass and experimental validation*, 7th International Conference on Modern Practice in Stress and Vibration Analysis, Journal of Physics: Conference Series 181 (2009) 012084.

[62] Francesco Ricciardelli and Carmelo Briatico, *Transient Response of Supported Beams to Moving Forces with Sinusoidal Time Variation*. J. Eng. Mech. 137, 422 (2011).

[63] R. Jaiswal and R. N. Iyengar, *Dynamic response of a beam on elastic foundation of finite depth under a moving force*, Acta Mechanica ,Volume 96, Numbers 1-4, 67-83, 1993.

[64] D. Thambiratnam and Y. Zhuge, *Dynamic analysis of beams on an elastic foundation subjected to moving load*s, Journal of Sound and Vibration Volume 198, Issue 2, 28 November 1996, Pages 149-169.

[65] Chen, Y.H., Huang, Y.H. & Shih, C.T. *Response of an infinite Timoshenko beam on a viscoelastic foundation to a harmonic moving load.* Journal of Sound and Vibration 241(5) 809-824,2001.

[66] Seong-Min Kim, Jose M Roesset, *Dynamic response of a beam on a frequency-independent damped elastic foundation to moving load, Canadian Journal of Civil Engineering,* 2003, 30:(2) 460-467, 10.1139/l02-109.

[67] Kim, Seong-Min, *Vibration and Stability of axial loaded beams on elastic foundation under moving harmonic loads.* Engineering Structures (26) 95-105, 2004.

[68] Roman Bogacz and Włodzimierz Czyczuła, *Response of beam on visco-elastic foundation to moving distributed load*, Journal of theoretical and applied mechanics 46, 4, pp. 763-775, Warsaw 2008.

[69] Lei Shi, Wen Liu & Chunyan Zhou, *A mathematic model for dynamic transient response of electromagnetic rail on elastic foundation*, Modern applied science,Vol.3, No.9, October, 2009.

[70] Shahin Nayyeriamiri and Mbakisya Onyango, *Simply supported beam response on elastic foundation carrying repeated rolling concentrated loads*, Journal of Engineering Science and Technology, Vol. 5, No. 1, p52 – 66,2010.

[71] Hanselman, Duane C. (2001) Mastering Matlab 6. Prentice Hall, Upper Saddle.

[72] Robert Cook and Warren Young, *Advanced mechanics of materials (2ndedition)*, Prentice Hall,1998, U.S.A.